Report Documentation Page Information

Title and subtitle:

AISI/DOE Advanced Process Control Program
Vol. 4 of 6: On-line, Non-destructive Mechanical Property Measurement Using Laser-Ultrasound

Authors:

André Moreau, Martin Lord, Daniel Lévesque, Marc Dubois, Jean Bussière, Jean-Pierre Monchalin, Christian Padioleau, Guy Lamouche, Teodor Veres, Martin Viens, Harold Hébert, Pierre Basséras, Cheng-Kuei Jen

Performing Organization Names, Addresses:

Industrial Materials Institute
National Research Council Canada
75 de Mortagne Boulevard
Boucherville, Québec J4B 6Y4
Canada

Abstract:

The goal of this project was to demonstrate the feasibility to measure the mechanical properties of low carbon steel sheets on the production line using laser ultrasound. Three types of steels were selected: ultra low carbon (ULC), low carbon (LC), and high strength low alloy (HSLA). The mechanical properties under study were yield strength (YS), ultimate tensile strength (TS), total elongation (TE), uniform elongation (UE), strain hardening exponent (n), and the two plastic strain ratio parameters, $\bar{r}$ and Δr. In addition, the ultrasonic techniques provided information on crystallographic texture, grain size, and sheet thickness. The measurement target accuracy for the various mechanical properties were (the "±" refers to one standard deviation):

YS:	± 0.5 ksi if YS < 50 ksi, ± 0.7 ksi if YS < 100 ksi
TS:	± 0.5 ksi if TS < 50 ksi, ± 0.7 ksi if TS < 150 ksi
n:	± 0.02
UE:	± 1%
TE:	± 1%
$\bar{r}$:	± 0.05
Δr:	not specified.

Laser ultrasound is a technology that allows to generate and detect ultrasound using lasers. The ultrasound generated by the apparatus travels mostly back and forth in the thickness of the steel sheet. By measuring the time delay between two echoes, and the relative amplitude of these two echoes, one can measure ultrasound velocity and attenuation. These are governed by the microstructure: grain size, crystallographic orientation distribution (texture), dislocations. Thus, by recording the time behavior of the ultrasonic signal, one can extract microstructure information. The measurement can then be utilized in a modified Hall-Petch equation that describes the effect of microstructure on the mechanical properties to infer these mechanical properties. The modified Hall-Petch equation also indicates that the mechanical properties depend on other microstructural factors that cannot be measured with ultrasound, i.e. they depend on friction stress, solid solution elements, and fine precipitates. However, if the heat chemistry is controlled sufficiently well, these contributions to the mechanical properties may be constant within the grade.

As a consequence to many technical and scientific achievements, all target accuracies were met or nearly met. In general, ULC and LC steels, with their simpler single-phase, nearly equiaxed and polygonal microstructure were more easily modeled and understood. However, the HSLA grades had more complex microstructure, their ultrasonic grain size measurement were less accurate and their microstructure-property relationships were not so easily established. Consequently, correlations between ultrasonic measurements and mechanical properties often included purely ultrasonic parameters, such as velocity and attenuation, as opposed to derived microstructural quantities. Some of the more important results are:

- The TS of ULC and LC steels varies with ultrasonic grain size measurements, although texture has a significant effect. For these grades, TS measurement accuracy varied between ± 0.3 and ± 0.9 ksi.

- For all grades and a constant amount of temper reduction, YS correlates extremely well with TS. However, temper reduction affects YS significantly. Absorption measurements were essential in probing the effect of temper reduction on YS. For ULC and LC grades, YS measurement accuracy varied between ± 0.5 and ± 1.0 ksi.

- For HSLA grades, YS and TS measurement accuracy varied between ± 0.7 and ± 1.5 ksi, with one exception. One HSLA grade from one of the sponsoring companies had such a low ultrasound absorption that it could not be measured even at very high frequencies. For this grade, YS and TS measurement accuracy were ± 2.3 ksi.

- TE, UE, and n depend on the same microstructural features as YS and TS, and they could be measured to within ± 0.4 to ± 1.5 %.

- The in-plane anisotropy of mechanical properties correlates with ultrasonic texture measurements.

- The in-plane average plastic strain ratio was measured to within ± 0.04 to ± 0.09 depending whether all grades from all companies were considered together or individually.

- Grain size measurement accuracy varied between ± 2 % and ± 14 % depending on grade.

- Sheet thickness could be measured to within ± 4 μm when all grades were considered together, although thicknesses measured within a single grade and thickness, variations of ± 1 μm could easily be detected.

A prototype aimed at validating the technology on the production line was installed at the #1 Inspection line at LTV, Cleveland. Overall, the prototype's performance was as good online as in the laboratory. Sheet vibrations as well as ambient mechanical and electrical noise did not adversely affect the measurement. Optical alignment was preserved over time scales of about two weeks, i.e. between two successive trips to the plant. And data acquisition and analysis were done in real time. Thus, the project reached its goal to demonstrate that mechanical properties can be measured online using laser-ultrasonics.

(RDP Standard Form, Form 298)

Sponsor TBD Report No.:

AISI/DOE Advanced Process Control Program

Vol. 4 of 6: 0N-LINE, NON-DESTRUCTIVE MECHANICAL PROPERTY MEASUREMENT USING LASER-ULTRASOUND

FINAL REPORT
May 1, 1993 – December 31, 2000

Edited By

Joe Vehec

March, 2001

Work performed under Cooperative Agreement No. DE-FC07-93ID13205

Prepared by
American Iron and Steel Institute
For
U.S. Department of Energy

DISCLAIMER

PROJECT PARTICIPANTS

Industrial Materials Institute

André Moreau:	Project leader, Research Officer
Jean F. Bussière:	Section Director
Jean-Pierre Monchalin:	Senior Research Officer
Martin Lord:	Technical Officer
Daniel Lévesque:	Research Officer
Marc Dubois:	Research Officer
Christian Padioleau:	Technical Officer
Guy Lamouche:	Research Officer
Teodor Veres:	Research Officer
Martin Viens:	Research Officer
Cheng-Kuei Jen:	Senior Research Officer
Harold Hébert:	Technical Officer
Pierre Basséras:	Research Officer

Three Steel Companies

American Iron and Steel Institute – Advanced Process Control Program

Lawrence W. Kavanagh:	Director
Joseph R. Vehec:	Director and Administrator

EXECUTIVE SUMMARY

The goal of this project was to demonstrate the feasibility to measure the mechanical properties of low carbon steel sheets on the production line using laser ultrasound. Three types of steels were selected: ultra low carbon (ULC), low carbon (LC), and high strength low alloy (HSLA). The mechanical properties under study were yield strength (YS), ultimate tensile strength (TS), total elongation (TE), uniform elongation (UE), strain hardening exponent (n), and the two plastic strain ratio parameters, $\bar{r}$ and Δr. In addition, the ultrasonic techniques provided information on crystallographic texture, grain size, and sheet thickness. The measurement target accuracy for the various mechanical properties were (the "±" refers to one standard deviation):

YS:	± 0.5 ksi if YS < 50 ksi, ± 0.7 ksi if YS < 100 ksi
TS:	± 0.5 ksi if TS < 50 ksi, ± 0.7 ksi if TS < 150 ksi
n:	± 0.02
UE:	± 1%
TE:	± 1%
$\bar{r}$:	± 0.05
Δr:	not specified.

Laser ultrasound is a technology that allows to generate and detect ultrasound using lasers. Compared to other ultrasound technologies, it offers several advantages. It is a truly remote sensing technology, requiring no couplant, and capable of working at standoff distances of up to several meters, thus allowing measurements on hot or moving parts. It has a much wider frequency bandwidth which results in more information and in the ability to instantly select the frequency most appropriate for the material under study. It generates all acoustic waves, yet its flexible geometry allows to select those waves that are of interest. And finally, because the measurement relies on the interaction between laser light and the material's surface, independently of laser beam angle, laser-ultrasound has much relaxed alignment requirements.

The ultrasound generated by the apparatus travels mostly back and forth in the thickness of the steel sheet. By measuring the time delay between two echoes, and the relative amplitude of these two echoes, one can measure ultrasound velocity and attenuation. These are governed by the microstructure: grain size, crystallographic orientation distribution (texture), dislocations. Thus, by recording the time behavior of the ultrasonic signal, one can extract microstructure information. The measurement can then be utilized in a modified Hall-Petch equation that describes the effect of microstructure on the mechanical properties to infer these mechanical properties. The modified Hall-Petch equation also indicates that the mechanical properties depend on other microstructural factors that cannot be measured with ultrasound, i.e. they depend on friction stress, solid solution elements, and fine precipitates. However, if the heat chemistry is controlled sufficiently well, these contributions to the mechanical properties may be constant within the grade.

To follow this approach, several scientific and technical challenges were surmounted. Laser-ultrasound detection bandwidth was extended from about 30 MHz to 300 MHz. A laser capable of generating high amplitude, high frequency ultrasound without marking the surface was found. Accurate and reliable ultrasound attenuation and velocity dispersion spectra were

measured over a wide bandwidth, thus resulting in accurate grain size measurements. A laser-ultrasound resonance spectroscopy technique was invented (and patented) to measure texture and thickness. Another technique was invented to measure ultrasonic absorption in large sheets and infer information about the effect of temper rolling (skin pass) on YS. And finally, empirical models were found to relate the measured microstructure and ultrasonic measurements to the mechanical properties.

As a consequence to these many technical and scientific achievements, all target accuracies were met or nearly met. In general, ULC and LC steels, with their simpler single-phase, nearly equiaxed and polygonal microstructure were more easily modeled and understood. However, the HSLA grades had more complex microstructure, their ultrasonic grain size measurement were less accurate and their microstructure-property relationships were not so easily established. Consequently, correlations between ultrasonic measurements and mechanical properties often included purely ultrasonic parameters, such as velocity and attenuation, as opposed to derived microstructural quantities. Some of the more important results are:

- The TS of ULC and LC steels varies with ultrasonic grain size measurements, although texture has a significant effect. For these grades, TS measurement accuracy varied between ± 0.3 and ± 0.9 ksi.

- For all grades and a constant amount of temper reduction, YS correlates extremely well with TS. However, temper reduction affects YS significantly. Absorption measurements were essential in probing the effect of temper reduction on YS. For ULC and LC grades, YS measurement accuracy varied between ± 0.5 and ± 1.0 ksi.

- For HSLA grades, YS and TS measurement accuracy varied between ± 0.7 and ± 1.5 ksi, with one exception. One HSLA grade from one of the sponsoring companies had such a low ultrasound absorption that it could not be measured even at very high frequencies. For this grade, YS and TS measurement accuracy were ± 2.3 ksi.

- TE, UE, and n depend on the same microstructural features as YS and TS, and they could be measured to within ± 0.4 to ± 1.5 %.

- The in-plane anisotropy of mechanical properties correlates with ultrasonic texture measurements.

- The in-plane average plastic strain ratio was measured to within ± 0.04 to ± 0.09 depending whether all grades from all companies were considered together or individually.

- Grain size measurement accuracy varied between ± 2 % and ± 14 % depending on grade.

- Sheet thickness could be measured to within ± 4 μm when all grades were considered together, although thicknesses measured within a single grade and thickness, variations of ± 1 μm could easily be detected.

A prototype aimed at validating the technology on the production line was installed at the #1 Inspection line at LTV, Cleveland. Overall, the prototype's performance was as good

online as in the laboratory. Sheet vibrations as well as ambient mechanical and electrical noise did not adversely affect the measurement. Optical alignment was preserved over time scales of about two weeks, i.e. between two successive trips to the plant. And data acquisition and analysis were done in real time.

However, at the time it was tested, the prototype suffered from two shortcomings. First, we could not guarantee that the laser used to generate the ultrasound would leave the sheet surface undamaged: a slight discoloration of the surface sometimes occurred. Since then, we have identified and successfully tested an alternate laser technology which can generate large amplitude ultrasound with no surface damage. The second shortcoming was YS measurement accuracy. Improved YS accuracies were obtained by adding laboratory measurements of absorption to the model. This resulted in the YS accuracies stated above.

Because we could not guarantee that the generation laser would not damage the surface, few coils were tested online. However, three coils from a set of five showed similar texture variations along their length. Another one of the five coils showed oscillations in the texture coefficient that correlates with plastic strain ratio. These oscillations were also found on another coil. The facts that few coils were measured and that reproducible variations of properties along the length of the coils were so easily found hints at the powerful ability of the sensor to detect variations in microstructure and mechanical properties that are typical of ordinary production conditions. It is the authors' opinion that systematic monitoring and analysis of such variability would lead to the identification of many of the process parameters that cause this variability. Corrective action could then be envisioned and implemented to produce more uniform product quality.

This project reached its goal to demonstrate that mechanical properties can be measured online using laser-ultrasonics. To go beyond and reach commercial success, we recommend the following: First, the latest generation laser must be re-engineered into a modern, affordable, and mill-worthy version. Second, the absorption measurements that were made using a laboratory setup must be incorporated into the online prototype. Following these developments, we recommend another series of online tests at the #1 inspection line at LTV. Given that the #1 Inspection line is equipped with all the required services, these tests would be relatively inexpensive and provide useful information to design and build a fully commercial prototype.

One key project development was the remote and real-time measurement of various microstructural quantities. The project was extended to demonstrate that laser-ultrasound could also measure austenite grain size and growth, phase transformations, sub-critical annealing, and ferrite grain growth at high processing temperatures. The microstructure was measured *in situ* and in real time, on a Gleeble 3500 thermomechanical simulator, the standard equipment used by the steel industry to physically simulate thermal and mechanical processes. At the rate of one microstructural measurement per second, this represents a technological breakthrough when compared to the time required to do similar work by quenching a new sample for each measurement, and doing metallographic analysis. This work is now being continued with the development of a new prototype to measure austenite grain size on hot pipes and tubing, online, at one of the APC member companies.

Table of Contents

LIST OF TABLES

LIST OF FIGURES

1 INTRODUCTION

1.1 Objectives

The goal of this project was to demonstrate the feasibility to measure the mechanical properties of low carbon steel sheets on the production line using laser ultrasound. Three types of steels were selected: ultra low carbon (ULC), low carbon (LC), and high strength low alloy (HSLA). The mechanical properties under study were yield strength (YS), ultimate tensile strength (TS), total elongation (TE), uniform elongation (UE), strain hardening exponent (n), and the two plastic strain ratio parameters, $\bar{r}$ and Δr. Additional benefits of using ultrasonic techniques is that information on crystallographic texture, grain size, and sheet thickness were also obtained. The measurement target accuracy for the various mechanical properties were (the "±" refers to one standard deviation):

YS:	± 0.5 ksi if YS < 50 ksi, ± 0.7 ksi if YS < 100 ksi
TS:	± 0.5 ksi if TS < 50 ksi, ± 0.7 ksi if TS < 150 ksi
n:	± 0.02
UE:	± 1%
TE:	± 1%
$\bar{r}$:	± 0.05
Δr:	not specified

1.2 Approach: Mechanical properties, microstructure, and ultrasonics

Mechanical properties of steels, such as yield strength (YS), are governed by the microstructure. For example, the phenomenological Hall-Petch equation states that YS increases with the inverse square-root of grain size. The modified Hall-Petch equation (Equation 1.1) also indicates that other microstructural and metallurgical parameters influence YS. These parameters are the friction stress (σ_0), solid solution strengthening contribution (σ_{ss}), precipitate strengthening contribution (σ_p), dislocations strengthening contribution (σ_d), crystallographic texture contribution (σ_t), and grain size (d). In Equation 1.1, k_{YS} is an empirical constant. By measuring at least some of these various microstructural quantities, one may be able to estimate the mechanical properties as long as the contribution of the other quantities does not vary significantly.

$$YS = \sigma_0 + \sigma_{ss} + \sigma_p + \sigma_d + \sigma_t + k_{YS} d^{-1/2} \tag{1.1}$$

In this project, ultrasound is used to probe as many as possible of the above parameters that contribute to YS and to other mechanical properties. To do this, ultrasound velocity, attenuation and absorption are measured. Both longitudinal and shear wave velocities are measured, as well as the frequency dependence of velocity, attenuation, and absorption. It will be shown that ultrasonic attenuation is primarily caused by scattering by grains and is a measure of grain size. Ultrasonic velocity is a direct measurement of elastic moduli, and angular variations and ratios of ultrasonic velocities are a measurement of crystallographic orientation distribution, or texture. Finally, ultrasonic absorption was indirectly shown to be sensitive to dislocations. Consequently, if a commercial grade is

produced with good chemistry control, then the contributions of friction stress (which is theoretically a constant), solid solution strengthening, and precipitates may be nearly constant for that grade, and reliable estimates of YS and other mechanical properties may be obtained using ultrasonics.

In accordance to this model, the approach we followed was to extract as much microstructural information as possible from ultrasonic measurements, and then correlate this information with mechanical properties using known (and discovering other) structure-property relations. Because the intermediate step of measuring the microstructure may be limiting, direct empirical correlation between ultrasonic measurements and mechanical properties were also sought.

To do the ultrasonic measurements, laser-ultrasound technology was selected. Laser ultrasound is a technology that allows to generate and detect ultrasound using lasers. Compared to other ultrasound technologies, it offers several advantages. It is a truly remote sensing technology, requiring no couplant, and capable of working at standoff distances of up to several meters, thus allowing measurements on hot or moving strips. It has a much wider frequency bandwidth which results in more information and in the ability to instantly select the frequency most appropriate for the material under study. It generates all acoustic waves, yet its flexible geometry allows to select those waves that are of interest. And finally, because the measurement relies on the interaction between laser light and the material's surface, independently of laser beam angle, laser-ultrasound has much relaxed alignment requirements.

1.3 Challenges and project overview

When the project began, some of the challenges were foreseen, others were not. In retrospect, here are the challenges that were met.

1.3.1 High-frequency laser-ultrasound

To measure ultrasonic attenuation and grain size in fine grain materials such as HSLA steels, ultrasonic measurements in the 50-100 MHz range are required. When the project started, and to our knowledge, laser-ultrasound measurements were usually made below 10 MHz, with occasional high-frequency components up to about 30 MHz. It was not known if high-frequency ultrasonic pulses could be generated or detected. The detection of high frequency ultrasound using a confocal Fabry-Perot interferometer is discussed in Section 2.2 (Detecting high frequency ultrasound). Its generation is discussed in Section 2.3 (Generating high-frequency high-amplitude ultrasound).

1.3.2 Laser-ultrasound measurements that do not damage the surface

When the project began, and today still, most of laser-ultrasonics systems employed Q-switched Nd:YAG lasers* which, when used in the ablation regime to generate high

* The main exception is laser-ultrasound systems dedicated to applications with polymers where a CO_2 laser is usually employed.

amplitude ultrasound, can cause substantial surface damage. At high enough laser energies, the damage results from partial melting of the surface and ejection of molten droplets, resulting in an alteration of the surface profile. Section 2.3 (Generating high-frequency high-amplitude ultrasound) describes how this surface damage was completely eliminated.

1.3.3 Measuring attenuation reliably

Laser-ultrasound was reputed to provide low signal-to-noise ratio (S/N). However, a high S/N was required to measure attenuation spectra. Moreover, it was generally believed that ultrasonic attenuation measurements were difficult to make using *any* technique and that the more reliable techniques were confined to the laboratory. In particular, to obtain reliable and accurate attenuation measurements, one had to solve the problems of ultrasound diffraction, acoustic noise, wedge effects, surface roughness effects and, if averaging over many locations, thickness variation effects. Section 2.4 (Measuring ultrasound attenuation, velocity dispersion, and grain size) describes how good S/N and reliable laser-ultrasonic attenuation measurements were obtained.

1.3.4 Obtaining enough uncorrelated information to measure all mechanical properties with sufficient accuracy. Being sensitive to the important microstructural parameters.

The original proposal emphasized measuring grain size through ultrasonic attenuation measurements, and using empirical equations based on chemistry and grain size to predict the mechanical properties. If these measurements were insufficient, they would be combined with NIST's magnetic measurements or with available processing information to provide better mechanical property estimates. Only a vague allusion was made to texture measurements. As the project evolved, the work on magnetic measurements was discontinued. In addition, it became clear that, to maximize the usefulness of the apparatus, *NO* processing information other than grade should be used. It was not even possible to rely on a thickness gauge to obtain the sheet thickness. Clearly, all properties, and especially YS, could not be simultaneously obtained using only grain size and grade number. Section 2.5 (Measuring ultrasound velocity, texture, and thickness using laser-ultrasound spectroscopy), Section 2.6 (Measuring ultrasonic absorption and temper reduction), and Section 2.7 (Other measurements in an attempt to measure temper reduction) describe how additional ultrasonic and microstructural (texture, dislocation) information were obtained.

1.3.5 Online measurements

The ultimate objectives were to demonstrate the measurement capabilities online. Engineering issues, such as transposition of the laboratory measurements to a production line, real-time data analysis, safety of the operation and so forth, are discussed in Section 3 (Prototype for online measurements)

1.3.6 Predicting yield strength and other mechanical properties

Once a maximum amount of information was gathered, there remained the task to predict the mechanical properties. But was the right information gathered? Would the approach discussed in Section 1.2 (Approach: Mechanical properties, microstructure, and

ultrasonics) be valid? Would the target accuracy for the various properties be met? These questions are discussed in Section 4 (Mechanical properties measurements).

1.4 Project extension: Exploratory measurements of microstructure at processing temperatures

One key capability developed in the project is the remote and real time measurement of various microstructural quantities. Simply attempting to estimate the mechanical properties seemed to under-exploit the technologies being developed. So it was proposed to demonstrate the ability of laser-ultrasound to measure austenite grain size and growth, phase transformations, and sub-critical annealing and ferrite grain growth. These capabilities were demonstrated first in a radiant furnace, and later in a Gleeble 3500 thermomechanical simulator, the standard equipment used by the steel industry to physically simulate thermal and mechanical processes. It is now possible to measure the microstructure *in situ* and in real time while the material is being processed. The measurement rate of one per second represents a technological breakthrough when compared to the time it takes to do the same work by quenching a new sample for each measurement, and doing metallographic analysis. This work was reported in a separate self-contained and comprehensive report and in several papers[1] and will not be reviewed here.

2 EXPERIMENTAL DEVELOPMENTS

2.1 Overall configuration

The chosen experimental configuration, Figure 2.1, relied on a pulsed laser and a laser interferometer to generate and detect ultrasound on opposite sides of the steel sheet. The generation laser sends a short burst of energy on the steel surface. At sufficiently high laser energies, a thin layer on the sheet surface may be ablated and the recoil energy generates a strong acoustic wave. When the acoustic wave reaches the opposite surface, the resulting surface motion is sensed with a detection laser whose light is collected in an optical fiber and analyzed with a Fabry-Perot interferometer. The output signal is then digitized using a fast oscilloscope and transferred to a PC where it is processed and stored. The more powerful is the detection laser, the more sensitive is the detection. Laser-ultrasound is a method of choice for online ultrasonic inspection because it can be performed at large standoff distances (several meters), the alignment procedure is simple, and it is broadband.

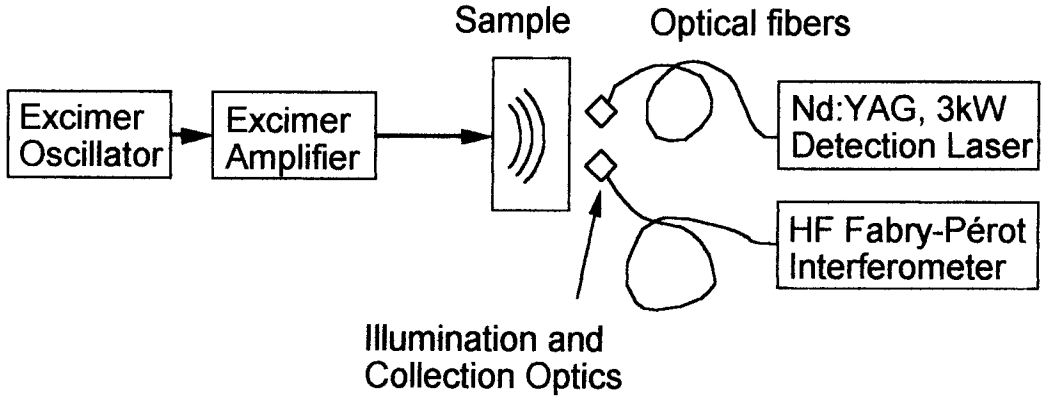

Figure 2.1 Laser-ultrasonic setup.
The generation laser is, in this case, made of an excimer laser oscillator followed by an amplifier. On the detection side, some experiments were made with the illumination and collection optics separate from each other (above) or using a coaxial configuration (not shown).

Figure 2.2 shows a typical example of the ultrasonic signal obtained with the setup of Figure 2.1. The large negative peaks are successive echoes of the longitudinal wave travelling back and forth between the sample's two surfaces. These negative peaks correspond to the sample surface moving toward the interferometer. Immediately following the negative peak, are positive peaks that are caused by high-pass filters. After the longitudinal wave has traveled a few round trips in the thickness of the sample, some shear acoustic signal appears. By measuring the time delay between two longitudinal echoes, one can obtain the longitudinal wave velocity. And by measuring the loss of amplitude between two longitudinal echoes, one can obtain the longitudinal wave attenuation. More information can also be extracted from such signals. This section of the report details the experimental configuration of Figure 2.1 and the information that can be extracted from signals such as the one shown in Figure 2.2.

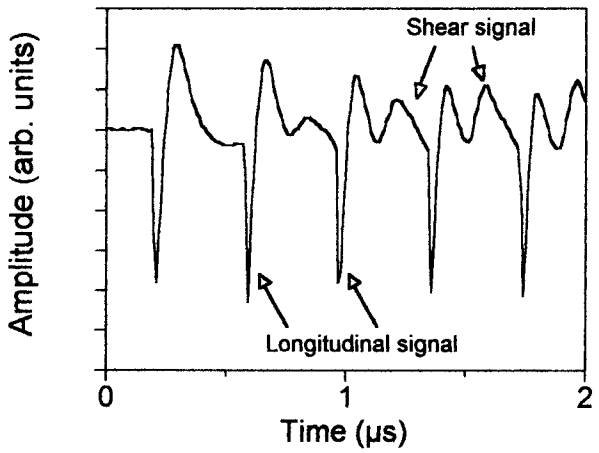

Figure 2.2 Typical laser-ultrasound signal
obtained with the experimental setup shown in Figure 2.1. The vertical axis corresponds to surface displacement in arbitrary units. Negative peaks represent the surface moving towards the interferometer. Longitudinal and shear acoustic echoes are identified.

2.2 Detecting high frequency ultrasound

2.2.1 High frequency Fabry-Perot interferometer

The Fabry-Perot laser-interferometer previously developed at IMI[2] was optimized to operate with higher sensitivity and at higher frequencies than ever before. To verify the behavior at high frequencies, the transfer functions of a 1 m interferometer operated using a He-Ne laser radiating at 632.8 nm and of a 50 cm interferometer operated using an argon laser radiating at 514 nm were measured and compared with theory. The measured amplitude and phase response of both interferometers precisely match our model's predictions. The model was verified at frequencies up to 180 MHz and predicts that the transfer function repeats has sharp drops in amplitude and sudden 180° phase shifts every 75 and 150 MHz for the 1 m and 50 cm interferometers, respectively. Figure 2.3 shows the case of the 50 cm argon-laser interferometer used for early laboratory measurements. The amplitude response is nearly flat with 10 MHz wide rejection bands every 150 MHz.

The response of the high-frequency interferometer used for the prototype could not be tested over its entire 300 MHz bandwidth because the light modulator used to produce Figure 2.3 was limited to 180 MHz in bandwidth. Other verifications of interferometer's behavior at frequencies up to 300 MHz and higher are shown in Figure 2.4 and were presented in detail elsewhere.[3] Here it is sufficient to mention that the amplitude and phase discontinuities illustrated in Figure 2.3 appear every 150 MHz as predicted by theory.

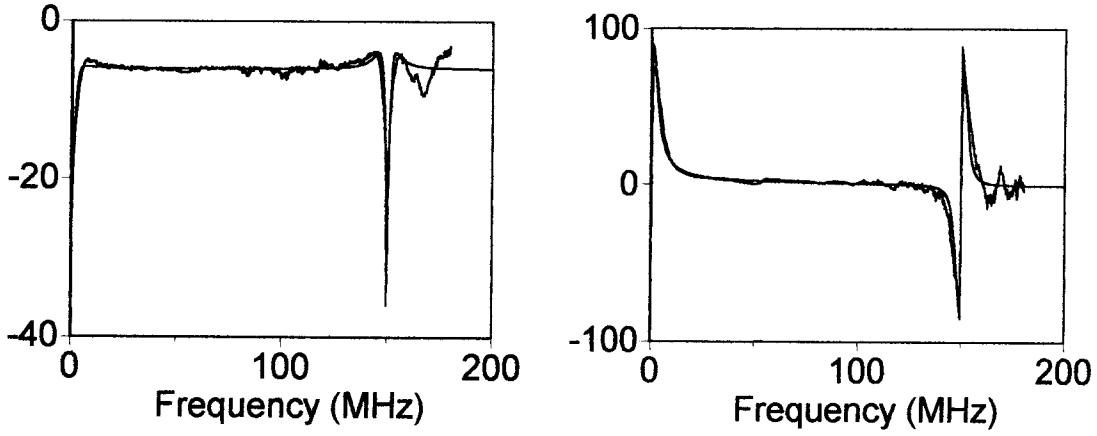

Figure 2.3 Amplitude and phase response of the 50 cm argon Fabry-Perot interferometer used for laboratory measurements. The smooth line is the model prediction and the jagged line is the experimental measurement.

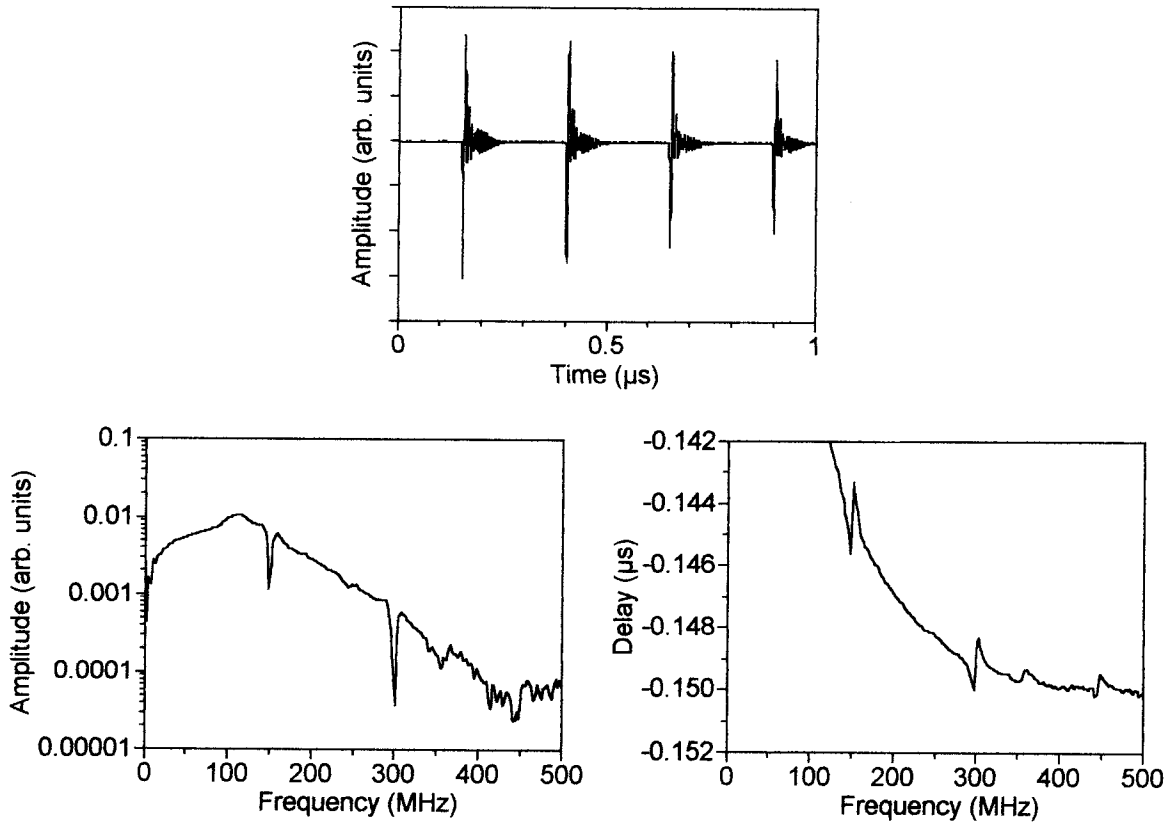

Figure 2.4 High frequency response of the Fabry-Perot interferometer.
Top: Amplitude as a function of time (A-scan) showing the first four acoustic echoes in an 800 μm thick aluminum plate (grade 6061-T6, chosen for its lower attenuation than steel). Left: Amplitude spectrum and Right: Delay spectrum of the first echo. Signal-to-noise ratio reaches unity near 500 or 600 MHz. The two spectra were calculated from the A-scan using a 350 ns rectangular window and Fourier transform techniques.

2.2.2 *Optical fiber*

The laser light received from the sample is coupled to the interferometer using an optical fiber. This allows one to locate the sensitive interferometer away from adverse environments. Optical mode dispersion in the fiber may attenuate the high-frequency components of the acoustic signal and this was studied experimentally. Modal dispersion causes the light received from the sample to travel in the fiber at a velocity that is a function of incidence angle. For a 20 m, step index fiber with a core of 400 μm diameter, we observed an increase in the propagation delay of a short light pulse of up to 3% when injected at an angle. A simple model shows that the high frequency, -3 dB sensitivity point occurs near 122 MHz for this fiber (Figure 2.5). Consequently, when building a prototype with long optical fibers, care must be taken to choose a fiber with low enough modal dispersion so that the high frequency response is not adversely affected.

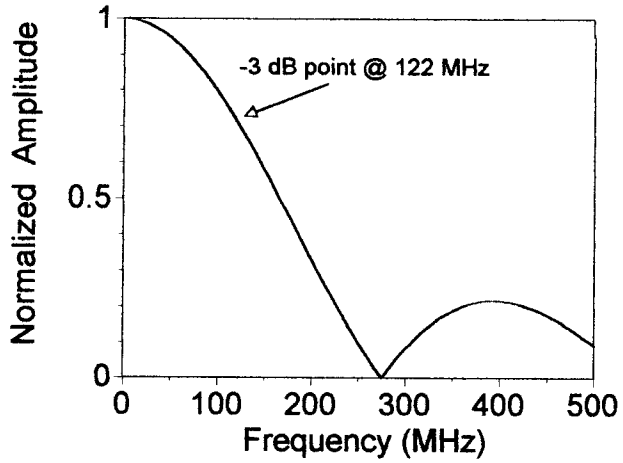

Figure 2.5 Amplitude response of a 20 m optical fiber with a 400 μm, step index core.

2.2.3 *Improvements in signal-to-noise ratio*

The 1 W argon detection laser used in the first two years provided sufficient light when measuring samples polished to near mirror conditions. But as-received (rough) samples scatter light in all directions and insufficient light is collected in the collection optics. Consequently, the argon laser was replaced with a 3 kW peak power Nd:YAG laser. The detection interferometer optics and optical detector were replaced to work at the new infrared wavelength. The detection electronics was much improved to better respond at high frequencies. Figure 2.6 compares the acoustic frequency spectrum of the first acoustic echo in an as-received HSLA steel sample obtained after the modifications (March 1996) to that obtained one year earlier on polished samples. The same generation laser was used in both cases, and the two curves are roughly normalized to equal noise levels. Clearly, the improvements offer much higher signal-to-noise ratio at all frequencies, and especially above 80 MHz. The drop at low frequencies in the March 1996 curve is due to a high pass electronic filter, and the drop between 140 and 160 MHz is due to the filtering effect of the Fabry-Perot interferometer, as shown in Figure 2.3. With this system, ultrasonic attenuation at frequencies of up to 120 MHz can be measured routinely in fine grain steels in their as-received conditions.

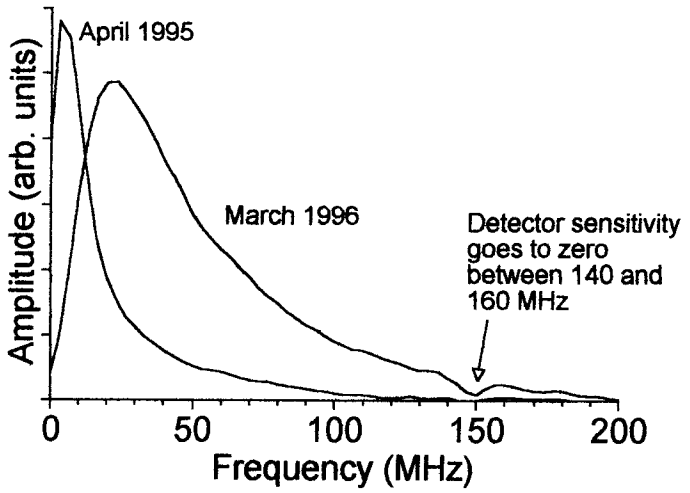

Figure 2.6 Improvement in high frequency laser-ultrasonic amplitude obtained between April 1995 on polished samples and March 1996 on as-received samples.

2.3 Generating high-frequency high-amplitude ultrasound

2.3.1 Shorter pulses generate higher frequencies

To study the frequency content of laser-generated acoustic waves with minimal acoustic diffraction effects, the generation and detection lasers were focused and aligned on opposite sides of steel sheets (point-source, point-detection). A Q-switched Nd:YAG infrared laser and an excimer UV laser were tried first. As expected, their respective pulse lengths, 8 and 15 ns full-width-at-half-maximum (fwhm), were too long to generate the required frequencies. To shorten the light pulse and generate higher acoustic frequencies, a plasma shielding cell previously developed at IMI was used. The infrared pulses were reduced from 8 ns fwhm to 3.5 ns fwhm. The highest acoustic frequencies obtained with this shortened laser pulse (signal-to-noise ratio of about 1) were of the order of 125 MHz. The plasma shielding cell was modified to be used with the excimer laser to combine short pulses with the more efficient UV radiation (see next sub-section) but the pulse width could be reduced from 15 ns to only 8 ns fwhm. Consequently, the plasma shielding cell was abandoned.[†]

The high frequencies generated with the infrared laser and the plasma shielding cell were sufficient to observe acoustic attenuation in LC and ULC steel samples but not enough for HSLA steel samples. To generate higher acoustic frequencies, an even shorter light pulse was required. Therefore we rented a frequency-tripled Nd:YAG laser that is Brillouin compressed to about 1 ns fwhm. The laser generated approximately 2.5 mJ at 355 nm (UV) and 30 mJ at 1.064 μm (IR). Acoustic frequencies in excess of 200 MHz were detected in HSLA steels with this system and an acoustic attenuation exceeding 6 dB/mm (an amount easily measurable) was observed at the highest frequencies.

[†] Later improvements (using IMI's internal funds and for internal purposes) to the cell with subsequent amplification allowed us to generate 1.7 ns fwhm pulses with 180 mJ of IR radiation energy, and to generate even higher ultrasonic frequencies. But IR radiation remained more damaging to the surface than UV radiation.

2.3.2 *UV light generates more efficiently that IR light*

Having generated sufficiently high acoustic frequencies, we studied the acoustic generation mechanism to improve generation efficiency. To compare the relative generation efficiencies of UV (355 nm) and infrared (1064 nm) radiation, the parameters influencing the measured acoustic amplitude were considered: spatial and temporal profiles of the laser, sample thickness, sample attenuation, and acoustic diffraction effects. The experiment was conducted in the strong ablation regime under a variety of conditions. The result is shown as two curves in Figure 2.7. For both types of radiation, the generated acoustic amplitude is proportional to the generation laser energy density (fluence). For a fixed fluence, the generated acoustic amplitude corrected for geometrical effects and diffraction is approximately five times larger when using the UV radiation. We can reasonably expect that UV radiation bursts will also be five times more efficient at generating ultrasound in the weak ablation regime. The generation efficiency was also somewhat improved when the steel surface was dirtied with finger prints or a thin layer of oil.

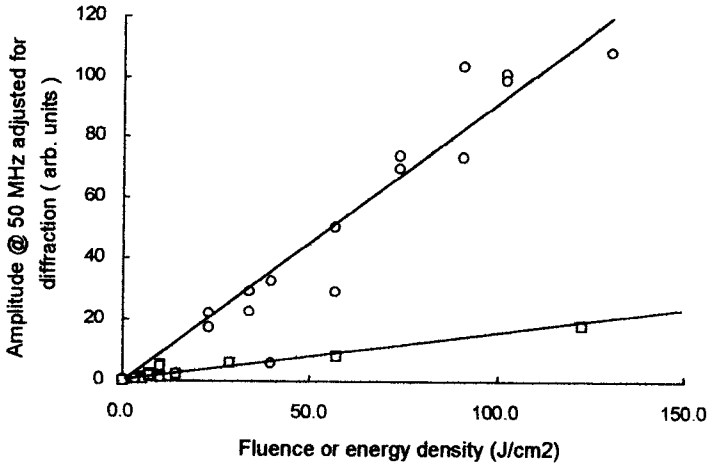

Figure 2.7 Relative generation efficiency of UV radiation IR radiation in steel.
Circular and square data points correspond to UV and IR radiation, respectively. The pulse duration was 1 ns, resulting in power densities (irradiance) of 0 to 150 GW/cm^2. The straight lines are guides to the eye.

2.3.3 *Generating high ultrasound amplitudes without damaging the surface*

While shortening the infrared (1064 nm) laser pulses from 8 ns to 3 ns using the plasma shielding cell and to 1 ns using the Brillouin compressed laser, it was observed that the severity of the damage caused by the laser to the sheet surface decreased. It was also observed that UV radiation obtained from the excimer laser (248 nm, 15 ns and 8 ns) or obtained by tripling the frequency of the Brillouin compressed laser radiation (355 nm, 1 ns) was less damaging than IR radiation of similar energy density and duration. As a general rule shorter the pulse duration and shorter the optical wavelengths (UV as opposed to IR) not only increased the high frequency content (Section 2.3.1) and increased generation efficiency (Section 2.3.2), but they also contributed to reducing surface damage.

Moreover, it was also observed that applying a thin layer of oil to the sample surface increases substantially the amplitude of the generated ultrasound while reducing surface damage even more. So a short pulse excimer laser (next section) was selected for the prototype, and this laser was to be used on oiled coils only. Depending on how the laser energy was focused on the sample surface, and depending on the thickness of the oil layer, it was possible to generate high amplitude, high frequency ultrasound with no damage to the surface. However, it was impossible to guarantee that the generation laser would be 100% reliable in not damaging the surface and this prevented large scale measurements on regular production material.

2.3.4 The short-pulse excimer laser solution

The 1 ns fwhm Brillouin compression laser used in the generation laser experiments is a laboratory instrument and cannot be used in an industrial environment. Moreover, its UV pulse energy of only 0.23 mJ cannot generate acoustic pulses with sufficient amplitude over large areas. Therefore, a new mill-worthy and more powerful generation laser had to be acquired. Based on these experiments, we determined that the optimal laser pulse duration should be of order 2 ns fwhm for efficient generation at the highest frequencies of interest (200 MHz). Other desirable laser characteristics were spatial uniformity of the beam, low beam divergence, sufficient pulse energies, and reliability. Our solution was to use a low energy, short pulse excimer laser whose output was amplified to 150 mJ using an excimer amplifier in a two-pass configuration (Figure 2.8).

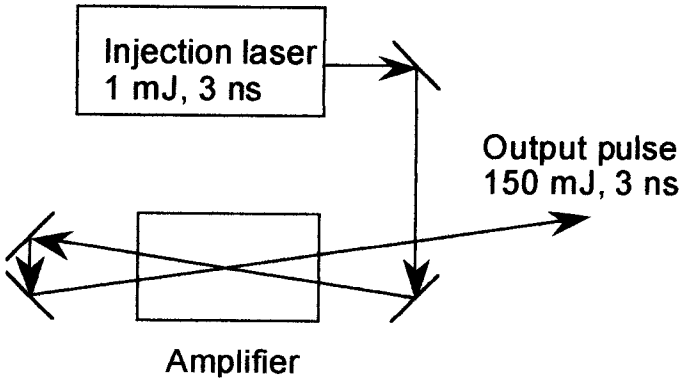

Figure 2.8 Schematics of the excimer laser system used to deliver 3 ns fwhm, 150 mJ light pulses of UV (248 nm) radiation.

2.3.5 The short- pulse CO_2 laser solution

The online tests at LTV confirmed that the short pulse excimer laser was only marginally capable of generating high amplitude ultrasound without damaging (discoloring) the sheet surface. So several other lasers were tested. Lasers with even shorter pulse duration, down to 1 ps showed further increases in generation efficiency but negligible improvements in surface damage. Eventually, a totally different solution was identified to generate high-frequency, high-amplitude ultrasound without damaging clean surfaces at all. This laser is based on a short pulse CO_2 laser. This laser radiates in the far infrared region and the mechanism by which ultrasound is generated is not understood. It is also the least efficient laser at generating high amplitude ultrasound in metals. However, a very high-energy

laboratory system was utilized and showed excellent S/N over a wide ultrasonic bandwidth, without damaging the surface, and over a wide range of laser pulse energies. It turns out that the inefficiency of the CO_2 laser at generating ultrasound is advantageously compensated by the high pulse energies that can be applied without damaging the surface. Moreover, the CO_2 laser does not require an oil layer to protect the surface against damage.

The laboratory system utilized in this project is too large, too expensive, and requires too much care for reliable in-plant operation. A smaller, cheaper, and more robust design is envisioned but time and budget constraints prevented upgrading the system to this novel solution.

2.4 Measuring ultrasound attenuation, velocity dispersion, and grain size

In Section 2.1 (Overall configuration), it was mentioned that attenuation of the longitudinal acoustic pulse could be obtained by comparing the amplitude of two successive echoes. The previous two sections (Detecting high frequency ultrasound and Generating high frequency ultrasound) detailed how one can generate and detect high amplitude ultrasound with excellent signal-to-noise ratio. But to measure ultrasonic signals accurately, good equipment is not sufficient: one must also avoid artifacts. Examples of such artifacts are diffuse ultrasound signal, acoustic diffraction effects, surface roughness effects, sample thickness variation effects, oil thickness effects.

In this section, we will describe how artifact-free signals are obtained, how the ultrasonic attenuation spectrum is calculated using Fourier analysis, sample requirements, and how attenuation spectra are used to estimate grain size.

2.4.1 Diffraction

Just as light can diffract while traversing a small hole, ultrasound can diffract. The equivalent of the hole is the finite dimensions of the ultrasound source. The Fresnel parameter, s, is defined as

$$s = \frac{\lambda z}{a^2}, \tag{2.1}$$

where λ is the ultrasound wavelength, z is the propagation distance of the ultrasound, and a is the radius of the ultrasound source. The Fresnel parameter may be used to identify three diffraction regions:

Near field:	$s \leq 0.1$
Intermediate field:	$0.1 \leq s \leq 10$
Far field:	$s \geq 10$.

In the near field, the ultrasound propagates like a plane wave of constant amplitude. In the far field, the ultrasound propagates as if it had been generated by a point source and its amplitude decreases as the inverse propagation distance. In the intermediate field, the ultrasound propagates in a complicated manner, sometimes increasing and sometimes decreasing in amplitude.

In Figure 2.9, ultrasound was generated and detected over a point-like area. In this far field setup, the ultrasound amplitude decreases as the inverse propagation distance ($1/z$). Consequently the ratio ultrasound amplitude of the first to second to third echo is roughly in the ratios of 1 to 1/3 to 1/5, and corresponds to a wave travelling through one, three times and five times the sample thickness. Therefore, this decrease in amplitude from one echo to the next is an artifact of the measurement and does not correspond to any material property. To avoid any diffraction problem, all measurements were conducted in the near acoustic field with generation and detection spots of nearly equal dimensions.[4]

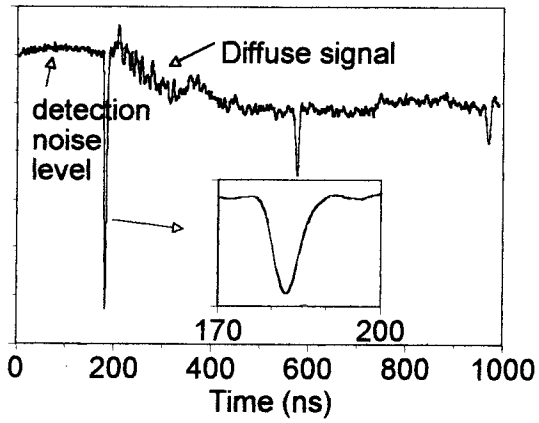

Figure 2.9 Acoustic signal generated by a 1 ns fwhm UV light pulse in HSLA steel. The experimental configuration was that of a point source and point detection.

2.4.2 Diffuse signal and spatial averaging

As will be seen later, grain size is obtained by measuring the loss of ultrasound amplitude caused by grain scattering. This scattered ultrasound does not disappear but travels in random directions. Some of it reaches the detection area where it is detected with random phase and amplitude. Although the equipment may produce ultrasound signal with excellent signal-to-noise ratio, this noise-like ultrasonic signal, which we call the *diffuse signal* or *incoherent signal*, degrades the measurement of the *coherent signal*, i.e. of the longitudinal echoes (Figure 2.9). Fortunately, this incoherent signal is not only incoherent in time, but also spatially on the sample surface. To greatly reduce this signal to negligible levels, it was spatially averaged by enlarging the source and detection area to several mm in diameter. One such spatially averaged signal was shown earlier in this report (Figure 2.2).

2.4.3 Attenuation spectra

As the ultrasound propagates in steel, its low and high frequency components are scattered in different amounts. Thus it is important to measure the frequency dependence of the ultrasonic attenuation. To do this, the first and second echoes are windowed and their amplitude spectra are computed using a discrete Fourier transform (DFT). The ratio of the two spectra is then calculated and converted to units of dB (a decrease in amplitude by a factor of 10 corresponds to 20 dB of attenuation). Finally, the calculated spectrum is divided by twice the sample thickness to yield the attenuation spectrum in dB/mm. Mathematically, one can write

$$\alpha(f)=\frac{1}{2h}20\log\frac{A_1(f)}{A_2(f)}, \tag{2.2}$$

where $\alpha(f)$ is the attenuation spectrum, $A_1(f)$ and $A_2(f)$ are the amplitudes of the first and second echoes, respectively, and h is the sample thickness. Examples of attenuation spectra are given in Figures 2.12 to 2.16.

2.4.4 Velocity dispersion spectra

Although we focused on attenuation spectra, the velocity dispersion spectra, i.e. the change in sound velocity as a function of frequency, were also measured. When a DFT is calculated, one obtains not only the magnitude of signal amplitude at each frequency, but also its phase. For a single frequency, the phase difference between two echoes is directly related to the time delay between the two echoes (to within an integer number of 2π radians). By converting this phase spectrum to a propagation delay spectrum, and by dividing twice the sample thickness by this delay, one obtains an ultrasonic velocity dispersion spectrum. Mathematically, the phase difference, $\Delta\phi(f)$, is expressed as

$$\Delta\phi(f)=\phi_2(f)-\phi_1(f), \tag{2.3}$$

where $\phi_1(f)$ and $\phi_2(f)$ are the phase spectra of the first and second echoes, respectively. The propagation delay spectrum, $\Delta t(f)$, is

$$\Delta t(f)=\frac{\Delta\phi(f)+2\pi n}{2\pi f}, \tag{2.4}$$

where n is an integer. Although n is unknown, it can be evaluated from an approximate time delay measurement between the two echoes. The velocity spectrum, $v(f)$, can then be expressed as

$$v(f)=\frac{2h}{\Delta t(f)}=\frac{4\pi fh}{\Delta\phi(f)+2\pi n}. \tag{2.5}$$

The velocity dispersion spectra are sometimes normalized by some mean velocity (Voigt average) and expressed as a percentage,

$$\frac{\Delta v(f)}{\bar{v}}=\frac{v(f)-\bar{v}}{\bar{v}}100\%, \tag{2.6}$$

where $\bar{v}$ is the mean velocity. An examples of a velocity dispersion spectrum is given in Figure 2.16.

2.4.5 Comparison with conventional ultrasonic attenuation measurements

Ultrasonic attenuation measurements are reputed to be difficult to make at all frequencies, and especially at high frequencies. Moreover, few laser-ultrasonic attenuation measurements, and no high frequency laser-ultrasonic measurements existed in the literature

before this project began. Therefore, to validate the accuracy of our measurements, laser-ultrasound attenuation values were compared to those obtained using a more conventional techniques based on piezo-electric transducers (Figure 2.10).[5] The data did not immediately agree and several technical improvements were made to both techniques until they agreed with each other. However, throughout this process it was generally felt that laser-ultrasound measurements were more reliable because fewer precautions needed to be taken and fewer difficulties were found. For example, laser-ultrasound does not require careful transducer alignment, does not involve reflection and transmission coefficients between the sample and a coupling medium, is less sensitive to surface roughness, can set up more easily in the near acoustic field, does not involve measuring the attenuation of the coupling medium, and covers a much wider bandwidth in a single experiment.

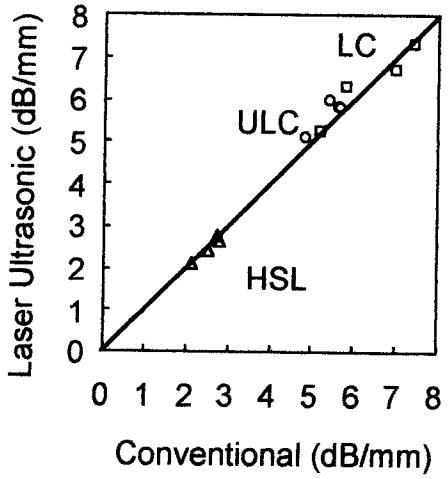

Figure 2.10 Laser-ultrasonic vs. conventional attenuation at 80 MHz in ULC, LC and HSLA steels. The samples were carefully polished parallel and to a mirror finish.

2.4.6 Surface roughness effects

As already discussed, it is desired to measure the attenuation of ultrasound pulses as they travel in the sheet thickness and are scattered by the grains. However, the ultrasound may also be scattered by surface roughness (surface finish). It was verified that typical surface roughness did not affect the attenuation measurement significantly (Figures 2.11 and 2.12).

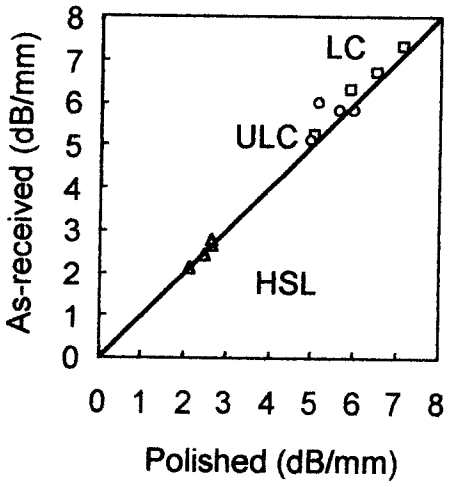

Figure 2.11 Surface roughness effect on laser-ultrasonic attenuation at 80 MHz for samples of ULC, LC, and HSLA steels in their as-received conditions vs. that obtained when the samples are carefully polished parallel and to a mirror finish.

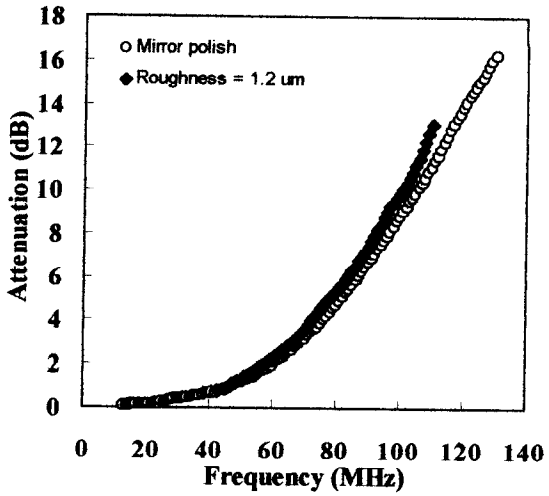

Figure 2.12 Laser-ultrasonic attenuation vs. frequency for polished and as-received steel samples. Surface roughness effects contribute only a small amount to the total attenuation, even for this least attenuating steel grade (HSLA). Sample to sample variations of surface roughness typical to production would likely be impossible to detect.

2.4.7 Effects of thickness variation

Changes in sheet thickness may also affect the measured attenuation spectra. This may occur in either of two ways: wedge effects and time averaging. If the two sample surfaces are not exactly parallel due to thickness variations, the ultrasound is reflected between the two faces of a wedge. With each successive reflection, it travels at an angle that is farther and farther away from the normal direction. Thus the plane acoustic wave is not parallel to the surface, but presents a phase shift as a function of position. If this phase shift is too large, the signal amplitude averaged over the detection area begins to cancel and the

detected signal is artificially low. This effect is modeled in detail elsewhere.[6] Applying the aforementioned model to typical thickness variations found on production material led to the conclusion that wedge effects do not affect our measurements significantly.

But sheet thickness variations did affect our measurements in a different way. To improve S/N, several signals were averaged in the time domain. If the sheet moves during the averaging process, then the signals may not exactly superimpose each other because of thickness variations. This effect is significant and increases with each successive echo, leading to errors in the measured attenuation spectra. This problem was solved by averaging the signals in the frequency domain rather than in the time domain (Figure 2.13).

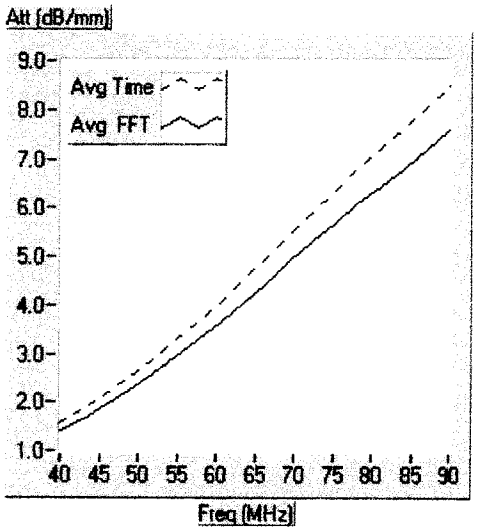

Figure 2.13 Attenuation spectra for a moving HSLA steel sample averaged in the time domain (dashed line) and in the frequency domain (solid line).
Averaging in the time domain causes an increase in the apparent attenuation because of thickness variations.

2.4.8 Oil thickness effects

Experiments were made to characterize the effect of oil thickness on ultrasonic behavior. We found that a "thin" layer does not affect the ultrasonic signal, while a "thick" layer has a large effect on the ultrasonic signal. Our measurements are consistent with the following explanation: When an ultrasonic pulse reaches the sheet's surface, part of its energy is immediately reflected into the sheet, but part of it is transmitted into the oil, where a resonance is excited. This resonance strongly affects the frequency content of the signal, and attenuation spectra can no longer be obtained reliably (Figure 2.14). The resonance frequency is too high to be observed when the oil layer is thin, but it is within the ultrasonic bandwidth when the oil layer is thick. The effect of oil on the attenuation spectra is nearly the same whether the oil is on the laser-ultrasonic detection or generation side of the sheet.

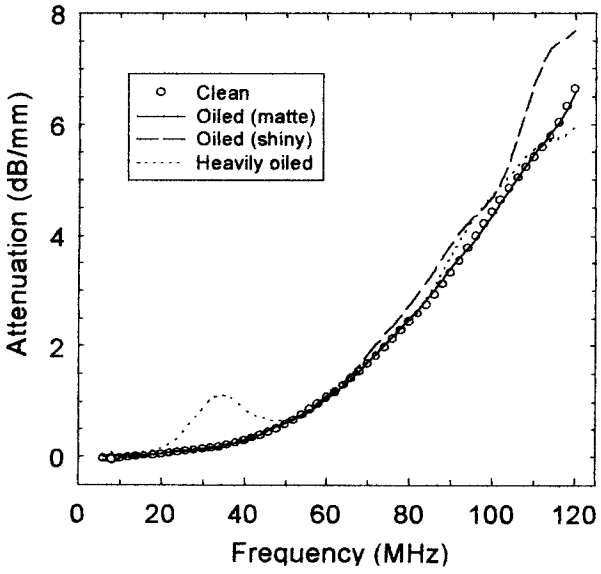

Figure 2.14 Attenuation spectrum of a HSLA steel sample for four surface conditions: clean (dots), lightly oiled with a matte surface appearance (solid line), lightly oiled with a shiny surface appearance (dashed line), and heavily oiled (dotted line).

Consequently, it is necessary to minimize the oil thickness on the coils to be inspected. A flow of compressed air at high enough pressure (about 85 psi) and flow rate was demonstrated to remove the excess oil.

2.4.9 Grain size measurements: method

The measured ultrasonic attenuation spectra were modeled in terms of ultrasound scattering by ferrite grains. Two models were adapted and expanded from the literature. The first model is based on the Born approximation, i.e. on the approximation that the ultrasound is weakly scattered by grains. In this model, a log-normal distribution of grain sizes is included. The second model is based on the Keller approximation, i.e. on the probability that the acoustic impedance (the product of the acoustic velocity and of the material's mass density) varies by a certain average amount over some average distance. No distribution of grain size can be included in this model. Grain shape and texture are included in neither models: the grains are assumed spherical or equiaxial and the texture is assumed isotropic.

Both models predict universal attenuation and velocity dispersion spectra (Figure 2.15). Here α is the attenuation, d is grain size (equivalent sphere diameter), $k = 2\pi/\lambda$ where λ is the acoustic wavelength, v is the acoustic velocity, and $\Delta v/v$ is the relative change of the acoustic velocity with respect to some calculated mean velocity (Voigt average). Therefore, αd is the attenuation per grain, and kd is a number proportional to the ratio of grain size to acoustic wavelength. For the frequency range accessible experimentally and for the current range of sample grain sizes, kd varies roughly between 0 and 4. Velocity dispersion was predicted by the model and later observed experimentally. This was an unexpected benefit to the project and provides a second estimate of grain size.

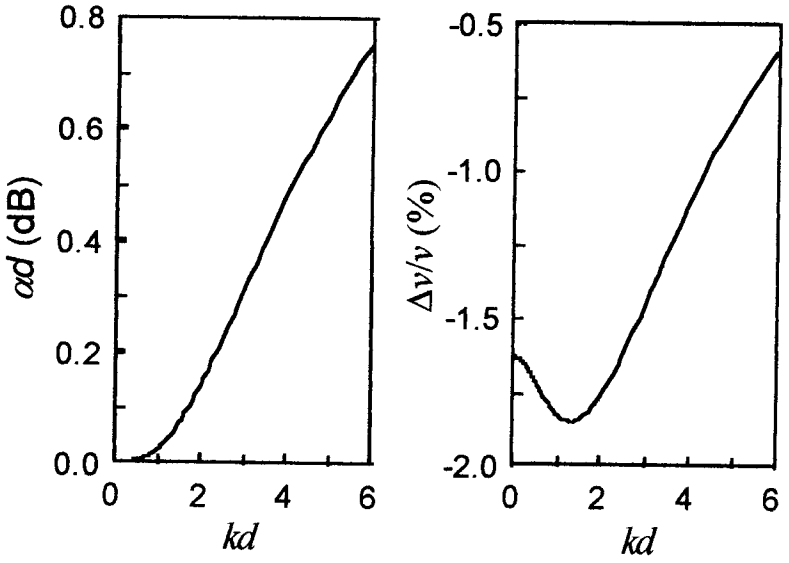

Figure 2.15 Normalized attenuation and velocity dispersion spectra predicted by the grain scattering model based on the Keller approximation.

The model attenuation and dispersion spectra were fitted to those obtained experimentally (Figure 2.16). Here, however, attenuation per unit length and relative velocity variations are plotted against acoustic frequencies to make the graphs correspond more closely to the experimental variables. The universal relationship of Figure 2.15 is not apparent anymore because of this change of axes. In general, the Keller model appears to fit the data slightly better than the Born model, and it is used systematically in our analyses. All fits of the models to the experimental data (either the attenuation or dispersion spectra) involve only two fitting parameters: d and a constant. The constant is necessary in the velocity dispersion spectrum because texture (which is not modeled) affects the average velocity. For the attenuation spectrum, the constant was introduced to verify if there was some unaccounted attenuation at low frequencies. Deviations from the model are possible because at low frequencies, other attenuation mechanisms (absorption, magnetoelastic effects) may be as important as grain scattering. But the fitted constant is nearly zero.

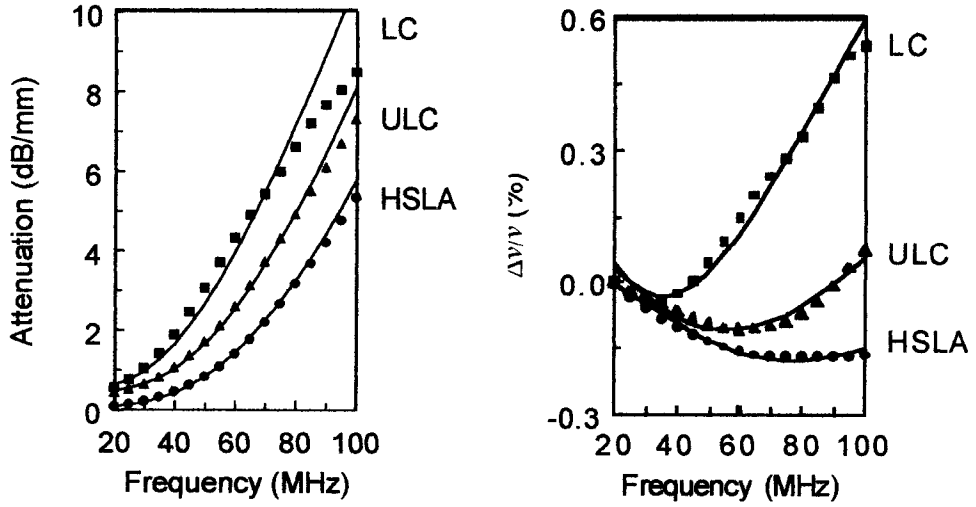

Figure 2.16 Fitted (solid lines) and experimentally measured (symbols) attenuation and velocity dispersion spectra for three steel samples of different grades.

The agreement between theory and experiment shown in Figure 2.16 is remarkable, especially given the simplifying assumptions of the model. The discrepancy observed in the attenuation spectrum near 90 MHz in LC steel is not significant. It is due to the low signal-to-noise ratio at high frequencies in this large grain and more strongly attenuating steel. Both attenuation and dispersion spectra predict grain sizes that are close to each other and close to that measured using standard metallographic practices for ULC and LC steels. However, the fitted values for HSLA steels are roughly twice as large as the measured values; no explanation for this phenomenon has been found.

2.4.10 Grain size measurements: results

The fitted grain sizes were compared to those obtained using standard metallographic practices (Figures 2.17 to 2.19). All laser-ultrasonic measurements were repeated twice; so for each sample, there is a horizontal pair of symbols on the figures. On these figures, the solid line is a linear least-squares fit to the data. For the ULC steel samples, the ultrasonic grain size is close the to metallographic grain size. The ULC grade is the closest to the ideal case of a single phase material with equiaxed polygonal grains and isotropic texture although texture was quite strong. The LC grade samples have an ultrasonic grain size close to the metallographic grain size but there is considerably more scatter in the data. This grade contained small amounts of a second phase, probably carbides, and also has a strong texture. The ultrasonic grain size of the HSLA samples was about twice the metallographic grain size. This grade was also farthest from the ideal microstructure used for the model, and contained substantial amounts of a second phase, probably pearlite, and had somewhat elongated grains.

By fitting our model to the data, we obtain an absolute grain size that has a small to large offset. But in all cases, the ultrasonic grain size is proportional the metallographic grain size. Therefore, one can correlate the two grain sizes to establish an empirical calibration. For such a correlation, the rms of the residual is a measure of the ability of laser ultrasound to estimate grain size. This rms residual is equal to 2 %, 14 % and 5 % of the mean grain size of ULC, LC, and HSLA steels, respectively.

Finally, the two ultrasonic grain sizes obtained by fitting our model to the velocity dispersion spectrum or to the attenuation spectrum correlate with each other to within the measurement repeatability. But they tend to differ by a small and systematic amount.

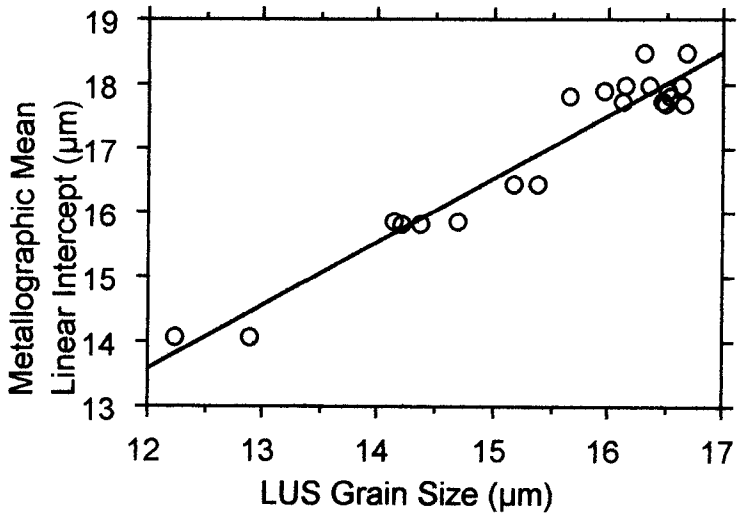

Figure 2.17 Metallographic vs. laser-ultrasonic attenuation measurements of grain size (mean linear intercept) for ULC production steel samples.
The rms residual of the correlation is 0.35 μm (±2 %).

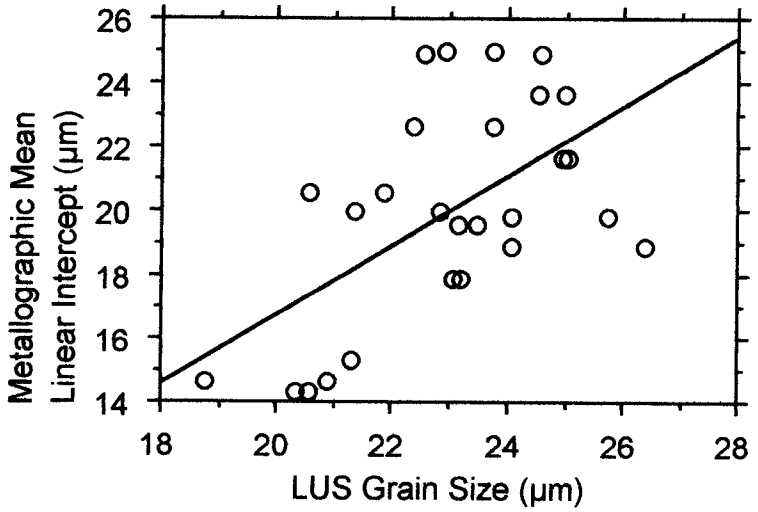

Figure 2.18 Metallographic vs. laser-ultrasonic measurements of grain size (mean linear intercept) for LC production steel samples.
The rms residual of the correlation is 2.9 μm (±14 %).

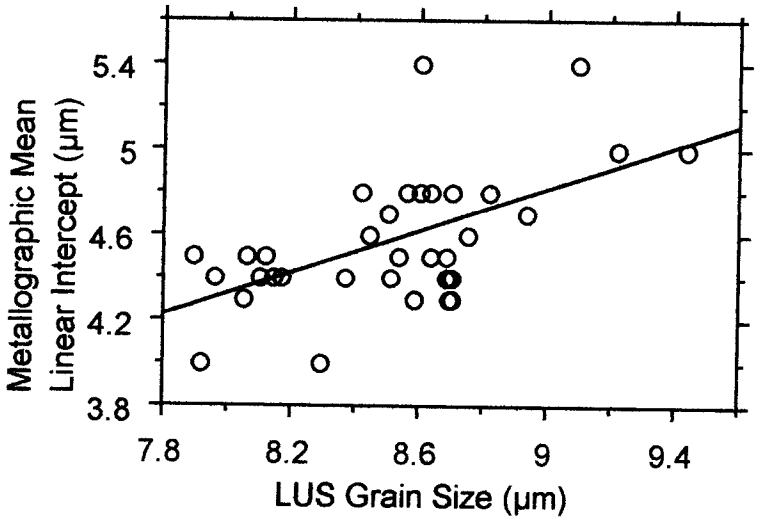

Figure 2.19 Metallographic vs. laser-ultrasonic measurements of grain size (mean linear intercept) for laboratory prepared HSLA steel samples.
The rms residual of the correlation is 0.25 μm (±5 %).

2.5 Measuring ultrasound velocity, texture, and thickness using laser-ultrasound spectroscopy

2.5.1 Ultrasound velocity

In the previous section it was shown how velocity dispersion spectra were obtained. Although this technique can accurately measure small velocity variations with frequency, it cannot measure the absolute value of the velocity because the phase is known only to within an additive constant of $2n\pi$, where n is an unknown integer. So an independent and absolute estimate of the time delay between two echoes is required. This estimate is obtained by calculating the crosscorrelation of the first two acoustic echoes. The maximum of the crosscorrelation yields the time delay between the two echoes (averaged over all frequencies). Dividing twice the thickness by this time delay yields the absolute value of the sound velocity.

2.5.2 Laser-ultrasound resonance spectroscopy (LURS)

Laser-ultrasound generates both longitudinal and shear acoustic waves. A shear acoustic wave signal is routinely observed after several acoustic round trips in the thickness of the sheet (Figure 2.2). However, the shear acoustic wave does not have sharp and easily identifiable features, and the two shear waves with orthogonal polarizations cannot be separated. Consequently, instead of attempting to measure the shear wave velocity in the time domain, as for the longitudinal wave velocity, it was decided to work in the frequency domain.

Figure 2.20 shows the first 20 μs of the acoustic signal obtained in a HSLA sample. Approximately 60 echoes can be seen. The signal envelope shows the decay of the ultrasonic wave caused by scattering, diffraction, and absorption.

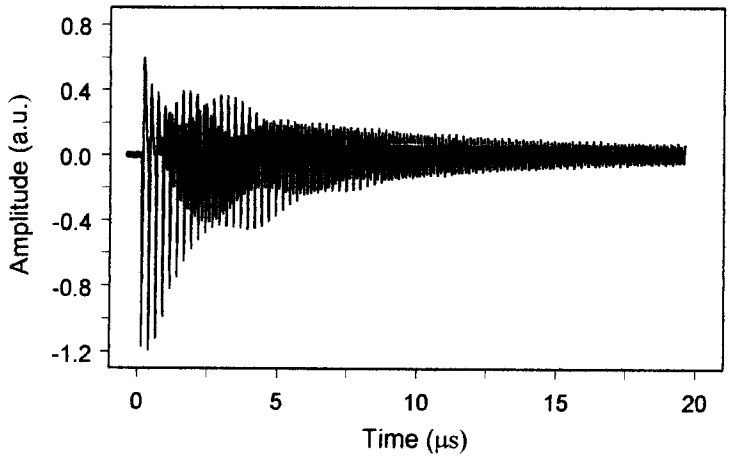

Figure 2.20 Example of time signal comprising roughly 60 of echoes.

To analyze the signal and extract information about the shear waves, the signal is windowed and Fourier transformed (Figure 2.21). An optimal window, such as the Blackman-Harris window, is used to minimize leakage while keeping good frequency resolution.[7] The observed resonance peaks in Figure 2.21 are harmonics of the longitudinal wave and of the two shear waves which are polarized in orthogonal directions in the plane of the sheet. The longitudinal resonances are identified as 1L, 2L, and 3L and shear wave resonances are identified as 1S, 2S, 3S, and 6S.

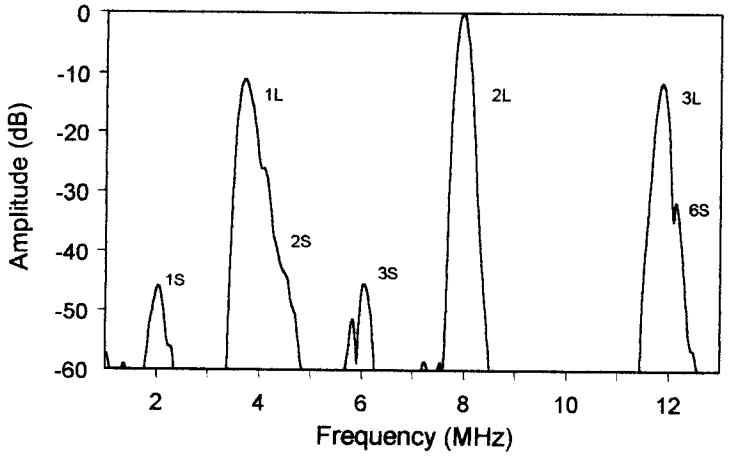

Figure 2.21 Amplitude spectrum corresponding to time signal of Figure 2.20.

Using this *laser-ultrasound resonance spectroscopy* (LURS) technique, the center frequency of the various resonances are measured very accurately. In the case illustrated here, the second harmonic, 2L, is selected for the longitudinal wave while for the two shear

waves, the 3S harmonics are selected because they are more easily separated than lower order harmonics. The best choice of harmonics depends on material properties as well as sheet thickness. As seen in Figure 2.21, however, the signal amplitude for shear harmonics is usually 40 dB lower than that for the longitudinal resonances. Therefore a signal-to-noise ratio of the order of 500 or higher is required. The system employed had a signal-to-noise ratio of more than 50 dB for single shot experiments in a 15 MHz bandwidth. Typically, 20 to 50 signals are averaged together to further improve the S/N.

Once the resonances have been identified and the center frequency normalized to the first harmonic, f_L, f_{S1}, and f_{S2}, are measured, the sample thickness, h, and the two texture coefficients, W_{400} and W_{420}, may be calculated using the following equations:

$$h = \sqrt{\frac{\lambda_M + 4\mu_M}{4\rho(f_L^2 + f_{S1}^2 + f_{S2}^2)}}$$

$$W_{400} = \frac{35\sqrt{2}\left[4\rho h^2 f_L^2 - (\lambda_M + 2\mu_M)\right]}{64\pi^2 c_M} \tag{2.7}$$

$$W_{420} = \frac{56\sqrt{5}\rho h^2 (f_{S1}^2 - f_{S2}^2)}{64\pi^2 c_M}$$

where ρ is the density of the metal sheet, and λ_M, μ_M , and c_M are the two average Lamé elastic constants and the average anisotropy factor (using either the Voigt, Reuss or Hill averaging procedure), respectively, of an ideal metal sheet having an isotropic crystallographic orientation distribution.[8]

2.5.3 Comparison with conventional ultrasonic measurements

Ultrasonics is well-established as a means to measure texture coefficients of order up to four for polycrystalline aggregates of cubic and hexagonal metals. Therefore, to show that texture can be measured using Equations 2.7, it is sufficient to show that the inverse of the harmonic resonance frequency divided by the order of the harmonic is the same as the ultrasonic round trip time delay measured using other ultrasonic transducers. Here the comparison was made with commercial piezoelectric transducers. The two techniques agreed to within 0.5% (rms residual) for 79 samples of low carbon steel having round trip time delays ranging from 200 to 800 ns (Figure 2.22).

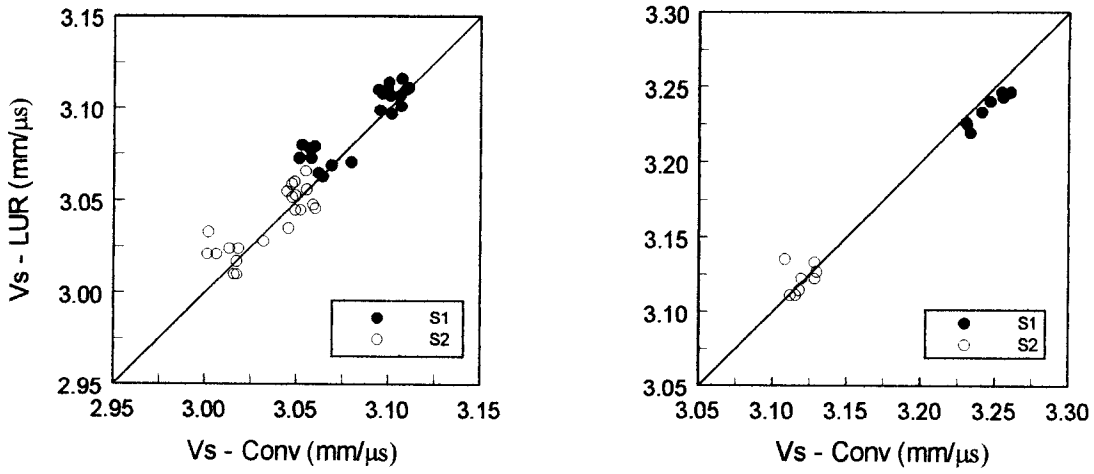

Figure 2.22 Comparison between laser-ultrasonic (vertical axis) and conventional ultrasonic (horizontal axis) measurements of the two shear velocities (black and white circles) for ULC (left) and HSLA (right) steel samples.

The spectroscopic data were also used to estimate the two texture coefficients W_{400} and W_{420}. These are compared to the values we obtained using conventional ultrasonics in Figure 2.23. Except for a systematic shift in the estimated absolute values, the agreement between both measurements is excellent.

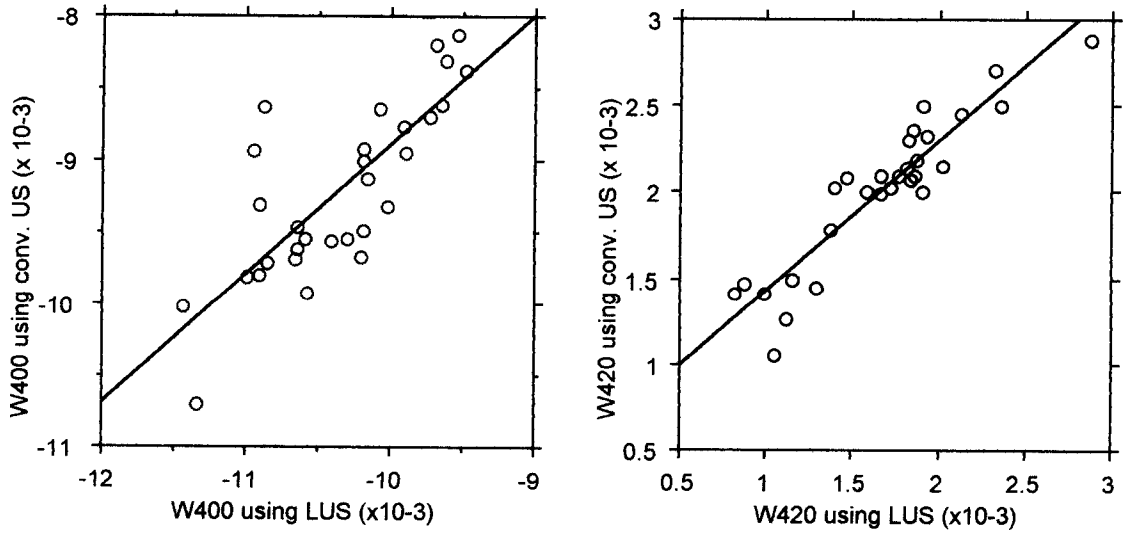

Figure 2.23 The W_{400} and absolute value of the W_{420} texture coefficients, as measured using conventional ultrasonics vs. that measured using laser-ultrasound resonance spectroscopy.

2.5.4 Thickness

Although thickness measurements were not a project objective, they are required to measure attenuation and velocities accurately. Moreover, one objective of the project was to have a sensor capable of operating independently of all external information with the

exception of chemistry grade. Finally, even if a thickness gauge were available, it is not certain it could provide thickness measurements with the required accuracy of the order of 0.1%.

Ultrasonic time-of-flight (TOF) measurements are often used to measure thickness, and several hand-held ultrasonic thickness gauges are commercially available. However, texture variations caused by common processing methods can significantly affect the ultrasonic velocity and consequently, affect the accuracy of the thickness measurement. In LURS, the texture coefficients that affect the velocity of the three acoustic modes propagating in the thickness direction are measured and the thickness calculated according to Equations 2.7 is corrected for texture variations.

This is illustrated in Figure 2.24. TOF and LURS measurements were made in three sets of roughly 30 samples each of ultra low carbon (ULC), low carbon (LC) and high-strength low-alloy (HSLA) steels sheets of 0.7 to 1.2 mm thickness. ULC carbon steels are used for deep drawing and are highly textured, with their {111} planes in the plane of the sheet. LC steels are also strongly textured, but less so than ULC steels. HSLA steels are weakly textured. In Figure 2.24a, the sample thickness as measured using a micrometer, is compared to the round trip TOF of the longitudinal wave as measured using conventional piezoelectric transducers. The solid line is a linear least squares fit with the intercept set to zero. Twice the slope of the graph is the mean ultrasonic velocity for all samples and it is equal to 6112 m/s. Clearly, the ULC and LC samples lie above the line and have higher ultrasonic velocity than the HSLA samples. This is not surprising because the ultrasonic velocity is highest (6426 m/s) in the <111> directions of the ferrite single crystal and lowest (5442 m/s) in the <100> directions (this may be calculated by substituting the single crystal elastic constants of ferrite[9] in the slowness curve equations of cubic materials[10]), and ULC and LC steels have strong {111} textures. If this mean velocity is utilized to measure sample thickness, then the measurement error (rms residual) is equal to ±22 μm. In Figure 2.24b, sample thickness for the same sample set is plotted against the LURS estimate. The measurement error is reduced to only ±5 μm and shows no systematic deviation for the various textures. In fact, this error is entirely due to the thickness measurement error using the micrometer. Unfortunately, the thickness and LURS measurements were not taken at the same locations. So the ±5 μm measurement error is attributed entirely to these thickness variations.

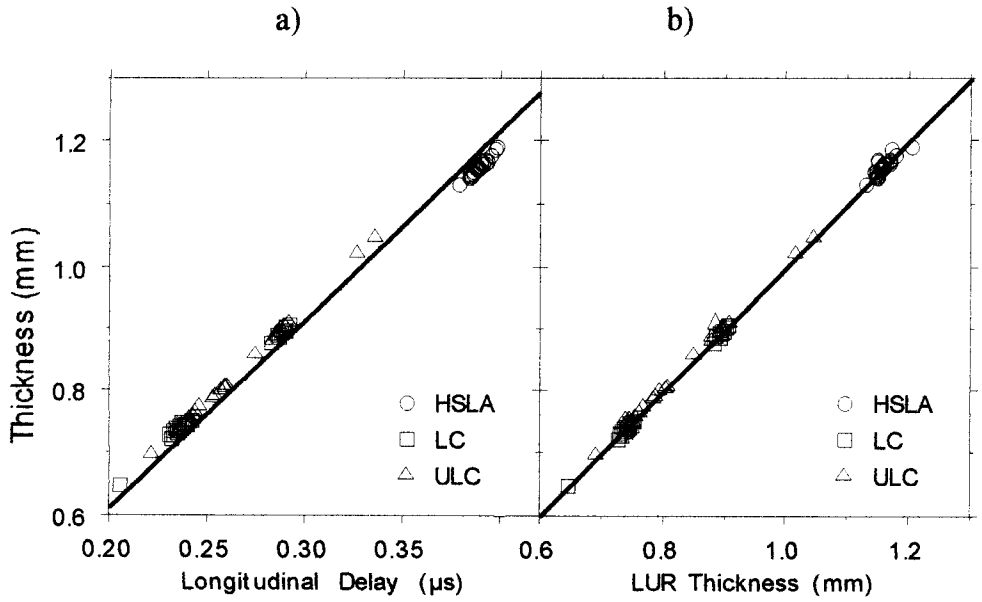

Figure 2.24 Sample thickness measured using a micrometer as a function of a) the round trip TOF of the longitudinal wave and b) the estimated thickness from LUR.
The solid lines are linear least squares fits with the intercepts forced to zero.

2.5.5 Sheet crowning

The measurement of sheet crowning was also made to further test the accuracy of the LURS thickness measurement. If the thickness of a single sheet is measured across its width using the LURS technique and careful micrometer measurements at the same locations (Figure 2.25), then it is seen that the LURS technique can measure thickness with an accuracy better than ±1 μm (rms difference between the two measurements), and sub-micron repeatability. This represents roughly a 0.1% measurement accuracy.

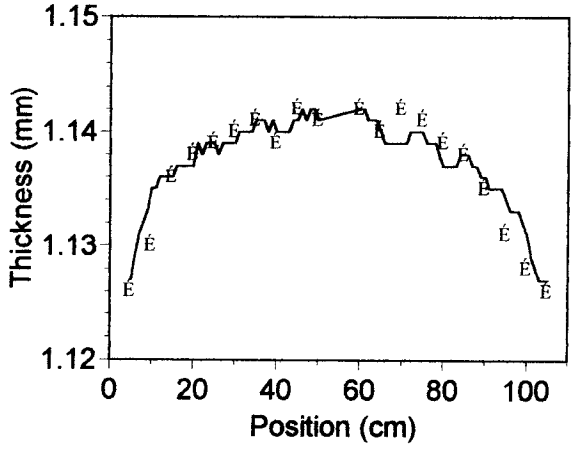

Figure 2.25 Crowning of a HSLA steel sheet
measured using LURS (solid line) and a micrometer (É symbols).

2.6 Measuring ultrasonic absorption and temper reduction (skin pass)

2.6.1 Introduction

Ultrasound absorption is the conversion of ultrasound energy into heat. This conversion is mainly due to two mechanisms that vary with the dislocation density: magnetoelastic effects and dissipative dislocation motion. Absorption is thus expected to provide a measure of the dislocation density and should reveal information useful to predict mechanical properties like the yield strength.

2.6.2 Measurements on small samples

Absorption measurements on small samples using the reverberation technique[11,12] were previously reported.[13] In this technique, a laser pulse is used to generate ultrasound that is scattered into the sample. After some time, due to the finite volume of the sample, the latter is filled with incoherent ultrasound that is sometimes termed « acoustic noise ». The measured decrease of the ultrasound amplitude in time is attributed to absorption and is called the « ultrasound absorption coefficient ». Examples of the dependence of ultrasonic absorption coefficient as a function of frequency is shown in Figure 2.26 for samples of three steel grades.

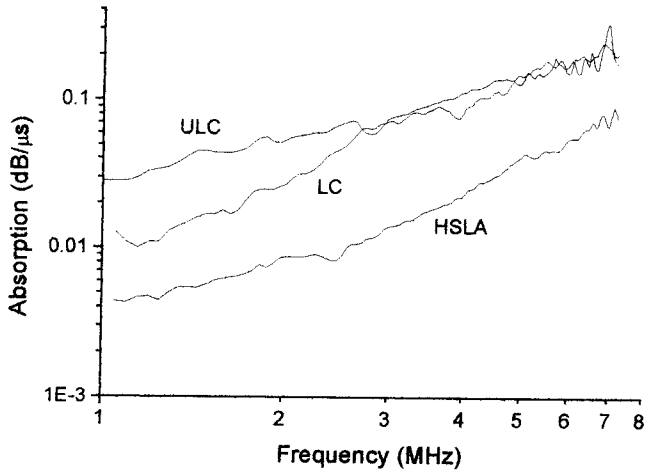

Figure 2.26 Ultrasonic absorption for typical samples of three steel grades between 1 and 7 MHz.

These measurements on small samples showed that, in the 1 to 7 MHz range, absorption varies almost linearly with frequency. It was also shown that absorption is dominated by magnetoelastic effects.[14] As reported in the literature,[15] it was expected that the absorption measurement would be a measurement of plastic deformation and consequently, be representative of some microstructural parameters related to dislocations. Consequently, we measured the ultrasonic absorption as a function of temper reduction (skin pass) for ULC samples with temper reduction varying from 0 to 3% (Figure 2.27).

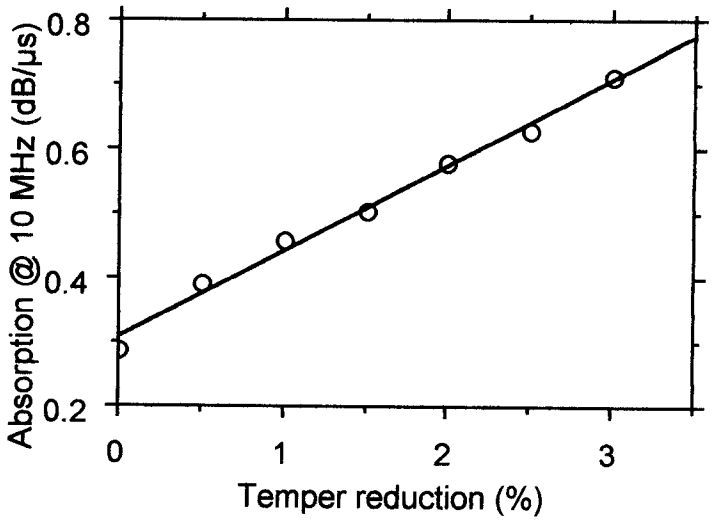

Figure 2.27 Ultrasonic absorption as a function of temper reduction (skin pass) for ULC steel samples taken from a single coil.

It was also found that ultrasound absorption combined with other ultrasonic measurements (grain size, texture) can be used to improve the prediction of the yield strength of ULC and LC samples from the production line (See Section 4.3.2).

2.6.3 Measurements on large sheets

The experimental configuration is depicted in Figure 2.28. A short laser pulse impinging on the sample surface generates an ultrasonic wave packet that bounces between the two faces of the steel sheet. This wave packet is scattered by the discontinuities it encounters at the boundaries of the metallic grains and loses its spatial coherence after a few microseconds. This gives rise to an ultrasonic energy cloud within which different area of the sample vibrate incoherently. Initially, this energy is localized near the generation point and then spreads in the sheet. The evolution of the ultrasonic field is monitored by measuring the surface motion from the opposite face at a point aligned with the generation. A typical measurement of surface motion is shown in Figure 2.29.

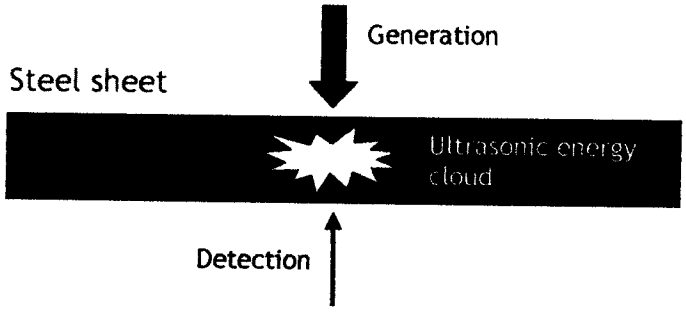

Figure 2.28 Experimental configuration to measure the absorption coefficient on large steel sheets.

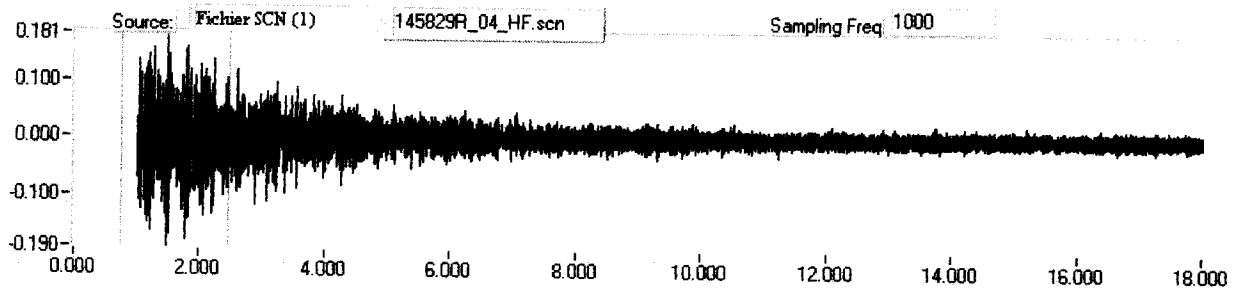

Figure 2.29 Incoherent ultrasonic signal measured on the surface of an ULC sheet. The x axis represents the time in microseconds and the y axis represents the surface displacement in arbitrary units. The generation pulse occurs at 0 μs and detection begins at 1 μs when the ultrasound field is in the diffusion regime.

Figure 2.29 shows that the surface motion is incoherent and that its amplitude decreases with time. This decrease is caused by two phenomena :

- diffusion: the energy cloud spreads in the sample following a two-dimensional diffusion process for thin steel sheets (1 mm thick);
- absorption: the ultrasound energy is absorbed by the material through magnetoelastic effects and dislocation motion.

These two contributions can be combined in a differential equation to describe the evolution of the ultrasonic field. The initial conditions of the problem are not easily defined since the initial appearance of the energy cloud is a complicated process. Fortunately, two limiting cases lead to very simple expressions for the evolution of the Fourier component U_f of the surface displacement at an ultrasonic frequency f as a function of time t.

In the first case the diffusion occurs rapidly. Consequently both diffusion and absorption are important and

$$U_f = A \exp(-\alpha t)/t^{0.5}, \tag{2.8}$$

where A is a constant and α is the absorption coefficient. A fast diffusion can be associated with a very localized initial energy cloud and/or a material showing very low ultrasound scattering, the phenomena underlying the diffusion process being the same as those responsible for the ultrasound scattering.

In the second case the diffusion occurs slowly enough to be neglected. The ultrasonic field decreases mainly due to absorption leading to :

$$U_f = A \exp(-\alpha t). \tag{2.9}$$

A slow diffusion is associated with an initial energy cloud showing a flat distribution near the detection point and/or a material that strongly scatters ultrasound.

These equations are used to fit the experimental data and evaluate the absorption coefficient α. The diffusion regime is influenced by the dimensions of the generation area,

the capability of the material to scatter ultrasound, and the ultrasonic frequency range of interest. In our measurements, we choose the equation that provides the best fit to the experimental data. But often, this choice is not obvious. Consequently, in some cases, the choice is based on the comparison of the absorption coefficients with those obtained on small samples using the reverberation technique.

The upper part of Figure 2.30 shows a typical spectrogram obtained from one hundred experimental measurements like the one shown in Figure 2.29. The sample was continuously rotated so that the measurements were taken on a circle of about 5 cm radius around the center of a 30 cm x 30 cm sample of 1 mm thickness. This spectrogram describes the time evolution of the Fourier components of the surface motion. The x-axis represents time from 0 to 20 μs (the ultrasonic generation occurred at –1 μs; the time scale is translated from that of Figure 2.29), the y-axis represents frequency from 50 to 113 MHz, and the color (gray scale) represents the amplitude of the Fourier components in dB. The lower part of Figure 2.30 shows the evolution of the 70 MHz Fourier component (in dB) with time (in μs). Depending upon the experimental configuration, Equation 2.8 or Equation 2.9 is used to fit the experimental data and extract the absorption coefficient. Typical values of the absorption coefficient as a function of frequency are shown in Figure 2.31 for an ULC sample. The figure shows that the absorption coefficient varies almost linearly with frequency.

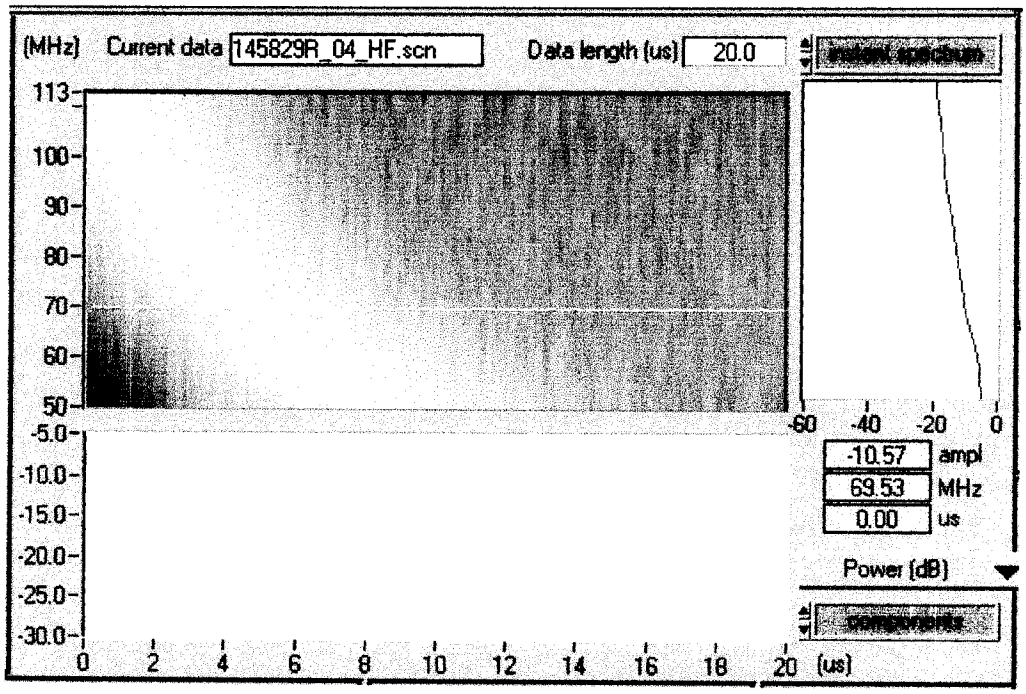

Figure 2.30 Top left : Joint time-frequency spectrogram showing the acoustic power (in dB, color coded z axis) as functions of Fourier components (in MHz, y axis) and time (in μs, x axis). Bottom left : Time dependence of the 70 MHz Fourier component in dB. Top right : Power spectrum in dB at time zero. Average of 100 measurements on an ULC sample.

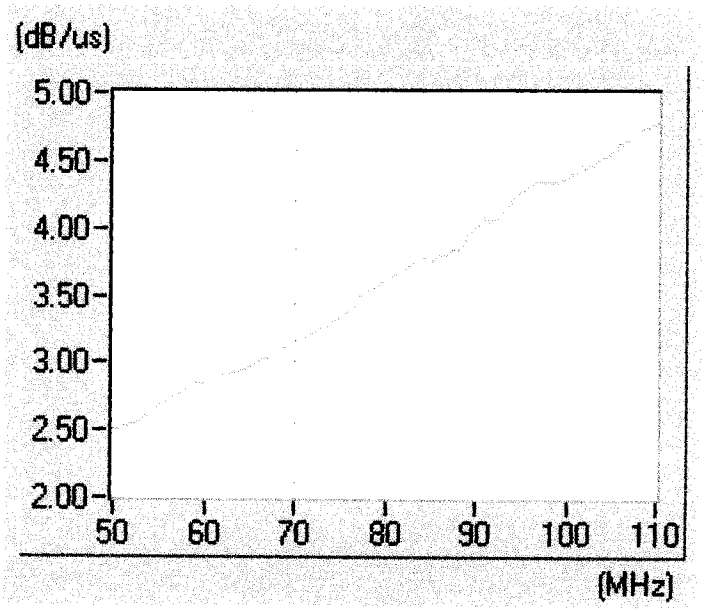

Figure 2.31 Ultrasound absorption coefficient (in dB/μs) dependence on frequency (in MHz) for an ULC sample of 1 mm thickness.

2.6.4 Validation of the technique

The absorption measurement technique on large sheets was validated in two ways:

1) The absorption coefficient was compared to the one obtained for small samples using the reverberation technique.

2) The absorption coefficient was correlated with the degree of temper reduction.

A first test to validate the large-sample technique is to compare the measured absorption coefficients to those obtained with the reverberation technique for small samples. Figure 2.32 presents the correlation between the absorption coefficients at 30 MHz measured on 29 large ULC samples (30 cm x 30 cm x 1 mm thick) and those measured on small samples (8 mm x 8 mm x 1 mm thick). Three adjacent small samples were extracted from each large sample and the average of the three measurements is plotted along the x axis. The samples were provided by one of the sponsoring companies.

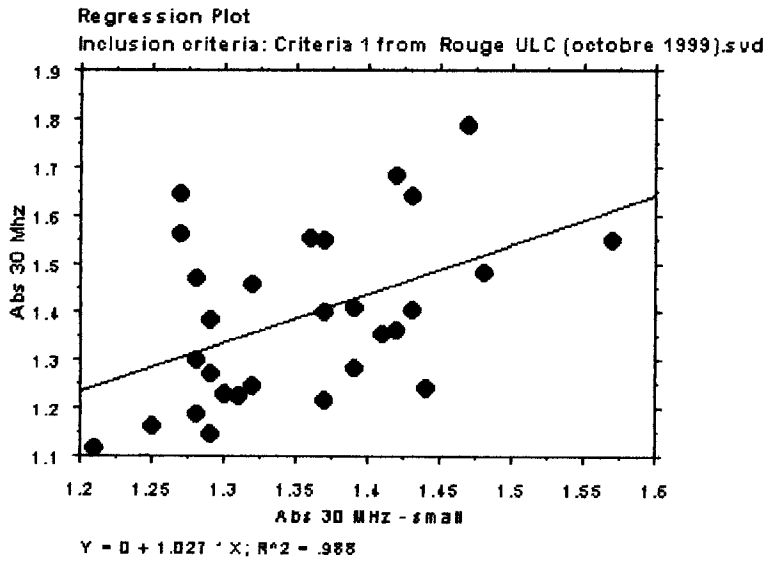

Figure 2.32 Absorption coefficients measured at 30 MHz for 29 large samples (y-axis) as compared to the coefficient obtained on small samples (x-axis) using the reverberation technique. The axes' units are dB/μs. The RMS residual is 0.16 dB/μs. The intercept value was forced to zero.

A first observation on Figure 2.32 is that the slope of the correlation is 1.025, i.e. almost exactly 1, which indicates that the two techniques show negligible systematic error with respect to each other. A second observation is that, despite the spread in the data, there is a definite correlation between the absorption coefficients. A good part of the RMS residual of ±0.16 dB/μs can be attributed to the experimental error estimated for the absorption coefficient of large samples. From measurements performed at 80 MHz, the measurement repeatability was estimated to 7.5 % which would correspond to approximately ±0.11 dB/μs for the 30 MHz absorption coefficient. For the small samples, the experimental error is estimated to be half. Another possible source of scatter in the data is related to the fact that the measurements on large samples were averaged over a larger area than the area of the small samples. Consequently, if there are inhomogeneities in the original steel sheet (and these have been found on occasion), different values of the absorption coefficients will be obtained depending upon where the small samples were extracted, or an unusual absorption value may affect the mean value of the averaged measurement.

As for the small samples, the absorption coefficient measured on large sheet is expected to be a good indicator of temper reduction and provide some information about dislocations. Figure 2.33 presents the absorption measured at 35 MHz for large ULC and HSLA samples taken from the same sheet and having received carefully applied amounts of temper reduction in the range of 0 to 3%. The strong relationship indicates that the absorption measurements on steel sheets are sufficiently accurate to provide a good measurement of temper reduction.

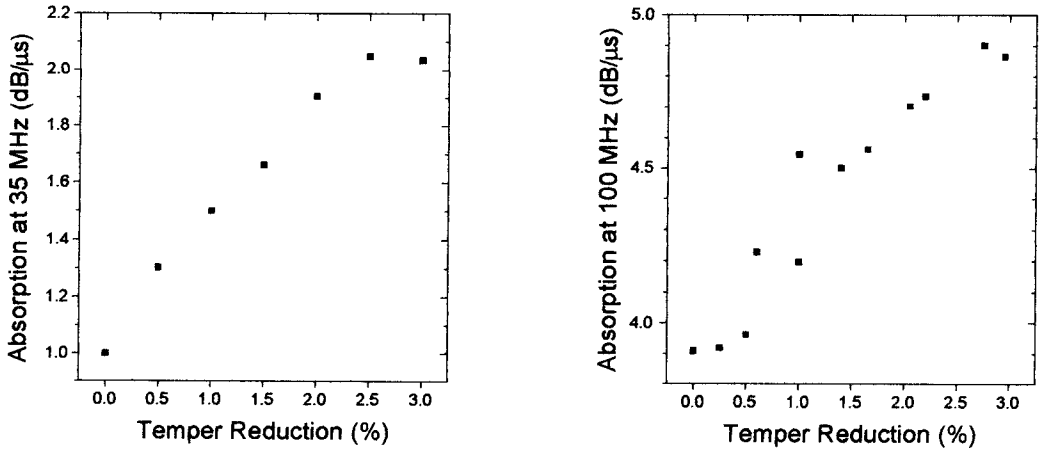

Figure 2.33 Absorption as a function of the temper reduction.
Left: Absorption at 35 MHz for ULC samples. **Right:** Absorption at 100 MHz for HSLA samples.

2.7 Other measurements in an attempt to measure temper reduction (skin pass)

2.7.1 Magnetoelasticity

To quantify the magnetoelastic effect, laser-ultrasonic measurements were repeated twice: once in the presence of a strong magnetic field, and once after demagnetizing the sample. It is expected that the magnetoelastic effect, i.e. the change in ultrasonic attenuation or in ultrasonic velocity caused by a magnetic field, should be sensitive to dislocation density and hence to temper reduction. The observed sample to sample variations, however, were of the same order of magnitude as the precision of the laser-ultrasonic measurements. But it was possible to measure differences between grades.

One way to improve measurement accuracy is to average a large number of measurements. Instead of remeasuring each sample several times, all 30 samples for a single steel grade were averaged together. This resulted in remarkable measurement accuracy: changes in ultrasonic attenuation of up to 1% and changes in ultrasonic velocity of up to 0.1% were easily measured as a function of frequency, as shown in Figure 2.34.

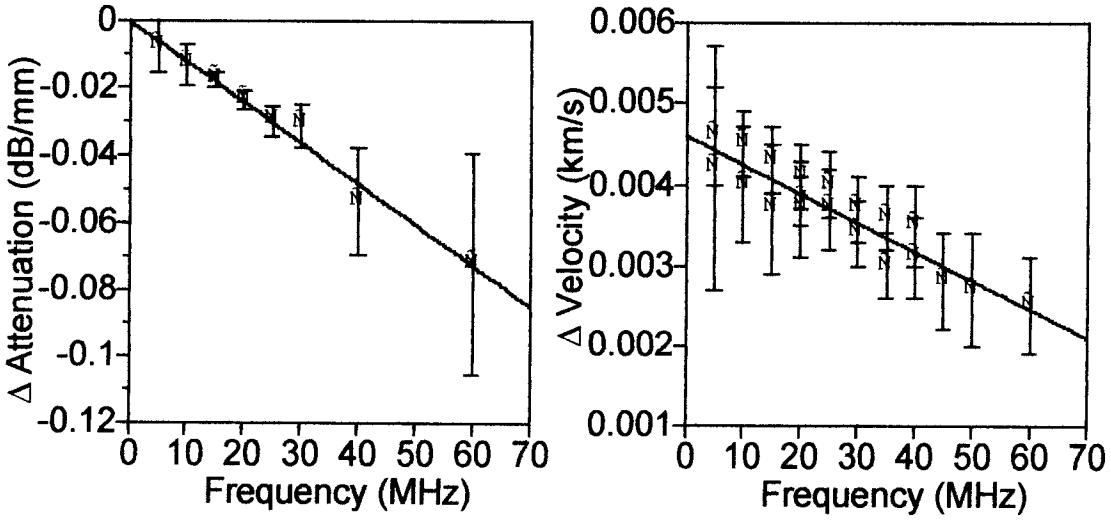

Figure 2.34 Average change in ultrasonic attenuation and velocity caused by the application of a strong magnetic field for 30 LC steel samples.

Variations in ultrasonic attenuation and velocity caused by the magnetic field were found to depend linearly on frequency. Variations over a frequency bandwidth of 40 MHz are summarized in Table 2.1. A smaller dependence of the magnetoelastic effect with frequency was observed in HSLA steel. This is as expected because the magnetoelastic effect is known to be larger in steels with lower carbon concentration.

Table 2.1 Variations in ultrasonic attenuation and velocity caused by a strong magnetic field. The signs indicate whether the magnetic field increases or decreases the quantity.

	Δ attenuation @ 40 MHz (dB/mm)	Δ velocity @ 0 MHz (m/s)	Δ velocity @ 40 MHz (m/s)
ULC	-0.050	+5.6	+4.2
LC	-0.048	+4.6	+3.2
HSLA	-0.027	+5.5	+5.3

2.7.2 Low frequency attenuation measurements

In April 1997, one of the sponsoring companies manufactured a set of ULC steel samples with carefully controlled amounts of temper reduction. The reductions were between 0.0% and 3.0% in steps of 0.5% and two samples were made for each value of reduction. The actual amounts of reduction, as measured from sample elongation, were within 0.1% of the intended values in all but one case. Ultrasonic measurements were performed on these samples using the laser-ultrasonic prototype installed at IMI to study the influence of temper reduction on ultrasonic velocity and attenuation, and to correlate these effects with yield strength variations caused by temper reduction.

Laser-ultrasonic thickness measurements were made to confirm that the amount of elongation corresponds to an equivalent reduction in thickness, and to evaluate once more, the precision of the thickness measurement. Figure 2.35 presents the thickness measured using laser-ultrasound vs. target temper reduction. For each intended reduction, two samples were made, and four ultrasonic measurements per samples were made. The slope of the graph is 0.94 ± 0.02 which indicates that the laser-ultrasonically measured reduction in thickness is 6% less than the target amount. The rms residual of the plot is 1.8 μm, which indicates that according to our ultrasonic thickness measurements, the achieved sample to sample manufacturing reproducibility was better than ± 0.2%. Using an analysis of variance, it was also determined that the laser-ultrasonic measurement repeatability on any sample was better than ± 0.3 μm. This analysis clearly demonstrates the ability of laser-ultrasonics to measure slight changes in thickness produced by temper reduction, and it also demonstrates the high level of precision and care used by one of the sponsoring companies in manufacturing the sample set.

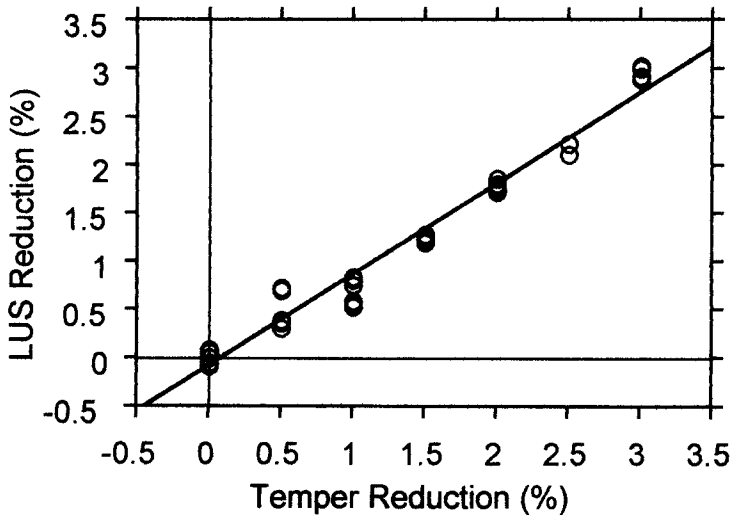

Figure 2.35 Laser-ultrasonic estimates of temper reduction based on thickness measurements vs. intended reduction for 14 ULC temper rolled samples.

The measured ultrasonic attenuation at 15 MHz and 40 MHz vs. reduction are presented in Figures 2.36 and 2.37, respectively. While the ultrasonic attenuation at 15 MHz increases by 50% between 0.0 and 3.0% reduction, the attenuation at 40 MHz and higher frequencies decreases. The decrease is especially large at 40 MHz. This measurement is unexpected because if temper reduction affects the material by introducing dislocations, then ultrasonic attenuation should increase with temper reduction at all frequencies. However, it is well known that large amounts of cold reduction can have a large effect on grain size and texture. Consequently, small amounts of cold reduction should also have some effect on texture and grain size, although such effect may be too small to be measurable and explain our data. These phenomena hint that attenuation measurements at two different frequencies may be used to measure two different microstructural parameters: dislocations and grain size.

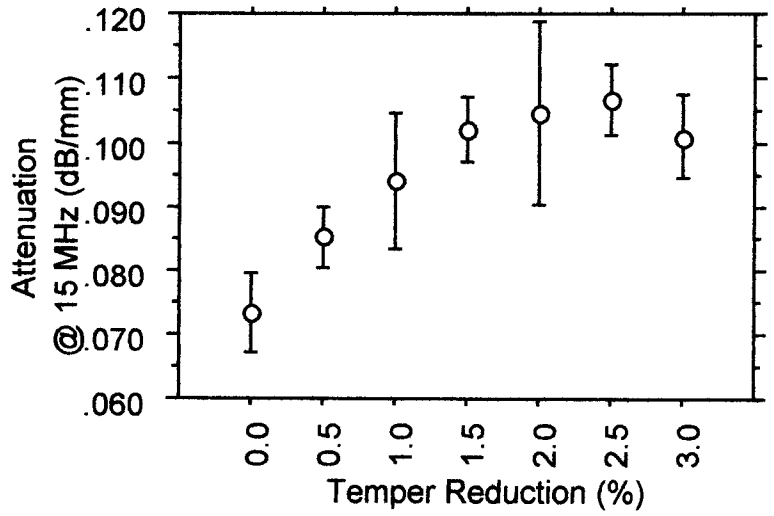

Figure 2.36 Ultrasonic attenuation at 15 MHz vs. reduction for ULC temper rolled samples. The error bars are equal to one standard deviation on a single measurement.

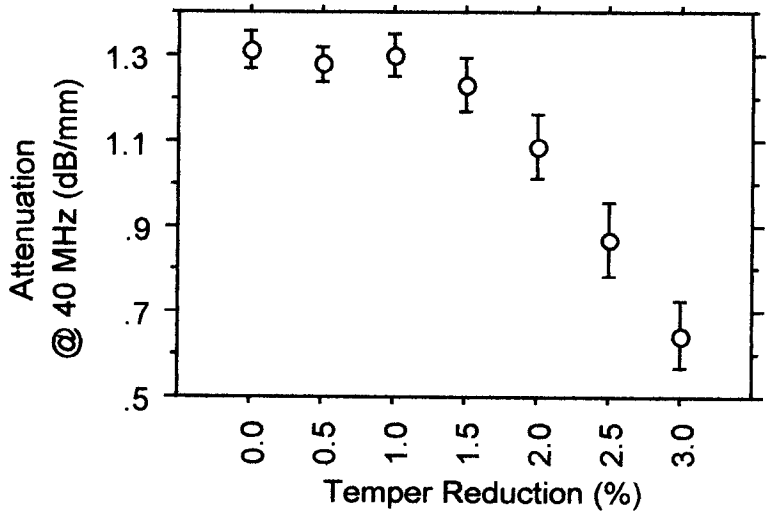

Figure 2.37 Ultrasonic attenuation at 40 MHz vs. reduction for ULC temper rolled samples. The error bars are equal to one standard deviation on a single measurement.

Our simple ultrasonic scattering model was applied to estimate what would be the reduction in grain size that could explain the drop in attenuation shown in Figure 2.37. If dislocations and texture effects are ignored, Figure 2.38 shows that the model predicts a reduction in grain size from 16.7 μm to 15 μm (i.e. 11%), as temper reduction increases from 0 to 3%. It was difficult for metallurgists to believe that a 3% cold reduction could reduce grain size this much. Consequently, these data likely indicate that grain size and dislocations affect the two acoustic spectra simultaneously.

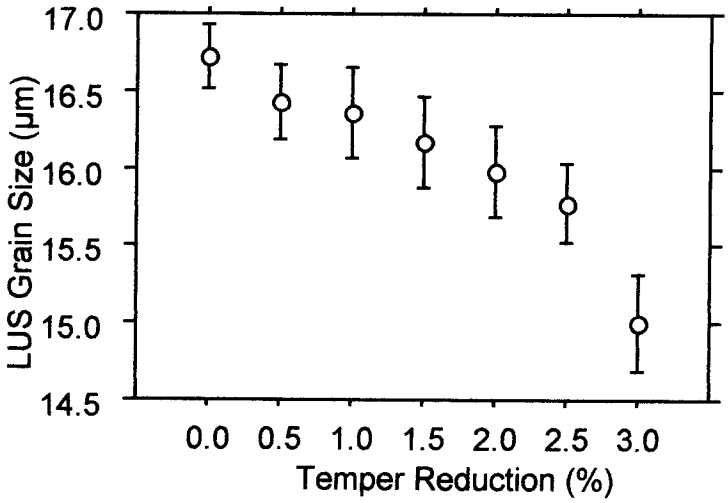

Figure 2.38 Grain size estimated from fitting the scattering model to the attenuation spectrum for ULC temper rolled samples.
The error bars are equal to one standard deviation on a single measurement.

Figure 2.39 presents the yield strength (YS) measured by one of the sponsoring companies vs. the YS estimated from a multiple linear regression using attenuation at 15 MHz and the ultrasonic grain size obtained from the scattering model. The rms residual is 0.7 ksi, which is approximately the error of the tensile test. Excellent correlations are also observed between the same two ultrasonic parameters and the total elongation, the uniform elongation, and the strain hardening exponent. If only the 15 MHz ultrasonic attenuation, which is expected to be an estimator of dislocation density, or only the ultrasonic estimate of grain size is used, then the correlations are not nearly as good. In conclusion, low and high frequency attenuation measurements appear to be sensitive to dislocations and to grain size at different levels. Combining these two parameters empirically allows to build an empirical model to estimate the YS of ULC steel samples. However, when low frequency ultrasonic attenuation was measured on regular production material, it did not improve YS measurement accuracy nearly as well as in Figure 2.39. Possible reasons are diffraction corrections that need to be carefully made at low frequencies, lack of resolution in the Fourier analysis, and thickness variation effects. This avenue was abandoned but it should be revisited because improvements to the prototype have been made since these measurements were last taken.

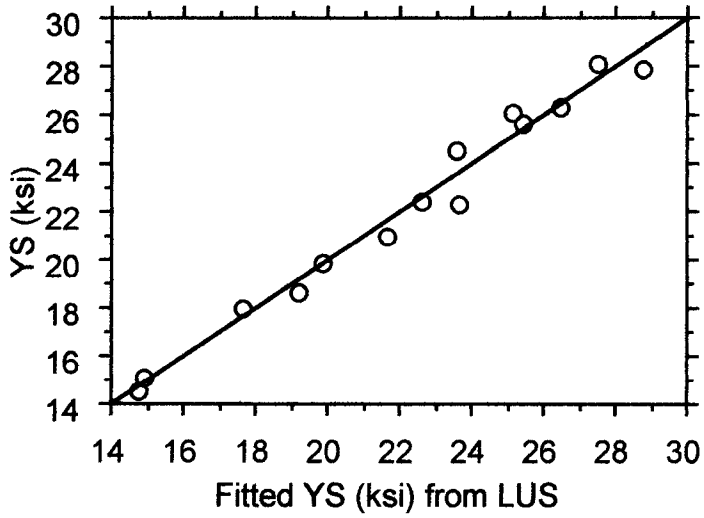

Figure 2.39 Measured yield strength vs. yield strength estimated from a multiple linear regression using attenuation at 15 MHz and grain size estimated using the scattering model.
The rms residual of the linear least squares fit is 0.7 ksi.

3 PROTOTYPE FOR ONLINE MEASUREMENTS

3.1 Overview

The system described here was installed at LTV's #1 inspection line in Cleveland (Figure 3.1). The generation laser was installed on a platform above the line. Typically, we employ 100 to 200 mJ of 248 nm radiation pulse lasting from 3 to 6 ns fwhm and focused on an area about 5 mm in diameter. This high power laser beam was steered with mirrors down to a horizontal rail installed above the line. The beam traveled along the rail up to a movable *generation head* which reflected and weakly focused the beam onto the sheet surface to generate the ultrasound.

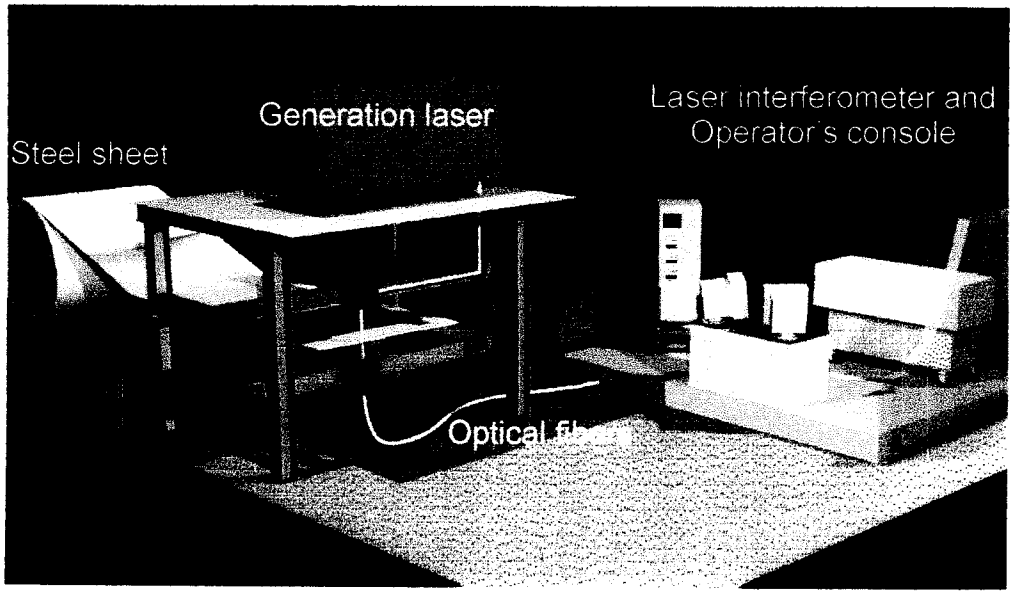

Figure 3.1 Schematic diagram of the laser-ultrasonic sensor installed at LTV Steel Company.

The detection laser and interferometer were located remotely from the line. As described earlier in Section 2.2 (Detecting high frequency ultrasound), the detection laser was a long pulse, 3 kW peak power, Nd:YAG laser with a variable attenuator to provide a large but stable amount of light for detection. The interferometer was a confocal Fabry-Perot interferometer which has a large light gathering capability and is insensitive to speckles. The detection laser light was carried using an optical fiber to another movable "detection head" located on another rail below the sheet. This detection head weakly focused the detection light onto the sheet and collected the reflected light, which was carried to the interferometer using a second optical fiber. The two sensing heads could be moved together manually to position the sensor anywhere across the sheet and to allow manual scans.

The two sensing heads were positioned about 30 cm from the sheet. Vertical fluttering of the moving sheet has no effect as long as the sheet remains within the depth of focus of the focusing optics (a few cm). Line speeds of up to tens of meters per second are possible depending on the optical properties of the Fabry-Perot cavity and of the sheet surface, and line speeds up to 4 m/s (800 feet/minute) were tested online.

The goal of the prototype was to demonstrate that the technology could be used online. Therefore, important practical features such as cost, size, and data acquisition rate were not optimized. However, a high level of automation was achieved and included real time data analysis and display, automatic recording of measurement position along the coil, line speed and sheet height (to shut off lasers in case of sheet buckling or other anomalous conditions), and end of coil detection, etc. The measured coils were oiled with an electrostatic oiler which spreads a thin and uniform layer of oil on the sheet surface.

Using this prototype, a large number of test samples were measured with the sensing heads positioned off the line, and many of the data points to be shown in the next section were taken in this way (others were taken while the prototype was being tested using rotating samples in our laboratories). However, a limited number of coils were also inspected on-line, along their length. Comparative tensile test specimens could only be gathered from the tail end of the coils, and the measured variations in mechanical properties could not be verified against tensile tests.

3.2 Laser ultrasound prototype features

This section details the features that are included in the prototype.

3.2.1 Mechanical and structural aspects

The prototype consists of a generation unit to produce the generation light pulses, a detection unit to generate the detection light and analyze the received light to extract the ultrasonic signal, and of two rails supporting two sensing heads that focus the generation and detection light and collect the detection light scattered by the steel surface. The generation unit is located on a platform above the line, the detection unit is located in a remote control cabin, and the two rails are directly above and below the steel sheet. Schematics and pictures of the prototype are shown in Figures 3.2 to 3.5. The following is a list of more specific features:

- The sensing heads move across the sheet so that optical alignment and off-line work on cut samples will be possible without interruption of production.

- The sensing heads are mounted on two rails. These rails are mounted on the four horizontal beams between the legs of the platform. Mounting plates welded on the beams hold the rails and allow fine adjustments of their position. The prototype's rails are designed to be installed in any position (horizontally, vertically) on any sufficiently sturdy support structure. The rails, sensing heads, and air jets (to remove excess oil, see below) form a structure only 22 inches wide. Consequently, it would be possible to design a supporting structure requiring only 22 inches along the length of the production line. Also, the rails are sufficiently long to allow scans across the whole width of an 80 inch strip, with some extra space to move the sensing heads off-line.

- Clearance between the generation head and the sheet is 15.5 inches and could easily be modified. Clearance between the detection head and the sheet is 7.5 inches and could

only be increased at the expense of signal-to-noise ratio. Note that at LTV's inspection line, a carry-over table with rollers prevents the sheet from reaching the detection head.

- Two air jets are mounted on pneumatic arms on the side of the rail opposite to the sensing heads. These jets were intended to blow away the excess oil that may hinder the ultrasonic measurements (see Section 2.4.8). However, the amount of oil deposited by LTV's electrostatic oiler was nearly ideal for laser-ultrasonics and the air jets were not be required. However, the jets may prove useful when other types of oilers are used to deposit uneven and thick oil layers.

- The air jets are mounted on retractable pneumatic arms. They assume either of two positions: up or down. When not in use, the arms are retracted away from the sheet. When in use, they are brought to a fixed, but manually adjustable position above the sheet. If for any reason, the sheet were to be raised unusually high, such as when buckling, the sheet would come in contact with rubber wheels that should offer good protection against scratches, and the pneumatic arms would retract against the pressure. Finally, a sensor also monitors the height of the sheet. If the sheet is too close to the sensor, a command is issued to automatically retract the air jets.

- The generation laser is water-cooled using a closed-cycle chiller. The cooled water from the chiller is also circulated in a heat exchanger to provide air conditioning of the generation unit. The detection laser is also water-cooled using a second closed-cycle chiller.

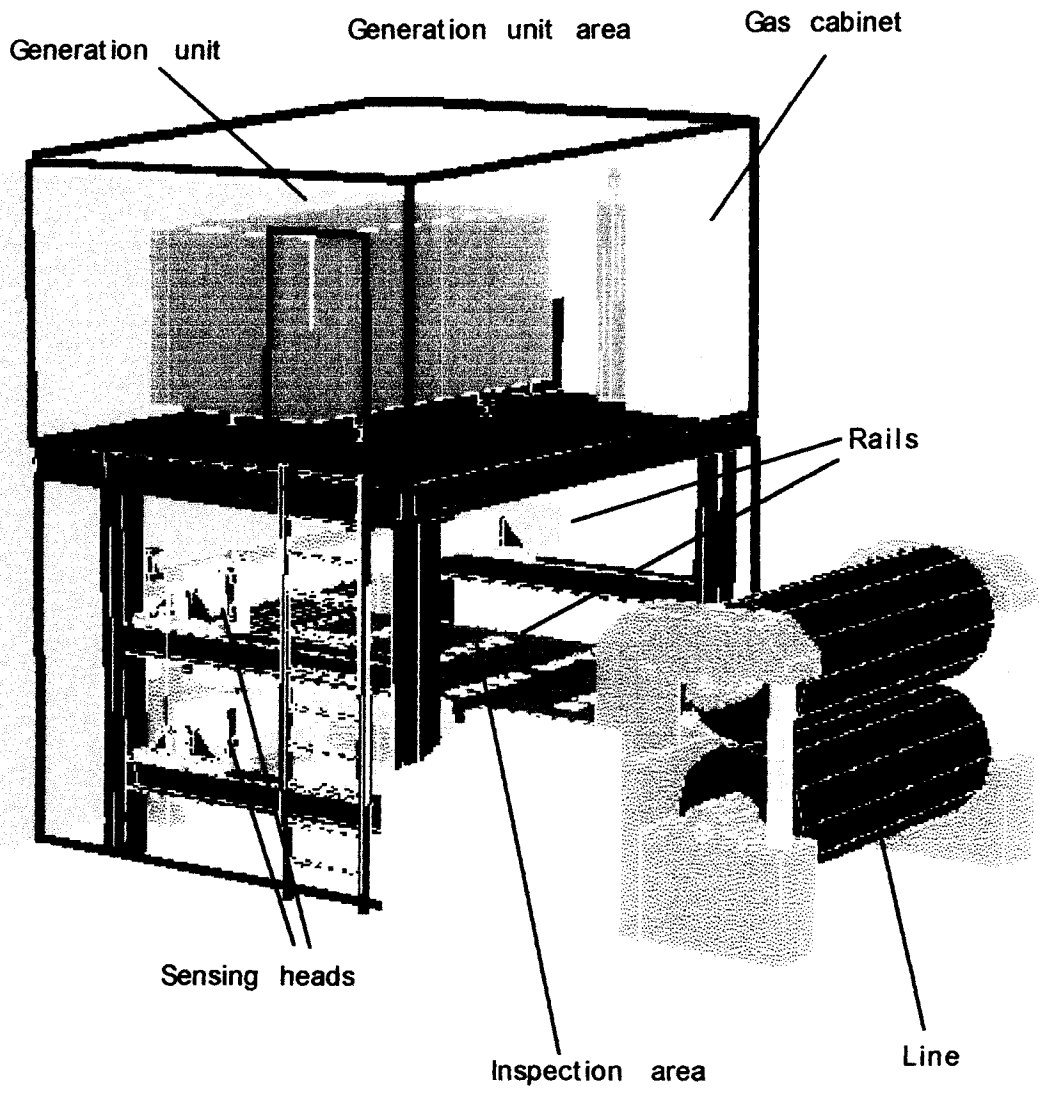

Figure 3.2 Overall schematics of the laser-ultrasonic prototype to measure the mechanical properties of steel sheets at LTV's #1 inspection line.

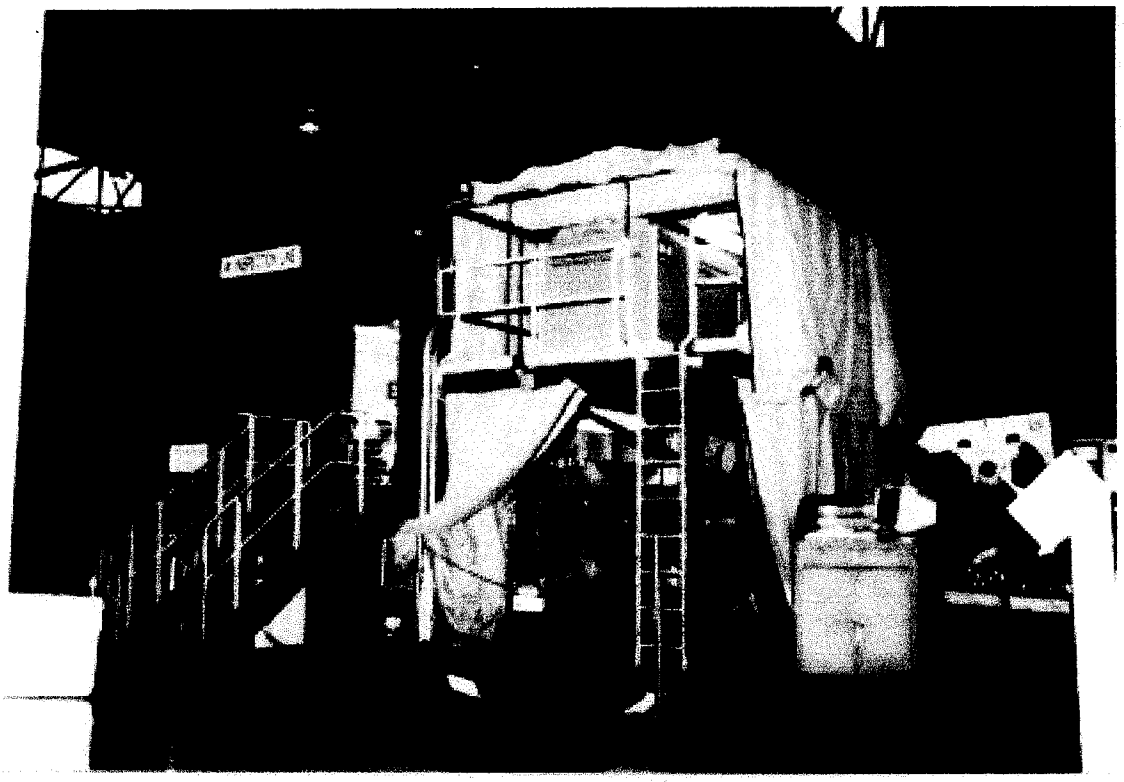

Figure 3.3 Overall view of the laser-ultrasonic prototype to measure the mechanical properties of steel sheets at LTV's #1 inspection line. The visual inspection booth is the blue construction on the left. The prototype is surrounded by curtains to block laser radiation.

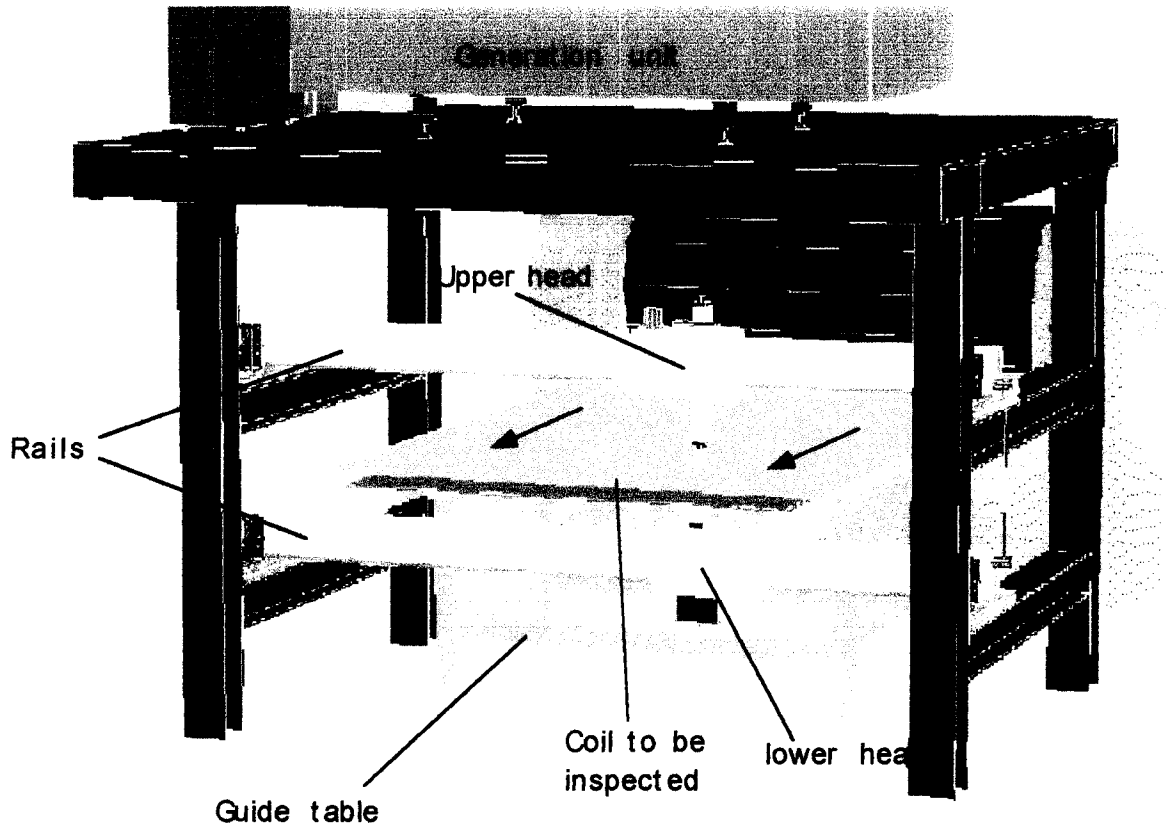

Figure 3.4 Enlargement of the inspection area showing the sensing heads and supporting rails.

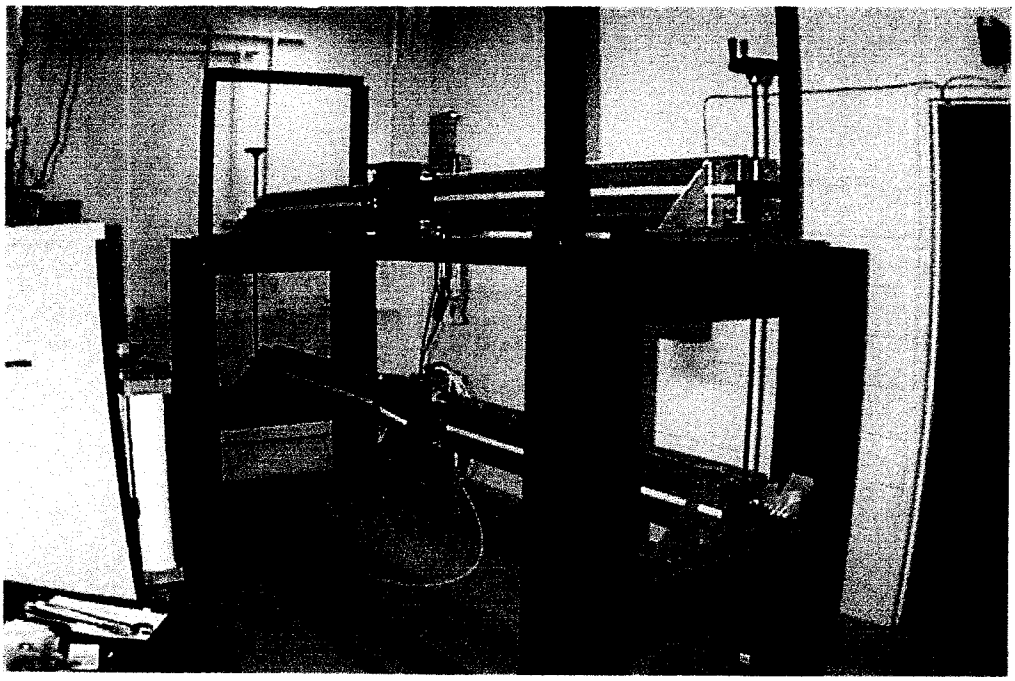

Figure 3.5 Rails and sensing heads mounted on a support structure at IMI to imitate LTV's installation.

3.2.2 Electronic and optical aspects

The following is a list of specific electronic and optical features:

- The generation head is oversized to allow modifications of the focusing optics. When the generation beam is focused more tightly, generation efficiency and signal-to-noise ratio increase, but surface damage also increases.

- Two computer-controlled optical shutters close the optical path at the exits of the generation and detection lasers to prevent accidental laser pulses from reaching the inspection area when the system is idle, and to allow the lasers to fire safely during warm up.

- The detection laser is equipped with an automatic attenuator to maintain a constant amount of light at the interferometer. This system is necessary because different types of steel have different reflection coefficients, and because variations in line tension may cause variations in the angle of the sheet and in the amount of light collected.

- The synchronization of the two generation lasers (oscillator and amplifier) is monitored automatically and natural long term and unavoidable drifts are automatically compensated.

- The generation head is equipped with an optical distance measuring device. Initially, this meter was intended to allow the air jets to follow slow height variations of the sheet caused by variations in line tension. However, it turns out that these variations are negligible. Nevertheless the device was kept to monitor 1) sudden stops of the line (the sheet then drops by about two inches), 2) the end of a coil, and 3) any possible anomalous condition that would cause the sheet to be raised abnormally high. In any of these three cases, the laser light is automatically shut off by the optical shutters, and the air jets are automatically retracted.

- The generation head is also equipped with a pyrometer. Temperature variations of the order of 10°C may cause small but measurable variations of ultrasonic velocities. If these variations were monitored, corrections could be applied to the data to improve accuracy. Therefore, a pyrometer was purchased to measure coil temperature and to evaluate whether these corrections would be significant in practice. However, laboratory tests have shown that the pyrometer output is much more sensitive to the amount of oil present on the sheet than to temperature. Consequently, the pyrometer was not used.

- The laser-ultrasonic signals are separated into high-frequency and low-frequency components using analog filters, and digitized using a two digital oscilloscopes running at two different speeds and gains. A smart averaging system allows to include only those ultrasonic signals within a predefined amplitude. The amplitude of the signal varies with generation efficiency and with the received light intensity. Sheet fluttering, variations in sheet reflectivity, and variations in oil thickness caused the signal to vary in amplitude, often saturating the electronics or being too small to be detected with sufficient signal-to-noise ratio. In such cases, the detected signal is rejected.

- LTV's footage gauge was interfaced with our equipment to monitor the location of the laser-ultrasonic measurements for future reference with mechanical tensile tests.

- A television camera was installed inside the inspection area to monitor the sheet while the safety curtains were drawn.

3.2.3 Computers and automation

The prototype is operated using two computers. The first computer automatically takes care of a number of repetitive background tasks. In particular, it constantly monitors sheet height using the optical distance measuring device, withdraws the air jets if an abnormal condition is detected, monitors the footage gauge, monitors the pyrometer, controls the optical shutters that block laser light under various conditions (laser warm up period, abnormal conditions, etc...), controls the triggering of the generation laser, limits the number of generation laser pulses on a single spot on the sheet to prevent unacceptable laser damage, and feeds information to the second computer. This background computer runs unattended and has very few controls. But it displays various prototype conditions.

The second (main) computer runs the main program which includes the main user interface and the acquisition and analysis software. This main program works as follows: The operator activates a button to let the system warm up and activate the air jets. The operator activates a second button to begin data acquisition. The program arms two digital oscilloscopes to average the ultrasonic signals coming from the interferometer. One average consists of 10 to 100 laser shots and lasts between one and ten seconds. The data are then transferred from the oscilloscopes to the computer where they are stored. The main computer also reads the information sent by the background computer, such as sheet temperature and footage. Data analysis is performed in real time and up to five mechanical or microstructural properties may be displayed simultaneously as a function of footage.

3.3 Software

This section shows a typical ultrasonic signal obtained online and the software utilized for its analysis.

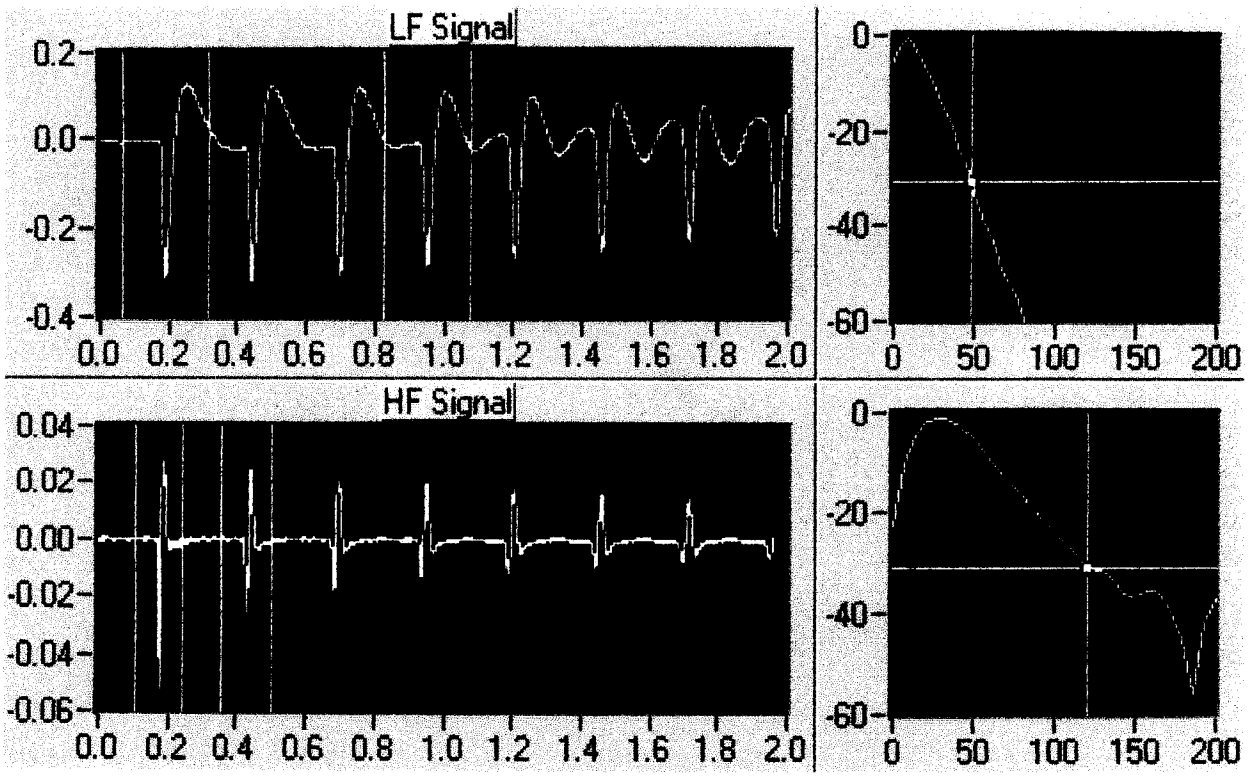

Figure 3.6 Online data analysis software showing the high and low frequency of the signal being analyzed.

Figure 3.6 shows, on the left, the low frequency (LF) and high frequency (HF) components of the ultrasonic signal (in arbitrary units) as a function of time (in μs). To the right, the Figure shows the frequency (in MHz) content of the fourth or second echoes contained within cursors (in units of dB relative to the maximum of each spectrum). In the LF display, the shear acoustic signal begins to appear after the fourth longitudinal peak. The shear signal contains only low frequencies and this is why it does not appear in the HF signal component.

In this example, typical of what is observed in LC or ULC samples, the S/N exceeds 60 dB at the lowest frequencies. The signal also exceeds the noise level over a frequency bandwidth greater than 100.

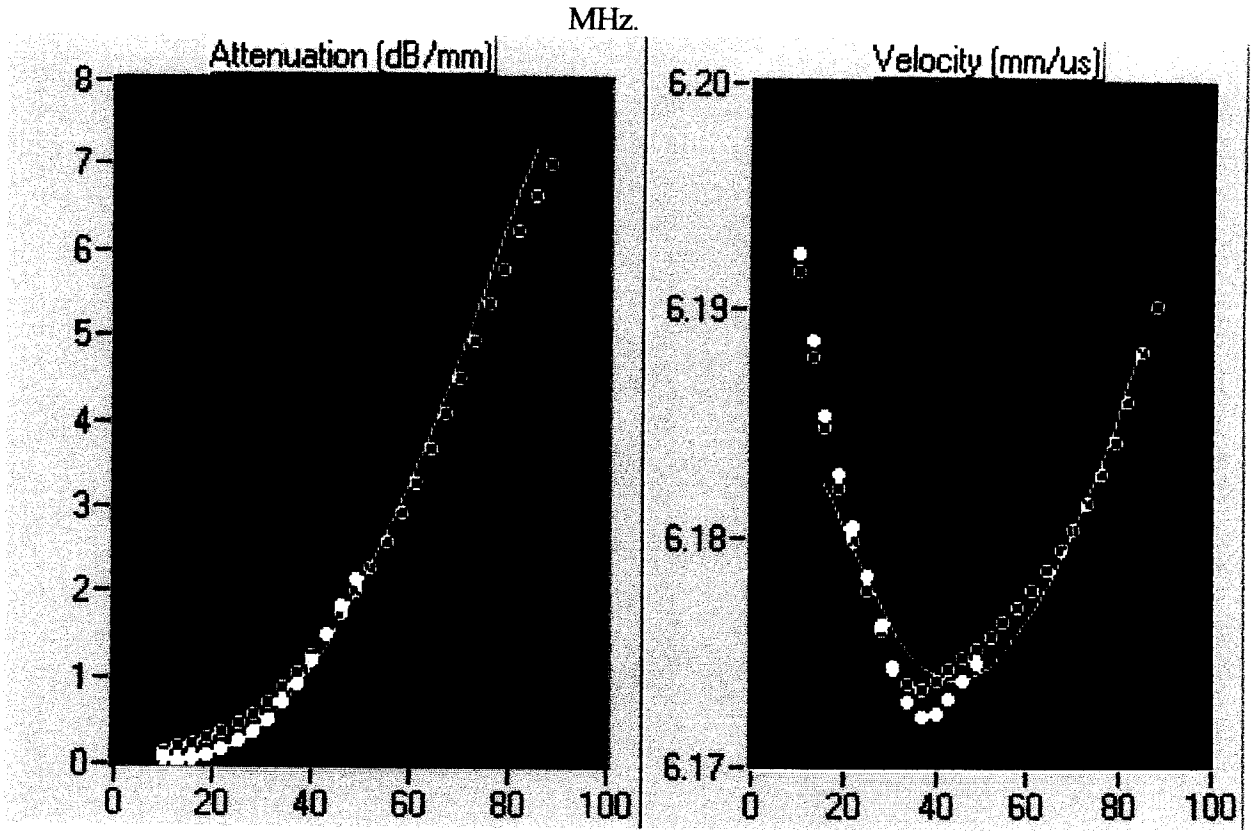

Figure 3.7 Online data analysis software showing computed attenuation and velocity dispersion spectra (dots) with the fitted scattering model (lines) used to estimate grain size.

The frequency spectra are obtained using Fourier transform techniques. By taking the ratio of the amplitude spectra of two echoes, one can obtain an attenuation spectrum. Additionally, by taking the difference of the phase spectra of two echoes, one can obtain a velocity dispersion spectrum. These are shown in Figure 3.7. The attenuation spectrum and velocity dispersion spectra are shown on the left and right, respectively (frequencies are in MHz). The open circles are obtained from the HF component of the signal while the white circles are obtained from the LF component. At low frequencies, the white circles are expected to be more reliable. The solid line is a non-linear least squares fit of the scattering model to the white circles at low frequencies, and to the open circles at high frequencies. The only fitting parameters are the ultrasonic grain size and a constant. One fit is obtained for each spectrum so two estimates of grain size are obtained. In general, both grain size estimates agree but there are small and systematic differences between them.

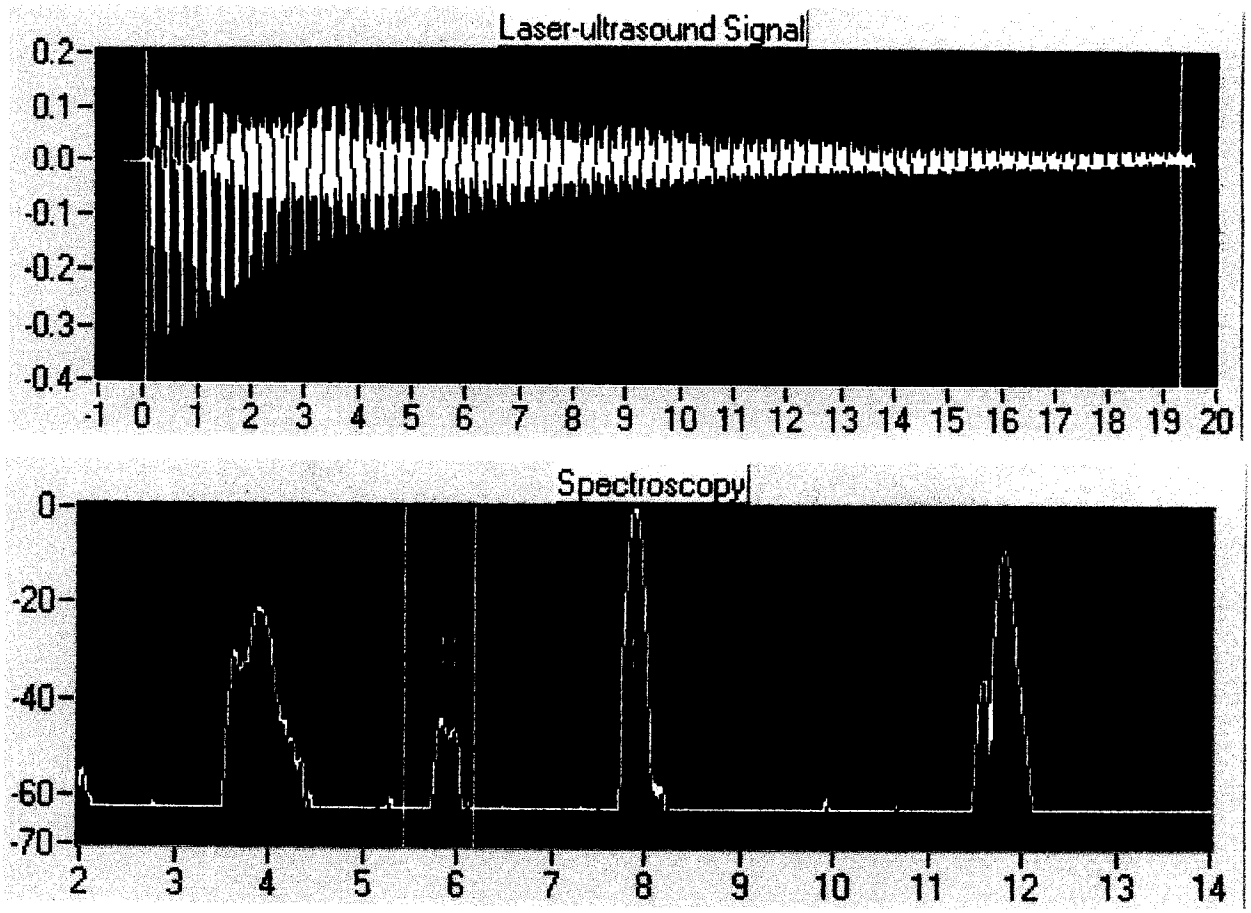

Figure 3.8 Online data analysis software showing the laser-ultrasound resonance spectroscopy analysis.

The signal's LF component is also used for the laser-ultrasound resonance spectroscopy technique (LURS). In LURS, the ultrasonic signal is acquired over roughly 20 μs or more (top of Figure 3.8, vertical axis in arbitrary units, horizontal axis in μs), which corresponds to at least 60 acoustic echoes. The amplitude spectrum of the entire signal (bottom of Figure 3.8, vertical axis in units of dB relative to the highest peak, horizontal axis in MHz) is calculated and the sheet's natural shear and longitudinal resonances are identified and their center frequency measured. In particular, it is usually possible to separate the two shear resonances which differ only by their polarization directions, as shown between the two cursor near 6 MHz in the bottom of Figure 3.8.

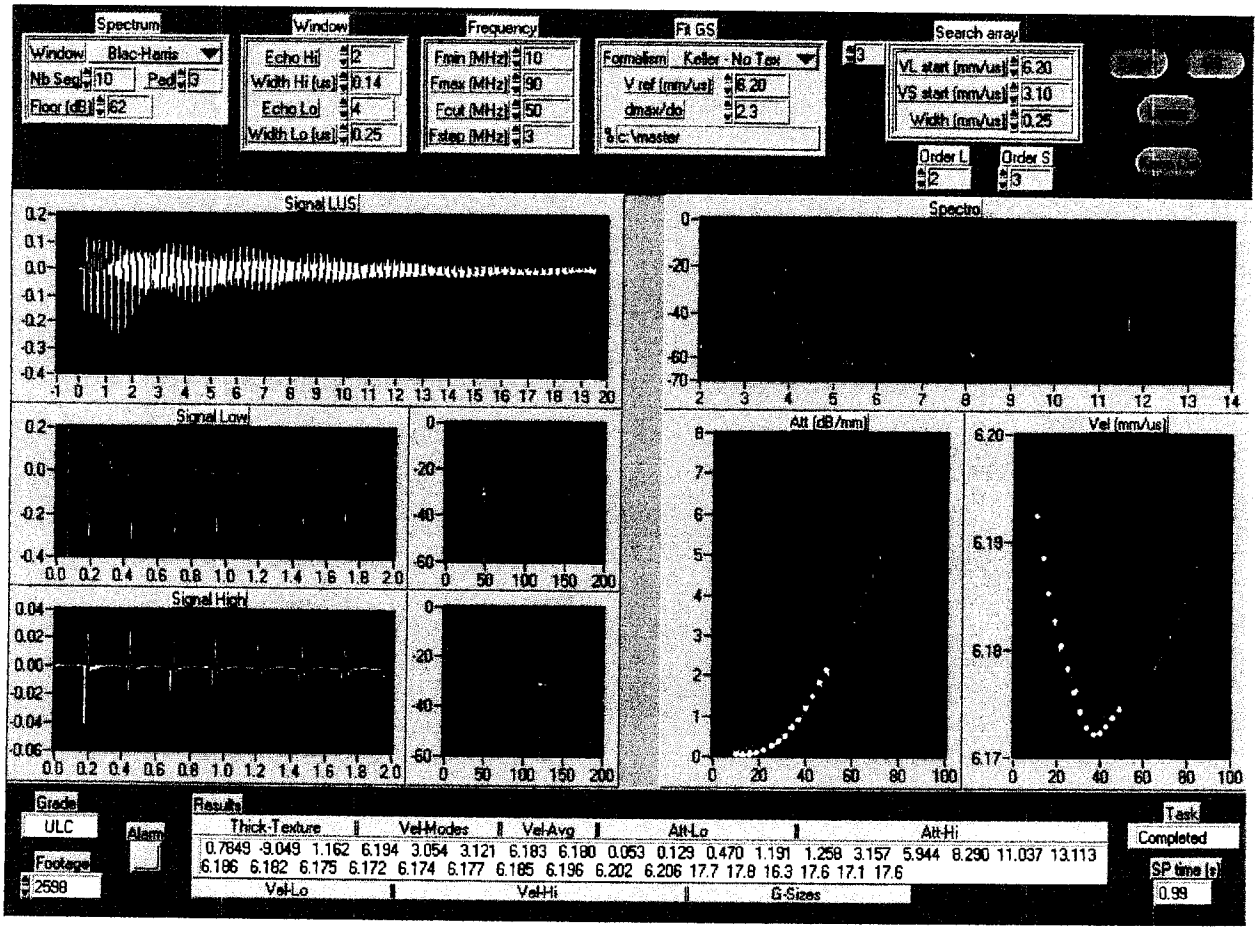

Figure 3.9 Online data analysis software showing the entire data analysis user interface. This interface is designed to meet the needs of the ultrasound scientist.

The signal processing software installed at LTV's inspection line regroups the ultrasonic data analysis in a single screen as shown in Figure 3.9. The software allows for easy modification of basic constants and data analysis parameters, such as window type and width, frequency bandwidth, initial values for automatic search of peak location and maxima, etc. The software also displays numerous computed values such as ultrasonic attenuation and velocity at selected frequencies, grain size, and texture coefficients, at the bottom of the screen. Once an acquisition is transferred from the digitizing oscilloscope to the computer, all above outputs are computed in less than one second on a 150 MHz Pentium computer.

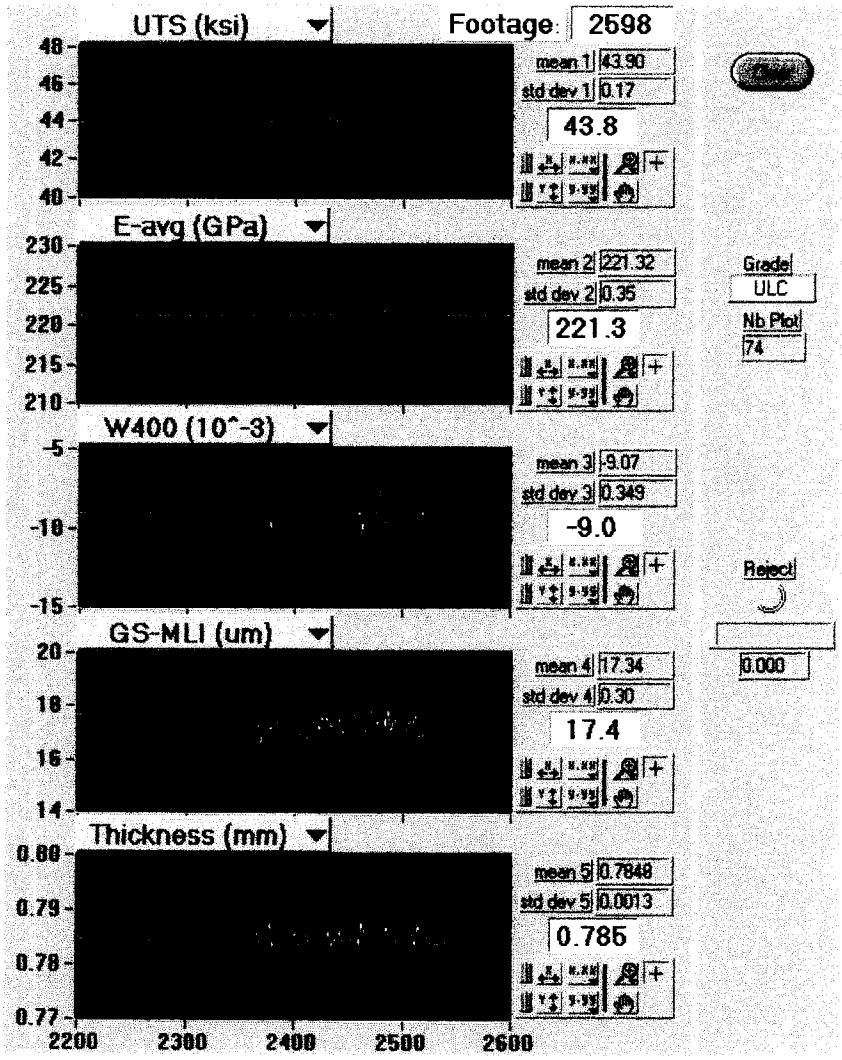

Figure 3.10 Online data analysis software showing the display of various properties along the distance of a coil as it is being measured. This is the interface that would be monitored by operators.

The acoustic parameters derived from the previous display are utilized to calculate the mechanical properties using pre-established correlations or models. Any five of a large number of mechanical or microstructural properties can be displayed in real time as a function of footage along the coil. The example of Figure 3.10 shows the ultimate tensile strength, Young's modulus, the W_{400} texture coefficient, grain size, and thickness at the tail end of an ULC coil. All raw ultrasonic data and derived quantities are also recorded electronically to allow for further or alternate data processing if desired.

3.4 Safety

A Safety Assessment Report was written to assess the risks of operating the prototype which was installed at LTV's #1 inspection line. The report was a comprehensive evaluation of the safety risks related to prototype operation. It identified several hazards, estimated the possible consequences, and described the safety measures implemented as well as specific procedural controls and precautions that should be followed. Table 3.1 lists the various

hazards that are considered in the report. The report also defined various procedures to be followed before operating the system and before shutdown for short or extended periods of time. The report was reviewed and accepted by LTV before the prototype was operated.

Table 3.1 List of hazards addressed in the Safety Assessment Report.

1.	Use of fluorine and inert gases
2.	Gas cylinder break
3.	Electrical shock
4.	Direct eye exposure to laser light
5.	Indirect eye exposure to laser light
6.	Direct skin exposure to laser light
7.	Indirect skin exposure to laser light
8.	Steel sheet damage due to laser misfire
9.	Fire hazards
10.	Loss of cooling water
11.	Dropping an object on the line
12.	Buckling of the sheet
13.	Vaporizing and burning oil on the sheet surface
14.	Others

Once installed, the levels of laser radiation were monitored and found much less than the conservative estimates presented in the Safety assessment report. The fumes generated by the ablation of the oil layer were not collected and removed as recommended in the report. They did incommode IMI's personnel when remaining in the enclosed area for extended periods of time. In those occasions, IMI's personnel felt discomfort in the throat area but the discomfort disappeared within minutes after leaving the area. No other hazard specific to the operation of the prototype was identified and no incident occurred.

3.5 Prototype performance

The prototype was installed without any major technical difficulty. **Overall, the prototype's performance was as good online as in the laboratory.** More specifically, the following conclusions were drawn:

- The prototype was robust against deviations from the optimal operation conditions. The pulse energy of the old generation laser can drop by a factor of three during the course of a day without significantly affecting the measurements. However, if the excimer amplifier were upgraded to a modern version, such a drop in pulse energy would occur only over a time scale of weeks.

- The laser beam alignment was preserved over time scales of about two weeks, i.e. between two successive trips at the plant. This was not tested over longer periods of time.

- The prototype included air jets to remove the excess oil when present. However, most coils inspected had been oiled with an electrostatic oiler and the air jets were not necessary.

- Good signal-to-noise ratio was obtained whenever the coils were oiled.

- When surface damage was tested, the operators and visitors agreed that there was no surface damage. But the authors, who by then had acquired considerable experience in observing laser damage, could observe a very slight amount of damage on some of the generation spots. Generally, it could not be guaranteed that the system would work without damaging the surface at all. Other measurements made in sub-optimal conditions resulted in more obvious surface damage.

The online measurements also uncovered some weaknesses that should be corrected in a commercial apparatus.

- When a very shiny, nearly mirror-like coil, such as a hot dipped galvanized coil, is measured, the contrast between the specular reflection and the diffusely scattered light is very high. When the sensing head collects the diffusely scattered light, the system adjusts by sending maximum detection laser light power. On the other hand, when the sensing head collects the intense specular reflection, the system adjusts by sending low detection-laser light power. However, the automatic adjustment is too slow and the photodetector was destroyed by such an intense specular reflection. Although the part can easily be replaced, a faster automatic light-power control system should be devised and built to adjust the detection-laser light power and eliminate this problem altogether.

- The data acquisition and transfer rates were slower than anticipated because of the highly variable signal strength caused mostly by the varying oil thickness, and because of the slow transfer rate of the digital oscilloscopes. This resulted in a slower measurement rate than expected: one data point every 10 seconds instead of one data point per 1 to 3 seconds. The fast automatic detection-laser power-control system described above would help solve this problem by maintaining a more constant signal strength. Replacing the digital oscilloscopes with ADC cards having a fast transfer rate would also improve the measurement rate. Finally, using the CO_2 laser to generate ultrasound on a clean surface, as opposed to an oiled surface, would also help stabilize the signal strength and improve measurement rate.

3.6 Online measurements

3.6.1 Online measurements along the length of coils

LURS spectroscopy was used to measure a limited number of coils along their length. In one case, five consecutive coils of low carbon steel manufactured for a single client were inspected. Three of these five coils showed identical variations of the W_{400} texture coefficient as a function of position, and two of the three coils also showed identical variations in the W_{420} texture coefficient. As shown in Figure 3.11, these features included identical absolute values of W_{400} and W_{420}, sudden jumps in W_{400} near 1500 feet, and similar increases of W_{420} along the coils' length. The fact that the prototype can sense similar features on coils produced in similar manners is strong evidence that the observed variations were real.

One of the same five coils showed a regular oscillatory pattern of the W_{400} texture coefficient with an apparent periodicity of 1100 feet (Figure 3.12). Another coil, not shown here, also showed oscillations in W_{400} of similar amplitude and with a periodicity of about 1400 feet. If these patterns were observed in more coils, one might be able to identify the source of the variability in the process and perhaps improve the process itself.

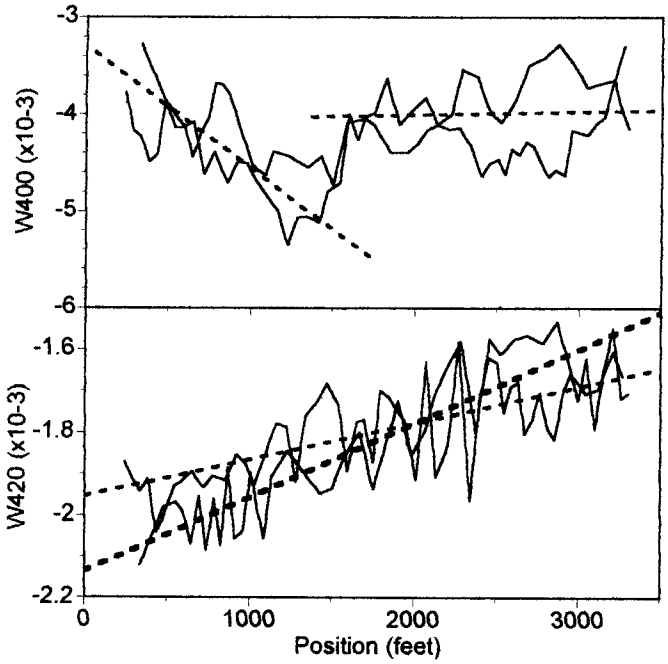

Figure 3.11 Variations in W_{400} and W_{420} along the length of two coils of LC steel.

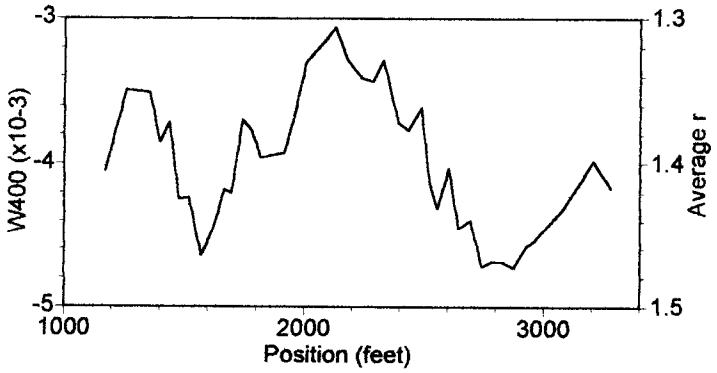

Figure 3.12 Oscillatory pattern of W_{400} observed in one of the five coils tested. The vertical scale on the right indicates the predicted $\bar{r}$ for the coil.

Even though the chemistry grade of these five coils was not studied within this project, if one uses the approximate empirical relation $\bar{r} = 1 - 1000\ W_{400}$ (see Figure 4.19), then this coil has a $\bar{r}$ of approximately 1.4 and the peak to peak amplitude of the $\bar{r}$ oscillations is about 0.15 (i.e. 1.4 ± 0.075). These variations are well within the sensing capabilities of the apparatus. In fact, from this figure, it is clear that the sensor's online $\bar{r}$ measurement repeatability of order ± 0.02 far exceeds the combined accuracy of the mechanical and ultrasonic measurements of ± 0.08 which was determined from Figure 4.19.

3.7 Projected cost of a commercial system

The Industrial Materials Institute is a not-for-profit research institute and not a commercial entity in the business of building commercial-quality sensing equipment. Therefore, we cannot speak for an eventual commercial partner. This project's research prototype was built at the lowest cost to the project. This is very different from building at the lowest commercial cost. For example, the lowest cost to the project meant that we built a relatively cheap box around our expensive optical table and expensive optical elements and supports. If a company wanted to duplicate and improve on our system, Table 3.2 shows a list of the most expensive items to be purchased, with approximate prices. This would amount to approximately 450 000 US$. Of all the components costs included in Table 3.2, the generation laser cost is the most uncertain.

Table 3.2 Estimated cost of the major components required to build a commercial prototype.

Main components	Sub components / Description	Company	Model #	Cost
				(x 1000 US$)
Generation Unit	Short pulse CO2 laser, or MOPA excimer laser			100
	Chiller	FTS Systems	RC150C0020	5
Detection unit	Interferometer	Ultra-Optec	LISOR	40
	Long pulse YAG laser & chiller	Ultra-Optec	LPDU-525	155
	Variable attenuator			10
	Housing structure			5
Detection Electronics	Fabry-Perot control card in a PC	National Instrument		3
	YAG Power control card in a PC	National Instrument		3
	Digital I/O multifunction card			2
	Acquiris A/D converter			30
	A/D converter for PC			10
	Housing cabinet			10
	2 industrial PCs			10
Others	Cables			10
	Miscelleneaous electronics			10
	Optics			30
	Optical mounts			10
	Software	LabView and LabView RT		5
			Total	**448**

4 MECHANICAL PROPERTIES MEASUREMENTS

As discussed in the Introduction, the general approach is to extract microstructural information from the ultrasonic data and to use that information to build correlations with the mechanical properties. The intermediate step of evaluating the microstructure is not absolutely necessary and may even introduce additional errors, so correlation with direct measurements of ultrasound velocity, attenuation, and absorption are also done. But evaluating the microstructure does present several benefits: It allows to combine the many interrelated ultrasonic data into a few independent variables; it allows to utilize and test structure-property relationships found by metallurgists (such as the Hall-Petch equation); it provides insights into what additional measurements might be needed; and it provides useful microstructural information.

In Section 2, it was shown how the various ultrasonic measurements reduce to the measurement of grain size, texture, and temper reduction. The importance of grain size was discussed together with the modified Hall-Petch Equation 1.1. As we will see, the measurement of temper reduction is assumed to provide some information about dislocations and is important to estimate YS. Texture is also extremely important in estimating the various mechanical properties, and especially their anisotropy.

This section begins with general considerations applicable to all steel grades studied in this project. It is shown that the problem of measuring six different mechanical properties (YS, TS, TE, UE, n, r) and their in-plane variation as a function of only four microstructural and ultrasonic parameters (grain size, W_{400}, W_{420}, and ultrasonic absorption) is not an impossible task because the mechanical properties are not independent from each other. First, insights into the physical meaning of the measured texture coefficients and a specific description of the in-plane anisotropy of the mechanical properties are presented, leading to a systematic approach to evaluate the in-plane anisotropy. Then we show how YS, TS, TE, UE and n are related to each other.

This section continues with empirical models which correlate the ultrasonic and microstructural data to the mechanical properties. Ultra low carbon (ULC) and low carbon (LC) grades were found to have nearly identical and relatively simpler predictive models compared to high strength low alloy (HSLA) grades. For these reasons, ULC and LC grades are treated together first, and HSLA grades are discussed afterwards.

4.1 Sample sets

The industry partners of this project decided that the mechanical property measurement sensor would be most useful for steel sheets (thickness of order 1 mm) of ULC, LC (about 0.05 %C) and HSLA (about 0.08 %C) grades because these grades constitute the bulk of their high added-value production. All samples are cold rolled, fully annealed (either continuously or in batch) and temper rolled. The LC samples from one of the partner companies were also artificially aged at 400°F (204°C) for 10 minutes to precipitate the carbon that would otherwise be in solid solution.

A typical sample set consisted of 30 samples. The mechanical properties were measured in the rolling, transverse, and 45° diagonal directions [except for some laboratory prepared samples that were measured only in the rolling direction]. Some of the measurements in the rolling direction were repeated two or three times, thus providing error estimates of the mechanical property measurements. Several samples were subsequently tested for their mechanical properties. Table 4.1 lists those sample sets included in this section of this report.

Table 4.1 Sample sets utilized in this project.

Company	Grade	# of samples	Comments
First Partner Steel company	ULC – A&B	30	A: Ti stabilized B: Ti-Nb stabilized
	HSLA - V	30	
	ULC - A	17	
	LC - A	2	
	ULC - C	14	Controlled temper reduction from 0 to 3%
	HSLA - W	16	Controlled temper reduction from 0 to 3%
	ULC - D	24	Laboratory prepared samples
	HSLA - V	18	Laboratory prepared samples
Second Partner Steel Company	LC - B	30	
Third Partner Steel Company	ULC - E	30	
	LC - C	30	
	HSLA - X	30	
	HSLA - Y	30	

4.2 General considerations applicable to all grades

4.2.1 In-plane anisotropy

The mechanical properties show in-plane anisotropy. To characterize this anisotropy, it is customary to measure the tensile properties in the rolling (or L for longitudinal, or 0°), transverse (T, or 90°), and 45° diagonal (D) directions. Hidden under this practice is the assumption that the anisotropy of a mechanical property (MP) as a function of in-plane angle from the rolling direction (θ) may be described as:

$$MP(\theta) = \overline{MP} + \Delta_2 MP \cos(2\theta) + \Delta_4 MP \cos(4\theta) \tag{4.1}$$

where $\overline{MP}$ is the in-plane average mechanical property and $\Delta_2 MP$ and $\Delta_4 MP$ are the two-fold and four-fold in-plane anisotropy of the mechanical property, respectively. These are defined as follows:

$$\begin{aligned} \overline{MP} &= [MP(0°) + 2MP(45°) + MP(90°)]/4 \\ \Delta_2 MP &= MP(0°) - MP(90°) \\ \Delta_4 MP &= [MP(0°) - 2MP(45°) + MP(90°)]/2 \end{aligned} \tag{4.2}$$

As will be seen, the anisotropy of mechanical properties is strongly related to the anisotropy of the crystallographic orientation distribution, or texture. The texture coefficients W_{400}, W_{420}, and W_{440}, in Roe's notation,[16] are the lowest order coefficients (for a cubic material like iron, and within the assumption that the macroscopic symmetry is orthotropic) of a series expansion of the crystallographic orientation distribution function in terms of generalized spherical harmonics. The better the {111} planes are aligned in the plane of the sheet, the more negative is the value of W_{400}, and the better the steel can plastically deform in the plane of the sheet. The second index in the texture coefficients indicates the in-plane order of symmetry of the particular spherical harmonic which is weighted by the texture coefficient. Therefore, W_{400}, W_{420}, and W_{440} indicate in-plane isotropic, two-fold, and four-fold symmetry, respectively, of texture in the plane of the sheet. Using these simple symmetry arguments, one may expect that $\overline{MP}$, $\Delta_2 MP$, and $\Delta_4 MP$ correlate with W_{400}, W_{420}, and W_{440}, respectively. Equivalent arguments were made on more solid mathematical grounds (and in a slightly different notation) by Bunge[17] for average and in-plane variations of the Young's modulus. Bunge also concluded that this approach would also apply for the plastic strain ratio. This was also found empirically by several authors.[18,19,20] For these reasons, correlations of in-plane averaged mechanical properties with W_{400}, and of in-plane anisotropy with W_{420} and W_{440} were sought and often found.

A recent model by Man[21] provides further justification for these simple relationships. Man applied the calculated (averaged) elastic constants of textured (orthotropic) polycrystalline aggregates of cubic materials to Hill's quadratic yield criterion of plastic deformation[22] to calculate a precise relationship between $\bar{r}$, $\Delta_2 r$, and $\Delta_4 r$ and the three fourth order texture coefficients. These relationships are:

$$\bar{r} = 1 - \frac{8\sqrt{2}\pi^2\beta}{7} W_{400}$$
$$\Delta_4 r = \frac{32\pi^2\beta}{\sqrt{35}} W_{440} \quad , \tag{4.3}$$
$$\Delta_2 r = \frac{64\pi^2\beta}{7\sqrt{5}} W_{420}$$

where β is a positive, semi-empirical material's constant. These equations show how the averaged and in-plane variations of the plastic strain ratio depend linearly on the lowest order texture coefficients. The same theory was extended to predictions of the anisotropy of YS. The calculations show that the in-plane average, four-fold anisotropy, and two-fold anisotropy of YS are given by

$$YS = \left(1 - \frac{6\sqrt{2}\pi^2\beta}{35} W_{400}\right) Y_0$$
$$\Delta_4 YS = \frac{8\pi^2\beta}{\sqrt{35}} W_{440} Y_0 \quad . \tag{4.4}$$
$$\Delta_2 YS = \frac{16\pi^2\beta}{7\sqrt{5}} W_{420} Y_0$$

In these equations, Y_0 is the isotropic YS, i.e. the YS averaged over all directions in 3-dimensional space (if it could be measured). These equations provide some theoretical justification for including texture in our models to predict various mechanical properties, either in the rolling direction, or averaged in the plane of the sheet.

4.2.2 Empirical relationships between UE, and n

In Leslie's book,[23] The Physical Metallurgy of Steels, it is written: "For expressing the stress-strain relation in a concise form, the empirical equation

$$\sigma = K \varepsilon^n \tag{4.5}$$

where σ is true flow stress, ε is true strain, and K and n are constants, developed originally by Ludwik, is used almost to the exclusion of all others. It is applied only in the region of uniform plastic strain. It does not allow for elastic deformation at low stresses, nor for necking." Leslie then shows that if this empirical relation is verified then "(...) the limit of uniform strain is equal to n."

If this empirical relation is so good, then our data should verify the relation UE = n. This is shown in Figure 4.1 for ULC, LC, and HSLA steel samples. The ULC and HSLA samples were measured by one partner steel company in the longitudinal, transverse and diagonal directions and the LC steels were measured by another partner company in the longitudinal direction only. The solid line is the equality relation.

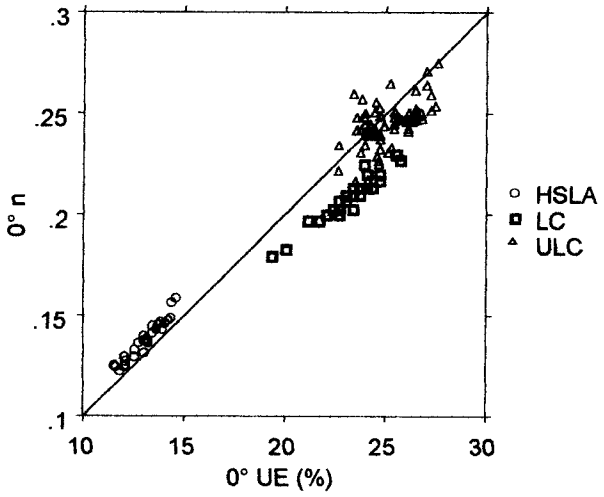

Figure 4.1 Strain hardening exponent as a function of uniform elongation in the rolling direction, for three grades of steels. The solid line is the equality between UE and *n*.

The equality UE = *n* was also tested more closely for each of the three steel grades. An excellent linear relationship was found for the LC and the HSLA grades.

In conclusion, the relationship UE = *n* is either verified or nearly verified for the three grades tested. Therefore, correlations with ultrasonic measurements were sought for both properties independently to check if one of them could be predicted more accurately.

4.2.3 Empirical relationship between n, UE and YS, TS

Figures 4.2 and 4.3 show that, for three of the grades studied (other grades were not considered in the analysis), *n* and UE can be expressed as linear combinations of YS and TS. The residual of the correlation using all three grades simultaneously is of order ± 0.01 for *n* and ± 1% for UE. This error corresponds to the target measurement accuracy or better. The residuals can be further reduced by considering only one grade at a time.

It is also interesting to note that the LC and ULC sample lots show identical relationships between UE and a combination of YS and TS, and that the two grades also show identical relationships between *n* and a combination of YS and TS except for a systematic offset. This offset is of order 0.02 in *n* values, and corresponds to the offset observed between UE and n in Figure 4.1. From this we conclude that if TS and YS can be measured with laser-ultrasound, then UE and *n* will also be measurable to within an accuracy close to the target accuracy.

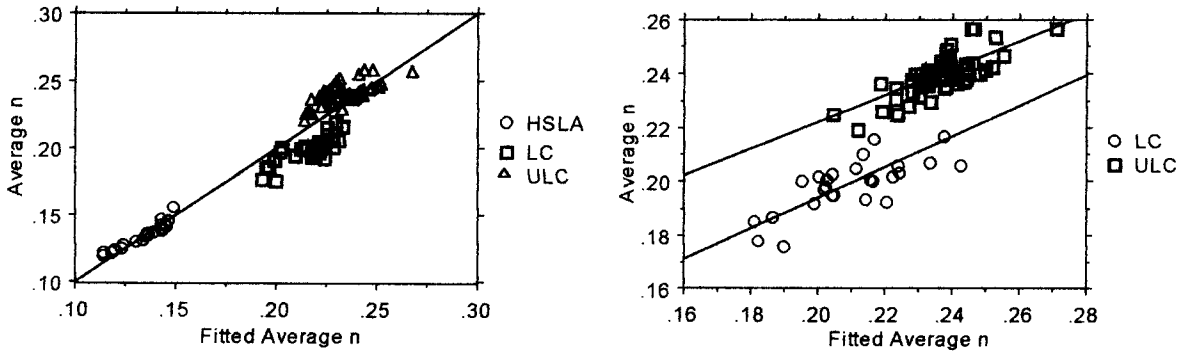

Figure 4.2 Average in-plane strain hardening exponent vs. a linear combination of YS and TS for 113 samples of LC, HSLA and ULC steels (left). If the HSLA grade is excluded (right), a single predictive model is found for the ULC and LC grades, but the two grades show a systematic offset.

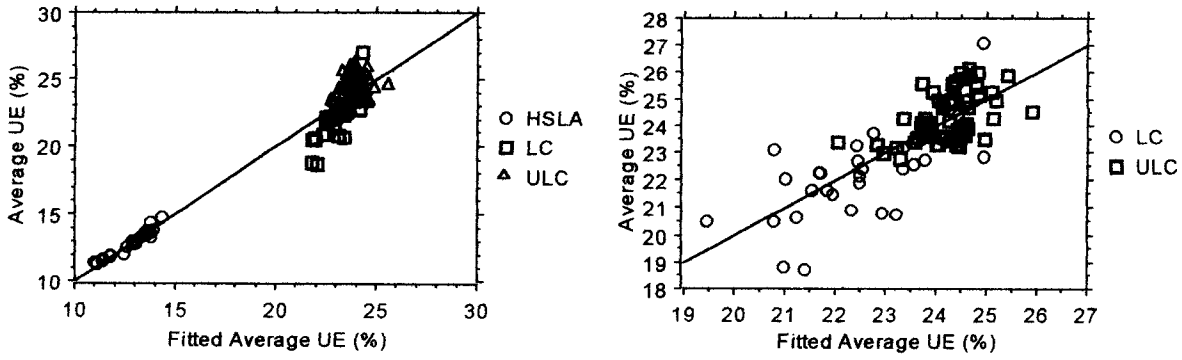

Figure 4.3 Average in-plane uniform elongation vs. a linear combination of YS and TS for 113 samples of LC, HSLA and ULC steels (left). The relationship improves for the ULC and LC grades if the HSLA grade is excluded (right).

4.2.4 Empirical relationships between UE and TE

Uniform and total elongation were also found to correlate with each other (Figure 4.4) for three of the grades studied (other grades were not considered in the analysis). The rms residual to the correlation is 0.7%, i.e. better than the required measurement accuracy. Therefore, if a sufficiently good correlation can be found for either one of these two properties, another correlation based on the same parameters can likely be found for the other property.

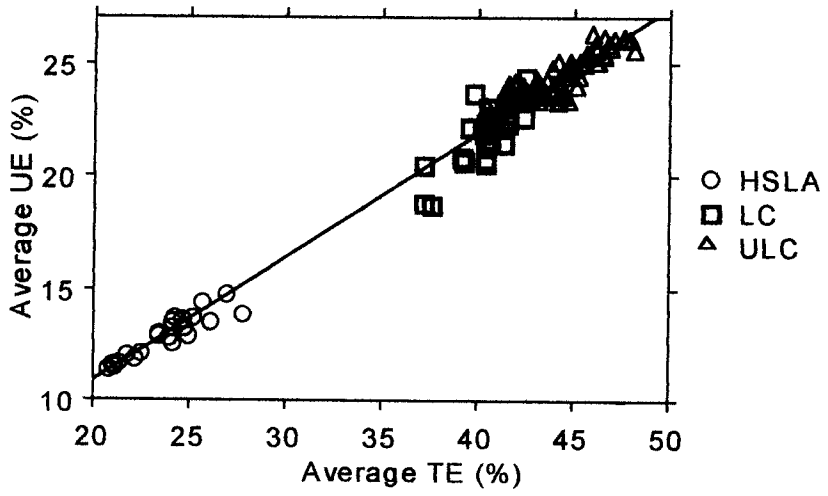

Figure 4.4 Correlation between the average in-plane uniform elongation and total elongation for 113 samples of LC, HSLA and ULC steels.

4.2.5 Conclusion

To estimate YS, TS, TE, UE, n, $\bar{r}$, and their in-plane anisotropy from grain size, texture, and temper reduction (dislocation) measurements only may seem an impossible task because fewer ultrasonic measurements than mechanical measurements are made. However, it was shown empirically that TE, UE, and n are related to each other and to a combination

of YS and TS. These relationships are valid when ULC, LC and HSLA grades are considered either together or individually. Moreover, there are good theoretical reasons to believe that the anisotropy of the mechanical properties is governed primarily by texture.

4.3 Ultra low and low carbon steels

4.3.1 Ultimate tensile strength

The ultimate tensile strength (TS) of ULC and LC grades was found to vary linearly with grain size, as shown in Figure 4.5. The Hall-Petch relationship for YS (Equation 1.1) and relationships found by other authors[24] for TS suggest that the dependence should be proportional to the inverse square root of grain size. Over a small range of grain sizes, however, the two relationships are indistinguishable. Here the linear relationship is used for simplicity.

Samples from five different grades from three companies are included in Figure 4.5. For each grade, a linear least squares fit is represented by a straight line. The two ULC sample lots (lots A & B) have essentially identical relationships between their average TS and grain size, while the ULC samples from another company have lower intercepts and the two LC grades have higher intercepts.

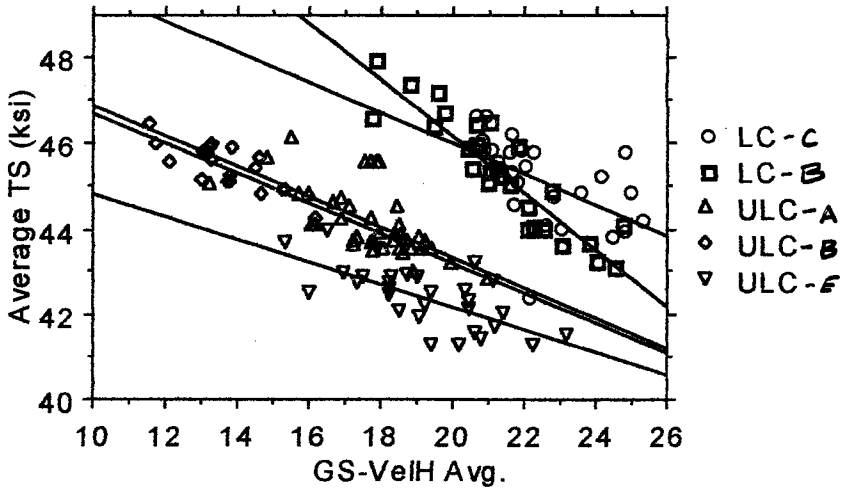

Figure 4.5 In-plane average of the ultimate tensile strength as a function of ultrasonic grain size for two grades of LC steels and three grades of ULC steels. The solid lines are linear least squares fits to each of the five grades.

The differences among various sample lots are probably explained by their respective chemistry which contain different amounts of carbon and solid solution elements. Pickering[25] states that

$$TS = 294 + 28\,Mn + 83\,Si + 3.85\,Pearlite + 7.7\,d^{-1/2}, \qquad (4.6)$$

while Klinman[26] states that

$$TS = 139 + 672\,C + 100\,Mn + 206\,Si + 11.6\,d^{1/2}, \quad (4.7)$$

where TS is expressed in units of MPa, Mn and Si are the concentration of Mn and Si in weight %, Pearlite is the percentage of pearlite in the structure (which may be equated to wt % of carbon divided by 0.77), and d is grain size in mm. Table 4.2 indicates the contributions of carbon and solid solution elements TS (converted into ksi) according to Equations 4.6 and 4.7. The differences observed between the LC and ULC grades in Figure 4.5 almost exactly agree with Pickering's estimate of solid solution strengthening

Table 4.2 Contribution of carbon and solid solution strengthening elements to TS.
These contributions are calculated according to Equations 4.6 and 4.7 for the LC and ULC carbon samples shown in Figure 4.5.

	Δ TS (ksi) Klinman	Δ TS (ksi) Pickering
ULC - lot A & B	2.3	0.7
ULC – lot E	2.8	0.9
LC – lot C	7.6	3.9
LC – lot B	9.1	4.8

According to Mintz,[27] the dependence of YS and TS on grain size, i.e. the slope of the Hall-Petch equation, increases with the concentration of interstitial elements that are free to diffuse to the grain boundaries. Increases in the concentration of stabilizing elements such as Al and Ti should reduce the slope.

The above argumentation shows that solid solution strengthening and the control of free solid solution elements possibly explain the differences among various sample lots. The laser-ultrasound sensor is not sensitive to chemistry and cannot sense these effects. In conclusion, the linear relationship between TS and grain size is the same for all LC and ULC grades, but the slopes and intercepts differ for each chemistry.

It is also well known that TS varies in the plane of the sheet in a manner as described by Equations 4.1 and 4.2. According to Section 4.2.1 (In-plane anisotropy) which led to Equations 4.3 and 4.4, one may expect that the in-plane anisotropy of TS correlates with texture. This was demonstrated unequivocally using conventional ultrasonics for ULC, LC, and HSLA grades.[28] Figure 4.6 shows the striking dependence of $\Delta_4 TS$ on W_{440}.

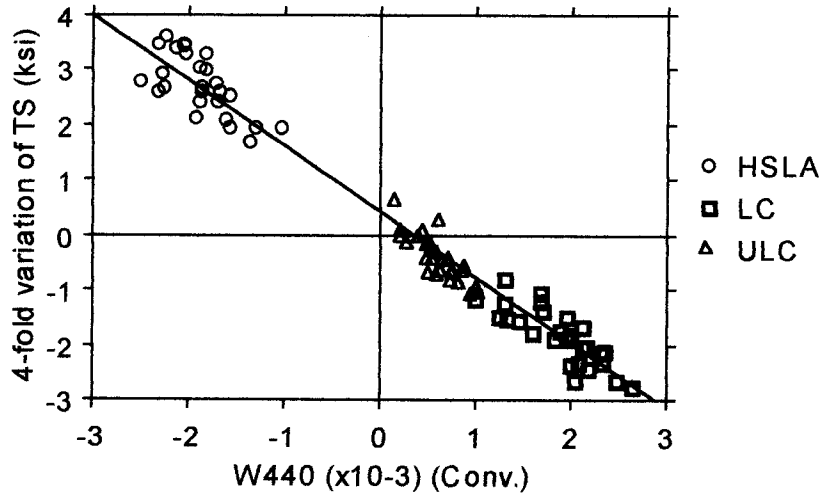

Figure 4.6 Dependence of the four-fold anisotropy of TS, $\Delta_4 TS$, on W_{440}, as measured using conventional ultrasonics on ULC, HSLA and LC steel samples.

For practical reasons, however, the laser-ultrasound prototype was built with the capability to measure W_{400} and W_{420} only, and not W_{440}. But it was also shown that processing affects the three texture coefficients in often correlated manners, and the four-fold, in-plane anisotropy of various mechanical properties such as TS can sometimes be correlated with W_{400} or W_{420} (Figure 4.7).

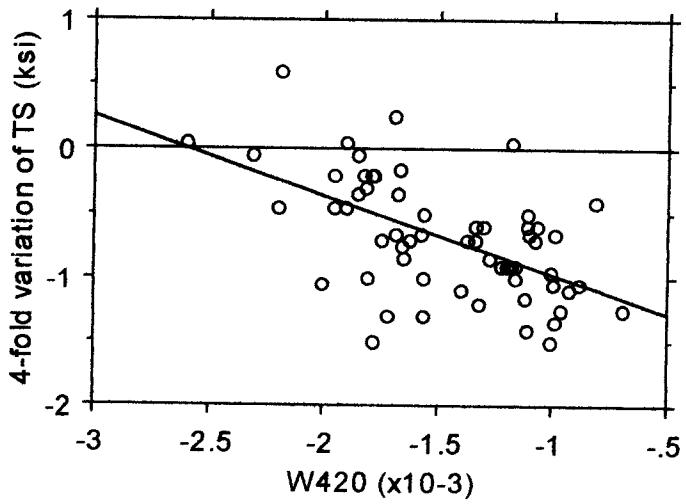

Figure 4.7 Dependence of the four-fold anisotropy of TS, $\Delta_4 TS$, on W_{420}, as measured using laser-ultrasound on ULC steel samples.

Figure 4.6, Figure 4.7, and Equations 4.1 to 4.4 are strong indications that texture does indeed affect the TS. This suggests that W_{400} may affect the average TS. The residual of the correlations between the average TS and the value predicted by the linear regression model of Figure 4.5 is plotted as a function of W_{400} in Figure 4.8. A positive residual indicates that the data point was above the fitted line. The line shown in Figure 4.8 represents a linear least squares fit through the data. The slope of the correlation indicates that the more strongly textured samples (the more negative values of W_{400} imply stronger {111} texture) have lower average TS. This is as expected because a stronger {111} texture should allow easier flow in the plane of the sheet which should lower the ultimate tensile strength. The rms residual to the correlation is 0.54 ksi which indicates that once grain size, texture, and chemistry effects are accounted for by our model, the average TS measurement precision for the five sample lots taken together is ±0.54 ksi.

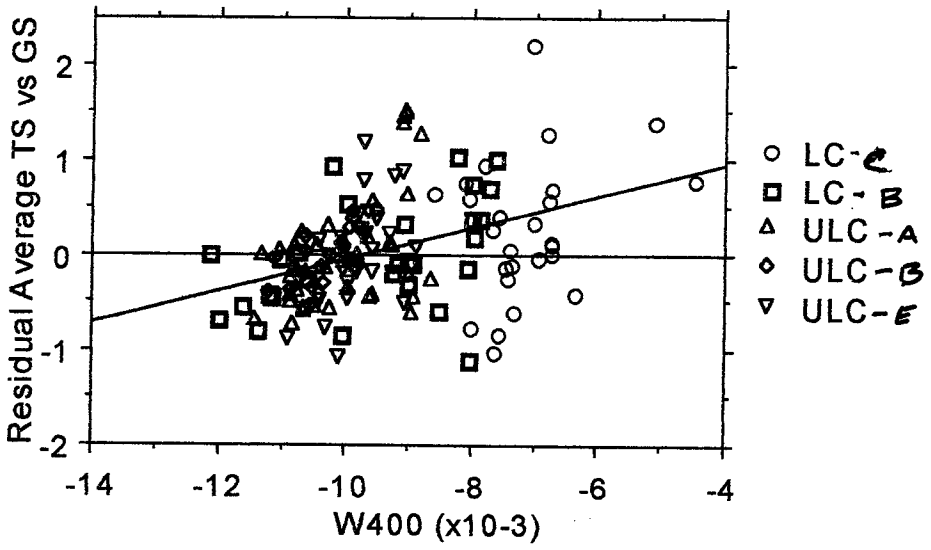

Figure 4.8 Difference between the data points and the linear least squares fit of Figure 4.5 (the residual) plotted as a function of W_{400}.
The straight line is a linear least squares fit and the rms residual of the correlation is 0.54 ksi.

In summary, all six LC and ULC lots behave in the same manner, except for systematic differences that can be explained by chemistry and solid solution strengthening. For a given grade, the chemistry is controlled sufficiently well so that sample to sample variations in solid solution strengthening are negligible. The ultrasonic grain size measurement is the main parameter utilized to estimate TS, sometimes to within the target accuracy of ±0.5 ksi. Texture accounts for the in-plane anisotropy and for a small correction on the value obtained using grain size alone. By building individual correlations for each chemistry grade, the ultimate tensile strength may be estimated to within an accuracy of ±0.3 to ±0.5 ksi,(±0.9 ksi for LC samples of lot C) as reported in Table 4.4. One example is shown in Figure 4.9.

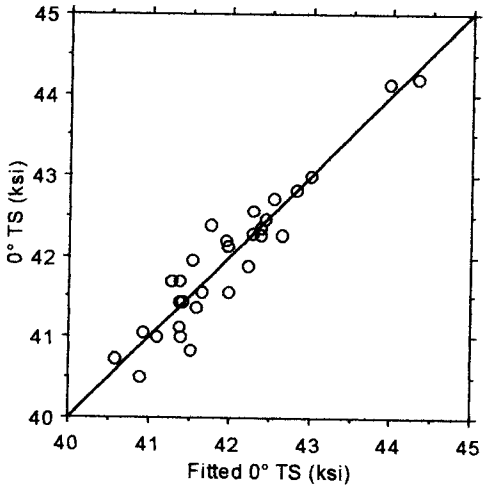

Figure 4.9 Ultimate tensile strength measured mechanically in the rolling direction as a function of the fitted ultrasonic model for 30 ULC steel samples.
The ultrasonic model is a linear combination of grain size and texture. The solid line represents the equality between model predictions and the measured values. The residual to the correlation is 0.31 ksi.

4.3.2 Yield strength

Temper reduction, also called skin pass, has a very large effect on YS but little effect on TS. Temper reduction is used to work harden steels and/or to remove the upper yield point. Figure 4.10 shows that an increase in temper reduction from 0 to 3% leads to an increase in YS from 15 to 28 ksi for a series of 14 ULC steel samples. At the same time, TS increases by less than 1 ksi.

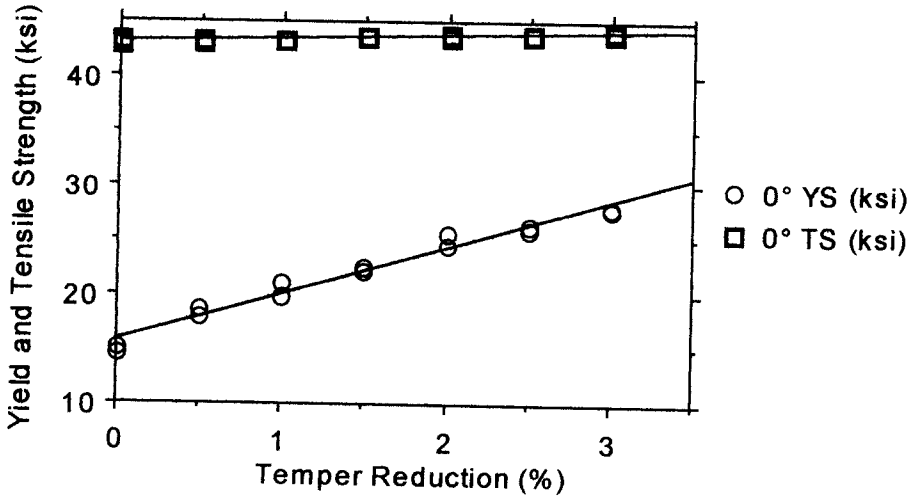

Figure 4.10 Dependence of YS and TS on temper reduction (skin pass) for 14 ULC steel samples.

Also, YS and TS are strongly correlated to each other if 1) the samples are of the same chemistry grade and if 2) they have the same amount of temper reduction. This is shown in Figure 4.11. Near TS = 43 ksi, an increase of 0.5% in temper reduction leads to an

increase of 4 ksi in YS, while an increase of 2 ksi in TS leads to an increase in YS of only 2 ksi. Clearly, temper reduction (also called skin pass) affects the YS behavior at least as much as TS.

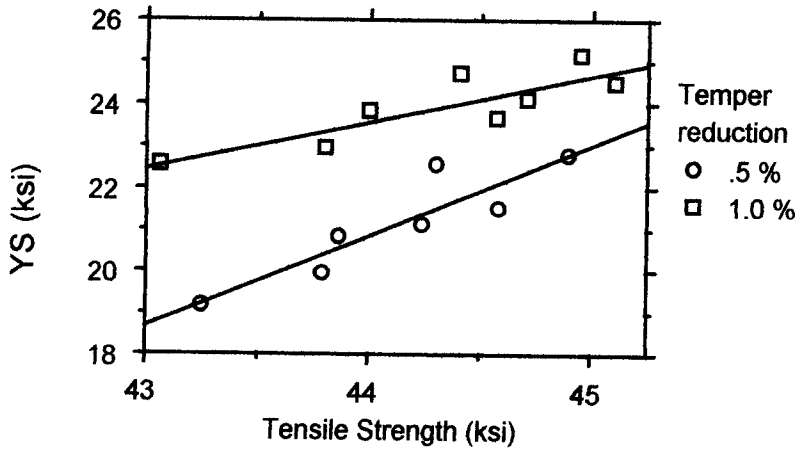

Figure 4.11 YS as a function of TS for 15 samples of ULC steel having received either 0.5% or 1.0% temper reduction in the laboratory.

Because TS can be obtained reliably, measuring YS reduces to measuring TS and temper reduction separately and then combining the measurements. As shown in Sections 2.6 and 2.7, temper reduction is best measured using absorption measurements, although it might be possible to use low frequency ultrasonic attenuation data as shown in Figure 2.27. Figure 4.12 illustrates the strong correlation between YS and either ultrasonic grain size or ultrasonic absorption for 29 ULC samples (lot E). A multiple regression involving absorption, grain size, and texture gives best results and a rms residual of 0.55 ksi, as shown in Figure 4.13.

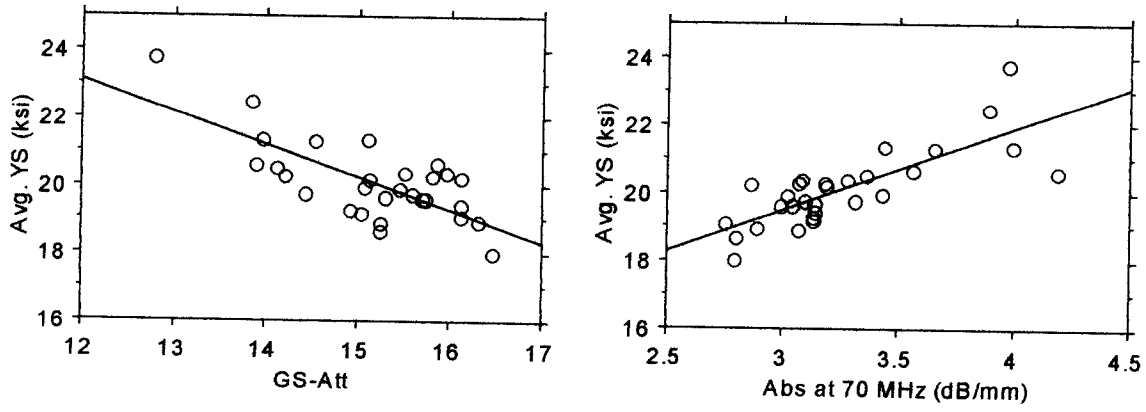

Figure 4.12 Dependence of the in-plane average YS on the ultrasonic grain size (left) and on ultrasonic absorption at 70 MHz as a measurement of temper reduction (right) for 29 ULC steel samples.
The rms residuals are 0.82 and 0.72 ksi for the left and right graphs, respectively.

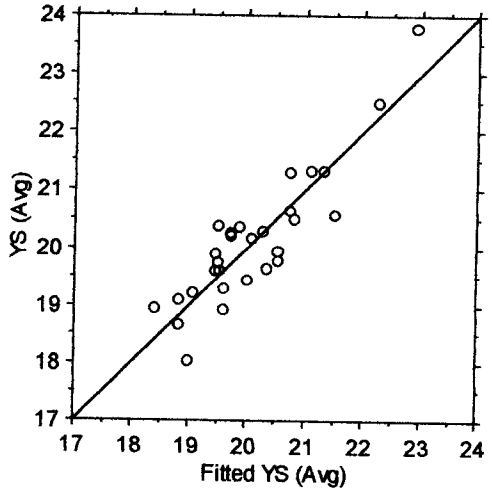

Figure 4.13 In-plane average YS as a function of the laser-ultrasonic value for 29 ULC steel samples.
The laser-ultrasound correlation model involves three parameters: grain size, texture, and absorption. The rms residual to the correlation is 0.55 ksi.

Another illustration of correlations between YS and a combination of grain size, texture and ultrasonic absorption measurements for 28 LC samples (lot B) is shown in Figure 4.14. In summary, YS can be estimated by using the same ultrasonic measurement and model as for TS and adding an independent measurement of temper reduction: ultrasonic absorption. All ULC and LC grades could be made to correlate with such ultrasonic measurements to within an rms residual of ± 0.5 to 1.0 ksi, as reported in Table 4.4.

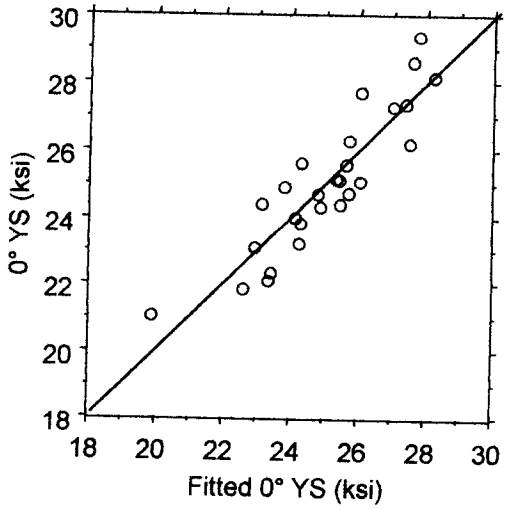

Figure 4.14 YS in the rolling direction as a function of the laser-ultrasonic value for 28 LC steel samples.
The laser-ultrasound correlation model involves three parameters combining four microstructural features: grain size, two texture coefficients, and absorption. The rms residual to the correlation is 0.69 ksi.

4.3.3 Total elongation

As TS, total elongation (TE) correlates with grain size (Figure 4.15) and texture (Figure 4.16). TE increases with grain size. However, simple chemistry arguments found in the literature and similar to those utilized to explain systematic differences for the relationship between TS and grain size do not account for the systematic differences observed between two grades. For example, Pickering[29] states that

$$TE = 140 - 290\,C + 20\,Mn + 16\,Si - 220\,S - 390\,P - 250\,Sn + 17\,d^{1/2}, \qquad (4.8)$$

where TE is expressed in %, the element names stand for their respective concentration in weight %, and d is grain size in mm. Table 4.3 indicates the contributions of elements present in each lot to TE according to Equations 4.8. Equation 4.8 overestimates the effect of chemistry on the total elongation by a factor of more than two. Moreover, the equation predicts that TE should decrease with increasing grain size, which is opposite to what is observed in Figure 4.15. But Equation 4.8 and Figure 4.15 do agree in predicting that chemistry should lower the total elongation of LC grades as compared to ULC grades thus providing a (shaky) explanation for the observed difference.

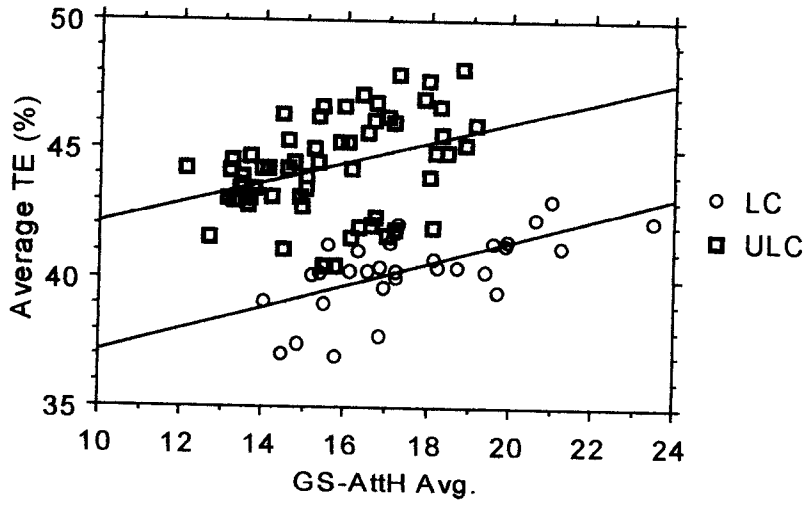

Figure 4.15 Variation of the average in-plane total elongation at fracture with ultrasonic grain size for 62 ULC steel samples and 31 LC steel samples.

Table 4.3 Contribution of various elements to the TE of LC and ULC carbon samples. These contributions are calculated according to Equation 4.8 for shown in Figure 4.15.

	Δ TE (%)
ULC – lot A & B	-4.2
LC – lot B	-17.2

The main texture effect found was an overall correlation between $\Delta_4 TE$ and W_{440} (Figure 4.16), although the correlation applies specifically much better to the ULC sample lots than to the LC sample lot. Correlations between W_{400} and the average TE were also sought. Although such a correlation could be observed for ULC grades (lot A & B), it could not be observed for LC grade (lot B). This result is somewhat surprising because it indicates that the degree of alignment of the {111} planes in the plane of the sheet did little to improve TE. The TE of all LC and ULC samples could be made to correlate with a number of ultrasonic parameters to within ± 0.8 to 1.1 % when each lot was analyzed separately.

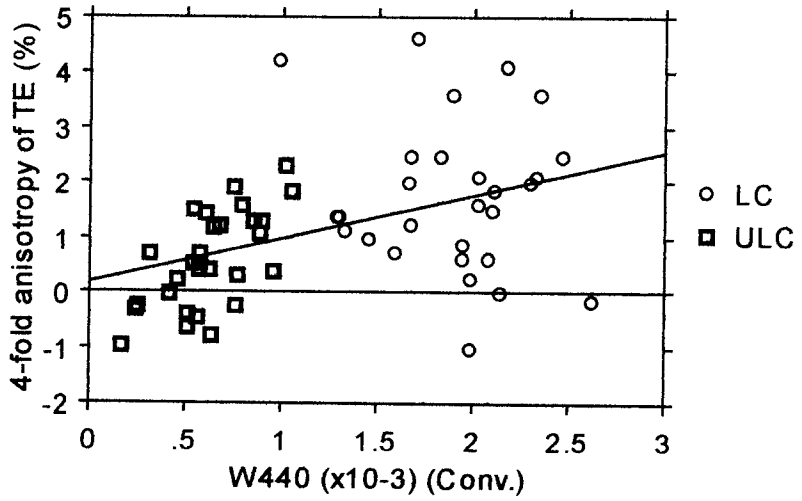

Figure 4.16 Correlation between the in-plane four-fold anisotropy of TE and the W_{440} coefficient measured using conventional ultrasonics for LC and ULC steel samples.

4.3.4 Uniform elongation

As discussed in Section 4.2.4, TE and UE are correlated. According to Pickering's book, the main difference between the two properties for low-carbon mild steels and HSLA steels is that the UE is sensitive to free nitrogen, while TE is sensitive to grain size. Our measurements are not sensitive to free N but Figure 4.17 indicates that UE does correlate with grain size, much like TE did, and in contradiction with Pickering. UE elongation was also found to correlate weakly with texture (Figure 4.18).

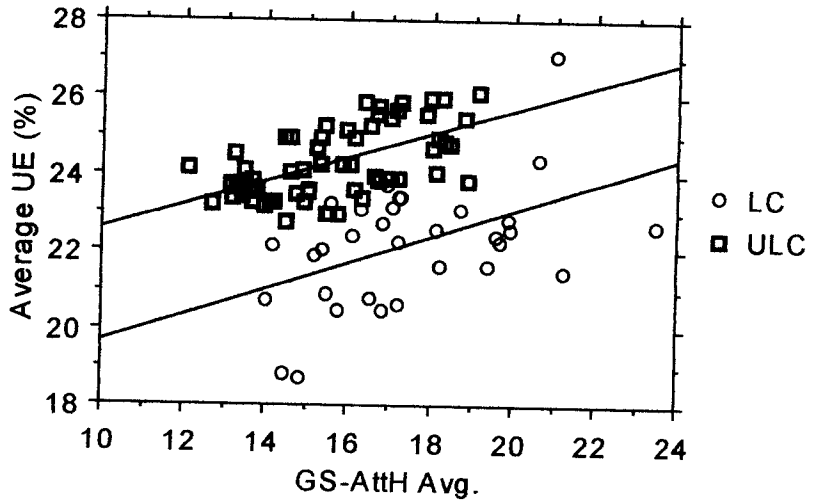

Figure 4.17 Variation of the average in-plane uniform elongation with ultrasonic grain size for 62 ULC and 31 LC steel samples.

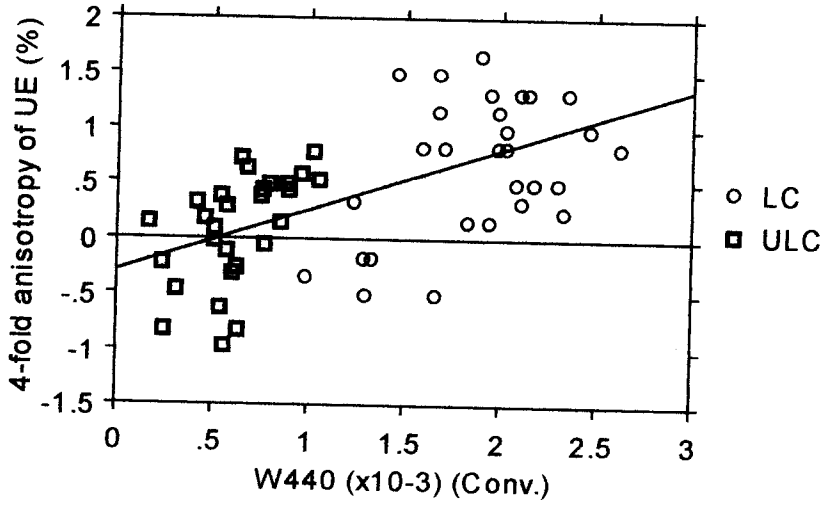

Figure 4.18 Correlation between the four-fold anisotropy of UE and the W_{440} texture coefficient as measured using conventional ultrasonics.

One major difficulty in finding an equation to estimate UE was that UE varied little within each sample sets. For example, in Figure 4.17, the total variability in ULC sample set was 3% only. In conclusion, ultrasonic measurements of UE were found for only some of the sample sets, and the empirical model predictions for UE resemble those found for TE. The ultrasonic measurements error (rms residual) was of the order of 1%.

4.3.5 Strain hardening exponent

As shown in Section 4.2.2, n = UE and the results shown in the previous section apply. Table 4.4 shows that the rms residual found for n are nearly equal to those found for UE. Here Pickering indicates that n should increase with grain size, which is as observed (see Figure 4.17 for UE).

4.3.6 Plastic strain ratio

Figure 4.19 shows the average plastic strain ratio, $\bar{r}$, as a function of W_{400} for 122 samples of ULC, HSLA and LC steels. Plastic strain ratio measurements were made by one company using the ASTM E517 standard on tensile specimens and by another using the Module-r apparatus, on the samples that they respectively produced. As predicted in Equations 4.3, HSLA steels samples, which have near zero values of W_{400}, have an $\bar{r}$ value of approximately one. Also, $\bar{r}$ is found to decrease linearly with W_{400}. If only the ULC steel samples are retained, and if a linear least squares fit of $\bar{r}$ to W_{400} is made, then the rms residual to the correlation is ±0.08. This rms residual approaches that found using the EMAR technique[30] (±0.04) and is comparable to the precision of the mechanical test, as stated in the ASTM standard (i.e., 3 to 8% of the r-values). Figure 4.19 also shows $\Delta_2 r$ as a function of W_{420} for the HSLA and ULC samples. As predicted by Equations 4.3, $\Delta_2 r$ appears proportional to W_{420} for the ULC steel samples, and perhaps also for the HSLA steel samples. The two straight lines are linear least squares fits with the intercept forced to zero for the two steel grades. The rms residuals to the correlations are ±0.13 and ±0.06 for the ULC and HSLA steel samples, respectively.

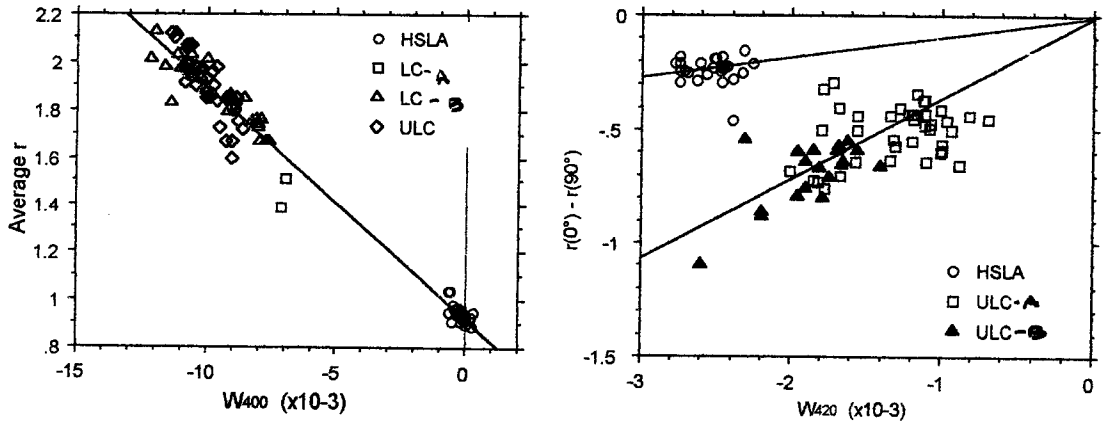

Figure 4.19 **Left:** $\bar{r}$ as a function of the W_{400} for three steel grades. **Right:** $\Delta_2 r$ as a function of W_{420} for two steel grades.

4.4 HSLA steels

4.4.1 Ultimate tensile strength and yield strength

Similar to the LC and ULC lots, YS and TS are linearly related to each other for the HSLA sample lots if the samples have received the same amount of temper reduction. This was shown for a sample set where 13 samples were given 2% temper reduction and 4 samples were given no temper reduction (Figure 4.20). The 2% temper reduction decreased YS by approximately 3 ksi. The effect of temper reduction on YS contrasts with the observed decrease in YS for ULC steels. The decrease in YS for HSLA is presumed to be caused by the removal of the upper yield point while the increase for ULC is caused by work hardening. For production samples, it would seem that temper reduction was controlled well and YS and TS are linearly correlated (Figure 4.21) with an rms residual of only 0.6 ksi, which is close to

the mechanical measurement accuracy of YS. Another similarity between HSLA and ULC & LC grades is the in-plane dependence of TS (and YS) with texture, as shown in Figure 4.6.

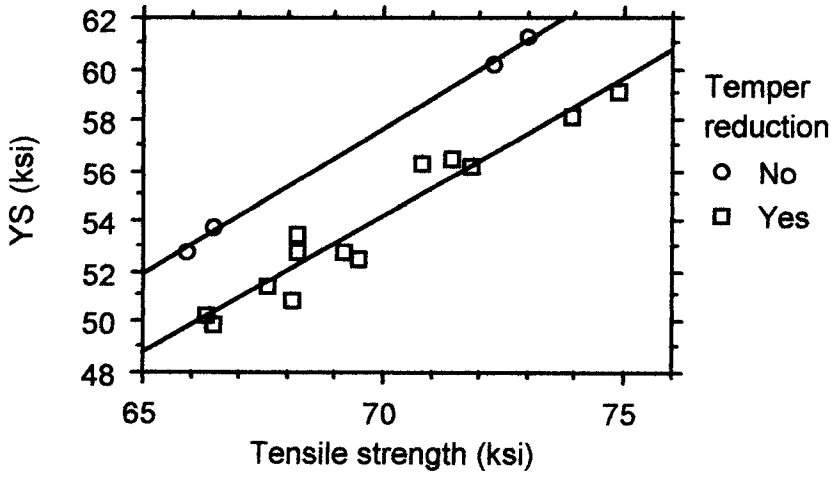

Figure 4.20 YS as a function of TS for 17 samples of HSLA steel with (squares) and without (circles) a 2% temper reduction.

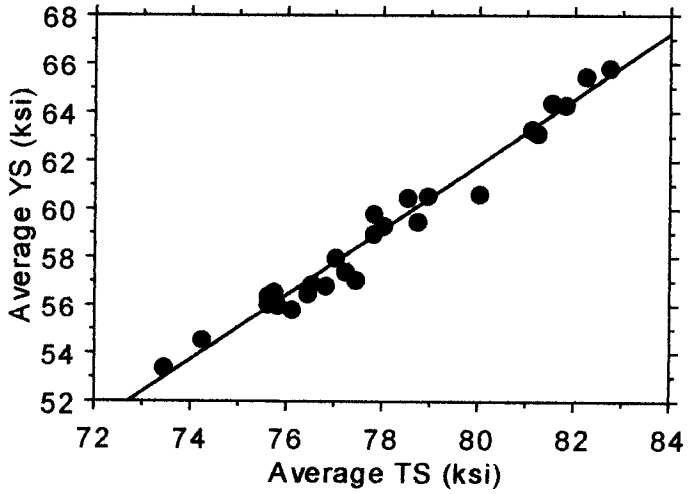

Figure 4.21 In-plane average YS as a function of in-plane average TS for 27 HSLA samples.

It was not possible to demonstrate a Hall-Petch dependence of YS or TS on grain size. This is perhaps not too surprising because, as shown in Section 2.4.10, although the grain size of HSLA steels did correlate with ultrasonic attenuation, the grain size estimate obtained by fitting the scattering model were a factor of two too large. The microstructure of HSLA steels is considerably more complex than that of ULC and LC grades. Something about it affects the ultrasonic behavior in a manner that has not been explained.

Consequently, our approach with HSLA steels has been entirely empirical, building multiple linear correlations with a number of measured parameters, hoping that the required information to predict the mechanical properties is contained in the data. Using mostly uncorrelated ultrasonic measurements (i.e. velocity is not correlated with attenuation, but the

attenuation at two different frequencies are highly correlated with each other), it was possible to correlate YS with a combination of four parameters with an rms residual of 1.5 ksi (Figure 4.22) for the above data set, and with a rms residual of 1.1 ksi for a 30 sample set from another company.

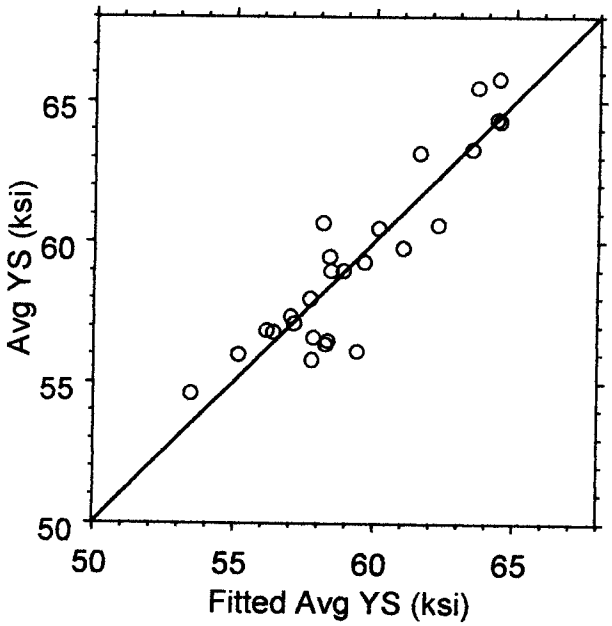

Figure 4.22 In-plane average YS for 25 HSLA samples as a function of a fitted empirical ultrasonic model involving 4 ultrasonic parameters.

For the first data set, a study of the obtained rms residual was made as a function of the number of parameters included in the correlation. Figure 4.23 shows that for 8 ultrasonic fitting parameters, the rms residual to the correlation drops to 0.7 ksi (Figure 4.24). The 8 ultrasonic parameters are evidently not all independent from each other. They combine into averages and differences. Averages of measurements likely increase measurement accuracy, while differences may isolate some information which is overlooked by the microstructural interpretation of the data. While empirical correlations with such high number of parameters and only 30 samples must be taken with skepticism, they may nevertheless be true. To test these correlations would require either larger data sets, or new insights into the microstructural parameters being measured and into their effects on the mechanical properties.

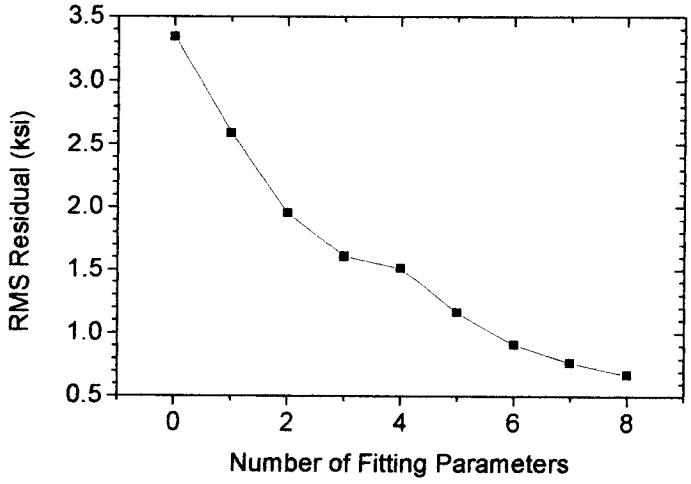

Figure 4.23 Reduction of the YS rms residual of Figure 4.22 for 25 HSLA steel samples when the number of ultrasonic fitting parameters increases from 0 to 8.
Zero ultrasonic parameters means that the data was fitted to a constant, the mean YS.

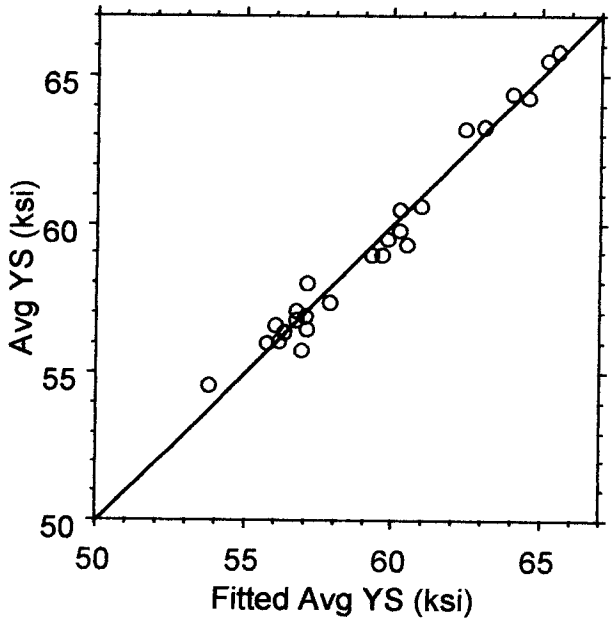

Figure 4.24 In-plane average YS for 25 HSLA samples as a function of a fitted empirical ultrasonic model involving 8 ultrasonic parameters.
The rms residual is 0.7 ksi.

4.4.2 Total elongation, uniform elongation, strain hardening exponent

As discussed in Section 4.2.2, the strain hardening exponent, n, is numerically equal to the value of the UE, except for a systematic offset, and UE correlates with TE. Empirical correlations with texture and grain size parameters yielded the rms residuals shown in Table 4.4.

4.4.3 Plastic strain ratio

The plastic strain ratio of HSLA is not commonly measured. However, this was done for a set of 30 samples from one company. The measurements showed relatively little sample to sample variation. Using laser-ultrasonics to estimate the $\bar{r}$ and $\Delta_4 r$ of HSLA steel samples was discussed with the ULC and LC grades in Section 4.3.6.

4.5 Summary table

Table 4.4 summarizes the measurement accuracy (rms residual of correlations, for a detailed explanation, see next section) obtained with the latest version of the prototype, data analysis software, and absorption measurements. All measurements were made on large (one square foot or more) rotating samples to simulate online conditions.

Table 4.4 Summary of achieved measurement accuracy.
Seven sample sets of approximately 30 samples each are included. Empty spaces indicate that correlations between ultrasonic and mechanical data were not evaluated. A set of three horizontal dashes indicates correlations were sought but not found for the data set.

	Target accuracy	ULC (lot A & B)	ULC (lot E)	LC (lot B)	LC (lot C)	HSLA (lot V)	HSLA (lot X)	HSLA (lot Y)
YS (ksi)	± 0.5 for YS < 50 ± 0.7 for YS < 100	1.0	0.5	0.7	0.7	0.7-1.5	2.3[a]	1.1
UTS (ksi)	± 0.5 for YS < 50 ± 0.7 for YS < 150	0.4	0.3	0.5	0.9	1.1	2.3[a]	1.3
TE (%)	± 1	0.9	0.8	1.1	1.0	1.5	1.5	1.2
UE (%)	± 1	---		1.2		0.6		
n	± 0.02	---	0.004	0.010	0.004	0.008		0.007
Average r	± 0.05	0.04	0.07	0.08	0.05	0.025		
Δr	not specified	0.09		0.05		0.04		
Grain size (μm)	not requested	0.35		2		0.25		
W_{400}, W_{420}	not requested	All grades: 5-10 %						
Thickness	not requested	One grade: 1 μm, Three grades: 4 μm						
ΔThickness[b]	not requested	All grades: Better than 1 μm						

[a] Reliable absorption measurement were unavailable for this grade. Absorption measurements are essential to further reduce the rms residual of YS.
[b] This refers to the ability to measure thickness variations, as opposed to absolute thickness.

In most cases, the target accuracies were either barely missed or somewhat exceeded. The most difficult target to meet was the measurement of YS which require delicate ultrasonic absorption measurements. Nevertheless, YS could be measured to ±1 ksi or better for all ULC and LC grades. HSLA grades proved especially difficult, but YS measurement accuracies in the range of ±0.7 to ±2.3 ksi could be achieved.

One of the most remarkable aspect of the prototype which is highlighted by Table 4.4 is the large amount of additional information that was obtained as a natural by-product of the laser-ultrasound technology: in-plane anisotropy, grain size, texture, thickness. Although the project goals were to build an instrument to measure the mechanical properties of finished products, the instrument could be used as an all-around sensor for online characterization of the microstructure for process diagnostic and process development purposes.

4.6 Measurement accuracies

To estimate the measurement accuracy of a sensor is a difficult task. For simplicity and practicality, the root mean square (rms) of the residual between the mechanical (or other reference) measurement and the laser-ultrasound measurement was chosen as the measurement accuracy estimator. To claim that a correlation existed between two quantities, an F-test was performed. As a rule, only those have been reported where correlations are significant to a confidence level of at least 95%, and each term in a multiple linear regression is significant to a 95% confidence level. Usually, the confidence levels largely exceeded 99%.

The rms residual is a good estimator of all sources of error combined: mechanical measurement error (y-axis error), laser-ultrasound error (x-axis error), and lack-of-fit. The lack-of-fit arises from inaccuracies in the model relating the ultrasonic measurement to the mechanical properties. For example, solid solution strengthening depends on chemistry variations that cannot be sensed. Therefore, if solid solution strengthening were to vary significantly, our model relating TS to grain size would not account for this variability which be accounted for in the lack-of-fit. Another example would be to choose a linear model instead of an inverse square root model to model the dependence of TS on grain size. All these sources of error, as well as a full analysis of their relative contributions to the rms residual, were fully analyzed. It was found that all three factors (mechanical measurement error, laser-ultrasound measurement error, and lack-of-fit) can contribute significantly to the rms residual of a specific measurement, but one of them usually dominates. Most often, it is the ultrasonic measurement accuracy or the lack-of-fit which dominates the rms residual.

The rms residual is a poor estimator of measurement accuracy when the correlation does not account for a large fraction of the total variance and displays a poor correlation coefficient, R^2. This might typically happen when there is too little variability in the sample set, or when the sample set is not representative of the entire production.

The many Figures shown in this report are typical of what was seen throughout the project. Over time, the rms residuals to the correlations with the mechanical properties slowly decreased. This indicated to us that the measurements and error estimates were reliable because they were repeatable, and improved slowly. Another reason to accept the

validity of the rms residuals is that they are nearly identical for different sample sets of equivalent grades from different companies. Finally, as discussed in the above paragraph, rms residuals also include mechanical measurement accuracies which, in a few cases, are significant. So the rms residuals can occasionally make the laser-ultrasonic measurement appears less accurate than it really is.

Another difficulty arises from *outliers*. Outliers are data points which do not fit the behavior of the rest of the sample set. Often, a specific cause may be identified, but often it cannot. Outliers are more easily identified when many repetitive measurements are made. For example, we have found that in some rare and specific locations on the sheet, the ultrasonic absorption can differ by a factor of up to four. Even if it differed by *only* 50%, our model would predict considerably different properties for this location. However, if such a measurement occurred online, the operator would immediately recognize the measurement as an anomaly and ignore it. But within the relatively few repetitions we made, we could not easily dismiss these outliers. Therefore, as the prototype is utilized online, algorithms will be developed to eliminate those glitches, average several measurements, improve data reliability, and further improve measurement accuracies.

5 CONCLUSION

5.1 Summary

The goal of this project was to demonstrate the feasibility to measure the mechanical properties of low carbon steel sheets on the production line using laser ultrasound. Three types of steels were selected: ultra low carbon (ULC), low carbon (LC), and high strength low alloy (HSLA). The mechanical properties under study were yield strength (YS), ultimate tensile strength (TS), total elongation (TE), uniform elongation (UE), strain hardening exponent (n), and the two plastic strain ratio parameters, $\bar{r}$ and Δr. In addition, the ultrasonic techniques provided information on crystallographic texture, grain size, and sheet thickness. The obtained measurement accuracies for the various mechanical properties are shown in Table 4.4 (p. 93)

The ultrasound generated by the apparatus travels back and forth in the thickness of the steel sheet. By measuring the time delay between two echoes or the resonance frequencies of the through-thickness excitations, and the relative amplitude of these two echoes, one can measure ultrasound velocity and attenuation. These are governed by the microstructure: grain size, crystallographic orientation distribution (texture), dislocations. Thus, by recording the time behavior of the ultrasonic signal, one can extract microstructure information. The measurement can then be utilized in a modified Hall-Petch equation that describes the effect of microstructure on the mechanical properties to infer these mechanical properties. The modified Hall-Petch equation also indicates that the mechanical properties depend on other microstructural factors that cannot be measured with ultrasound, i.e. they depend on fiction stress, solid solution elements, and fine precipitates. However, if the heat chemistry is controlled sufficiently well, these contributions to the mechanical properties may be constant within the grade.

To follow this approach, several scientific and technical challenges were surmounted. Laser-ultrasound detection bandwidth was extended from about 30 MHz to 300 MHz. A laser capable of generating high amplitude, high frequency ultrasound without marking the surface was found. Accurate and reliable ultrasound attenuation and velocity dispersion spectra were measured over a wide bandwidth, thus resulting in accurate grain size measurements. A laser-ultrasound resonance spectroscopy technique was invented (and patented) to measure texture and thickness. Another technique was invented to measure ultrasonic absorption in large sheets and infer information about the effect of temper rolling (skin pass) on YS. And finally, empirical models were found to relate the measured microstructure and ultrasonic measurements to the mechanical properties.

As a consequence to these many technical and scientific achievements, all target accuracies were met or nearly met. In general, ULC and LC steels, with their simpler single-phase, nearly equiaxed and polygonal microstructure were more easily modeled and understood. However, the HSLA grades had more complex microstructure, their ultrasonic grain size measurements were less accurate and their microstructure-property relationships were not so easily established. Consequently, correlations between ultrasonic measurements and mechanical properties often included purely ultrasonic parameters, such as velocity and attenuation, as opposed to derived microstructural quantities. A summary table of the

measurement accuracies is shown on page 93 of this report. Some of the more important results are:

- The TS of ULC and LC steels varies with ultrasonic grain size measurements, although texture has a significant effect. For these grades, TS measurement accuracy varied between ± 0.3 and ± 0.9 ksi.

- For all grades and a constant amount of temper reduction, YS correlates extremely well with TS. However, temper reduction affects YS significantly. Absorption measurements were essential in probing the effect of temper reduction on YS. For ULC and LC grades, YS measurement accuracy varied between ± 0.5 and ± 1.0 ksi.

- For HSLA grades, YS and TS measurement accuracy varied between ± 0.7 and ± 1.5 ksi, with one exception. One HSLA grade from company C had such a low ultrasound absorption that it could not be measured even at very high frequencies. For this grade, YS and TS measurement accuracy were ± 2.3 ksi.

- TE, UE, and n depend on the same microstructural features as YS and TS, and they could be measured to within ± 0.4 to ± 1.5 %.

- The in-plane anisotropy of mechanical properties correlates strongly with ultrasonic texture measurements.

- The in-plane average plastic strain ratio was measured to within ± 0.04 to ± 0.09 depending whether all grades from all companies were considered together or individually.

- Grain size measurement accuracy varied between ± 2 % and ± 14 % depending on grade.

- Sheet thickness could be measured to within ± 4 μm when all grades were considered together, although thicknesses measured within a single grade and thickness variations of ± 1 μm could easily be detected.

A prototype aimed at validating the technology on the production line was installed at the #1 Inspection line at LTV. Overall, the prototype's performance was as good online as in the laboratory. Sheet vibrations as well as ambient mechanical and electrical noise did not adversely affect the measurement. Optical alignment was preserved over time scales of about two weeks, i.e. between two successive trips to the plant. And data acquisition and analysis were done in real time.

However, at the time it was tested, the prototype suffered from two shortcomings. First, we could not guarantee that the laser used to generate the ultrasound would leave the sheet surface undamaged: a slight discoloration of the surface sometimes occurred. Since then, we have identified and successfully tested an alternate laser technology which can generate large amplitude ultrasound with no surface damage. The second shortcoming was YS measurement accuracy. Improved YS accuracies were obtained by adding laboratory measurements of absorption to the model. This resulted in the YS accuracies stated above.

Because we could not guarantee that the generation laser would not damage the surface, few coils were tested online. However, three coils from a set of five showed similar texture variations along their length. Another one of the five coils showed oscillations in the texture coefficient that correlates with plastic strain ratio. These oscillations were also found on another coil. The facts that few coils were measured and that reproducible variations of properties along the length of the coils were so easily found hints at the powerful ability of the sensor to detect variations in microstructure and mechanical properties that are typical of ordinary production conditions. It is the authors' opinion that systematic monitoring and analysis of such variability would lead to the identification of many of the process parameters that cause this variability. Corrective action could then be envisioned and implemented to produce more uniform product quality.

One key project development was the remote and real-time measurement of various microstructural quantities. The project was extended to demonstrate that laser-ultrasound could also measure austenite grain size and growth, phase transformations, sub-critical annealing, and ferrite grain growth at high processing temperatures. The microstructure was measured *in situ* and in real time, on a Gleeble 3500 thermomechanical simulator, the standard equipment used by the steel industry to physically simulate thermal and mechanical processes. At the rate of one microstructural measurement per second, this represents a technological breakthrough when compared to the time required to do similar work by quenching a new sample for each measurement, and doing metallographic analysis.

5.2 Expected benefits

The expected benefits that would be achieved by an eventual commercial apparatus capable of measuring the mechanical properties and the microstructure of steel sheets are:

- reduction in mechanical testing cost
- inspection along 100% of the length of a coil for improved product quality and consumer satisfaction
- fewer returned shipments caused by property variations in the body of the coil
- detection of slow drifts in production quality which could then be compensated to yield more consistent product properties
- detection of end-of-coil anomalies and smart decision on how much must be cut off leading to increased productivity
- immediate detection of coil properties and possibility to take immediate action to reduce the amount of downgraded production
- real time diagnostic of processes during production shifts from one grade to another, resulting in shorter set-up and delivery times and reduced inventories

- generic microstructure sensor for process diagnostic and process development, thus shortening product development times

- reduction in energy consumption arising from more efficient production

Finally, secondary benefits include the development of a measurement platform that can measure other parameters of interest with relatively little modifications. Some of these parameters are:

- hot ferrite and austenite grain size
- the onset and end of phase transformations and of recrystallization in hot rolling mills

- the end of recrystallization and the onset of grain growth during annealing

It is worth noting that two other laser-ultrasound prototypes are currently being developed by IMI for online measurements in the steel industry. One of them will exploit the results of the high temperature work developed under this project to determine the grain size of austenite at high temperatures during the controlled thermomechanical processing of seamless pipes.

5.3 Future work

This project reached its goal to demonstrate that mechanical properties can be measured online using laser-ultrasonics: the target accuracies for the mechanical properties were met or nearly met, and it was shown that online measurements are as good as in the laboratory. However, at the time of the online measurements, there remained two difficulties: 1) the achieved YS measurement accuracy needed some improvements, and 2) the laser used to generate ultrasound occasionally caused a slight discoloration of the sheet surface. In addition, minor problems were identified online: specular reflections by shiny sheet, such as hot dipped galvanized sheets[‡], can destroy the photodiode, and measurement rate was slower than expected due to varying signal strength and slow data transfer rate.

Since these online tests, YS accuracy has been improved by including ultrasonic absorption measurements which are sensitive to dislocations and temper reduction. It was also shown that a CO_2 laser can generate large amplitude ultrasound without any surface damage on clean (not oiled) coils. Finally various solutions are envisioned to protect the photodetector and increase measurement rate. To continue this project with the aim of reaching an eventual commercial success, we recommend to demonstrate that these new laboratory developments do work in the plant. Additional online tests are also likely to further demonstrate the usefulness of full-length mechanical testing. Such a project extension would require the following tasks:

[‡] The project was supposed to address bare sheets only, but a few tests were made on coated products. In general, electrogalvanized and hot dipped galvanized sheet coatings are so thin that the coatings do not affect the laser-ultrasound measurements in the frequency bandwidth of interest for this project.

- New generation laser: Develop a new CO_2 generation laser that will be an affordable, reliable, easy to maintain and compact version (4' x 8' x 4' high) of a laboratory laser that currently fills an entire room.

- Absorption measurements: Develop a new sensing heads to measure absorption while preserving the current measurements.

- Miscellaneous improvements: Develop a fast optical attenuator to protect the photodetector and stabilize signal strength. Replace slow digital oscilloscopes with fast ADC cards. Add any other improvements that would help speed up or reduce risk in a subsequent commercialization of the system.

- System integration: Integrate the above developments in the current prototype. Upgrade the software code to take advantage of new functionalities.

- Online tests: Mechanical property measurements along the full length of commercial coils and comparison with mechanical tests near the end of coils or near locations where coils are cut for other purposes at LTV's #1 inspection line. A calibration procedure will also be developed and tested during these online tests.

Upon the successful completion of this project extension, the technology will be ready for development into a commercial system. At this time, we do not know what will be the cost of such a commercial system. The cost of the laboratory components used in the proof-of-principle prototype is estimated at 450 000 US$. But laser, optical and electronic technologies are evolving rapidly toward improved performance at lower cost. In addition, the prototype developed for this project utilizes expensive laboratory equipment for added flexibility and lower cost to the project (lower cost to the project because many components are borrowed from IMI). An optimized design will likely lower component costs further.

APPENDIX – LIST OF PUBLICATIONS MADE UNDER THIS PROJECT

Patent

D. Lévesque, A. Moreau, M. Lord, C. Padioleau, M. Dubois, J.-P. Monchalin and J. F. Bussière. "Laser-Ultrasound Spectroscopy Apparatus and Method with Detection of Shear Resonances for Measuring Anisotropy, Thickness, and other Properties." US Patent # 6,057,927.

Published Papers

Marc Dubois, André Moreau, and Jean F. Bussière. "Ultrasonic Velocity Measurements During Phase Transformations in Steels Using Laser-Ultrasonics." In preparation for publication in *Journal of Applied Physics.*

A. Moreau, D. Lévesque, M. Lord, M. Dubois, J.-P. Monchalin, C. Padioleau, and J. F. Bussière. "On-line Measurement of Texture, Thickness, and Plastic Strain Ratio Using Laser-Ultrasound Resonance Spectroscopy." Submitted to *Ultrasonics*, 1999.

A. Moreau, M. Lord, D. Lévesque, M. Dubois, and J. F. Bussière. "Laser-Ultrasonic Absorption Measurements in Low Carbon Steels." *Journal of Alloys and Compounds* **310**, 1-2 (2000) p. 427-431, *Proceedings of the Twelfth International Conference on Internal Friction and Ultrasonic Attenuation in Solids*, Buenos Aires, Argentina, 18-23 July 1999.

M. Dubois, M. Militzer, A. Moreau, and J. F. Bussière, "A New Technique for the Quantitative Real-Time Monitoring of Austenite Grain Growth in Steel", *Scripta Materialia* **42**, 9 (2000) p. 867-874.

D. Lévesque, A. Moreau, M. Lord, M. Dubois, J.-P. Monchalin, C. Padioleau, and J. F. Bussière. "On-line Measurement of Texture, Thickness, and Plastic Strain Ratio on Steel Sheets Using Laser-Ultrasound Resonance Spectroscopy." *Advanced Sensors for Metals Processing.* Proceedings of the International Symposium on Advanced Sensors for Metals Processing, Quebec City, Canada, 22-26 August 1999. Edited by B. W. Brusey, J. F. Bussière, M. Dubois, and A. Moreau. Canadian Institute of Mining, Metallurgy and Petroleum, Montreal, 1999. p. 53-65.

A. Moreau, D. Lévesque, M. Lord, M. Dubois, J.-P. Monchalin, C. Padioleau, and J. F. Bussière. "On-line Measurement of Texture and Plastic Strain Ratio on Steel Sheets Using Laser-Ultrasonics." *Proceedings of the Twelfth International Conference on Textures of Materials*, Montreal, Canada, 9-13 August 1999. Edited by Jerzy A. Szpunar (NRC Research Press, Ottawa, 1999). p. 493-498.

M. Dubois, M. Militzer, A. Moreau, and J.F. Bussière. "Real-Time Monitoring of Austenite Grain Growth in Steel Using Laser-Ultrasonics." *Grain Growth in Polycrystalline Materials III*, Proceedings of Third International Conference on Grain Growth, Pittsburgh, PA, 14-19 June 1998. Edited by H. Weiland, B. L. Adams and A. D. Rollett. p. 593-598.

M. Dubois, A. Moreau, A. Dawson, M. Militzer and J. F. Bussière. "Laser-Ultrasonic Measurement of Microstructure Evolution During Metals Processing." NATO RTO Workshop I - Intelligent Processing of High Performance Materials, Brussels, Belgium, 13-14 May 1998. Published in RTO MP-9 (November 1998), p. 11.1-11.9.

M. Dubois, A. Moreau, M. Militzer and J. F. Bussière. "Laser-Ultrasonic Monitoring of Phase Transformations in Steels." *Scripta Materialia* **39**, 6 (1998) p. 735-741.

M. Dubois, A. Moreau, M. Militzer and J. F. Bussière. "Monitoring of Attenuation During Phase Transformations in Steel Using Laser-Ultrasonics." *Nondestructive Characterization of Materials* **VIII**, edited by Robert E. Green, Jr. (Plenum Press, New York, 1998). p. 323-328.

A. Moreau and M. Lord. "High-Frequency Laser-Ultrasonics." *Nondestructive Characterization of Materials* **VIII**, edited by Robert E. Green, Jr. (Plenum Press, New York, 1998). p. 27-32.

Progress, internal, industrial, and other reports

André Moreau, Martin Lord, Teodor Veres, and Guy Lamouche. "How to Generate High-Amplitude, High-Frequency, Laser-Ultrasound on Steel Without Damaging the Surface" Produced for the "Advanced Process Control Program" of the American Iron and Steel Institute (confidential), *Industrial Materials Institute*, #IMI2000-87091-C, 2000, 10 pages.

André Moreau, John A. Nilson, Martin Lord, and Jean-Pierre Monchalin. "Novel, Discharge Pumped, KrF Excimer, Oscillator-Power-Amplifier Laser System to Generate 2-3 ns UV Light Pulses" Produced for the "Advanced Process Control Program" of the American Iron and Steel Institute (confidential), *Industrial Materials Institute*, #IMI2000-87090-C, 2000, 6 pages.

Teodor Veres, Guy Lamouche, André Moreau, Daniel Lévesque and Martin Lord. "Error Analysis on Laser-Ultrasound Measurement of Tensile Properties for ULC, LC, and HSLA Steel Samples from Rouge Steel Company" Produced for the "Advanced Process Control Program" of the American Iron and Steel Institute (confidential), *Industrial Materials Institute*, #IMI2000-87089-C, 1995, 44 pages.

André Moreau, Christian Padioleau, Martin Lord, and Marc Dubois. "Safety Assessment Report Concerning the Laser-Ultrasonic Prototype to be Installed at LTV's #1 Inspection Line in Cleveland." Produced for the "Advanced Process Control Program" of the American Iron and Steel Institute (confidential), *Industrial Materials Institute*, #IMI2000-87093-C, 1998, 40 pages.

André Moreau, Marc Dubois, Daniel Lévesque, Martin Lord, Christian Padioleau, Jean-Pierre Monchalin, Jean F. Bussière. "On-line, Nondestructive Mechanical Properties Measurements Using Magnetic and Ultrasonic Techniques - Annual Report May 1, 1997 to April 30, 1998" Produced for the "Advanced Process Control Program" of the American Iron and Steel Institute (confidential), *Industrial Materials Institute*, #IMI98RT-70300-77395-C, 1998, 43 pages.

André Moreau, Jean F. Bussière, Jean-Pierre Monchalin, Daniel Lévesque, Marc Dubois, Martin Lord, Christian Padioleau. "On-line, Nondestructive Mechanical Properties Measurements Using Magnetic and Ultrasonic Techniques - Annual Report May 1, 1996 to April 30, 1997" Produced for the "Advanced Process Control Program" of the American Iron and Steel Institute (confidential), *Industrial Materials Institute*, #IMI97RIS-70300-73585-C, 1997, 46 pages.

Marc Dubois, André Moreau, and Jean F. Bussière. "High Temperature Monitoring of Steel Microstructure Using Laser-Ultrasonics" Produced for the "Advanced Process Control Program" of the American Iron and Steel Institute (confidential), *Industrial Materials Institute*, #IMI96RT-70300-72386-C, 1996, 55 pages.

A. Moreau. "On the Measurement Errors of Tensile Properties of Low Carbon Steel Samples" Produced for the "Advanced Process Control Program" of the American Iron and Steel Institute (confidential), *Industrial Materials Institute*, #IMI2000-87092-C, 1996, 36 pages.

André Moreau, Jean F. Bussière, Jean-Pierre Monchalin, Daniel Lévesque, Marc Dubois, Pierre Basséras, Martin Lord, Harold Hébert, Martin Viens. "On-line, Nondestructive Mechanical Properties Measurements Using Magnetic and Ultrasonic Techniques - Annual Report May 1, 1995 to April 30, 1996" Produced for the "Advanced Process Control Program" of the American Iron and Steel Institute (confidential), *Industrial Materials Institute*, #IMI96RIS-70300-70198-C, 1996, 40 pages.

André Moreau, Jean F. Bussière, Jean-Pierre Monchalin, Pierre Basséras, Martin Lord, Martin Viens, Harold Hébert, and Cheng-Kuei Jen. "On-line, Nondestructive Mechanical Properties Measurements Using Magnetic and Ultrasonic Techniques - Annual Report May 1994 - April 1995." Produced for the "Advanced Process Control Program" of the American Iron and Steel Institute (confidential), *Industrial Materials Institute*, #IMI95RIS-70300-66784-C, 1995, 15 pages.

P. Basséras, M. Lord, M. Viens, and A. Moreau. "Laser-Ultrasonic Generation Using a 1 ns Laser Source and Acoustic Attenuation Measurements in Steels." Technical report produced for the "Advanced Process Control Program" of the American Iron and Steel Institute (confidential), *Industrial Materials Institute*, #IMI95RT-70300-64234-C, 1995, 23 pages.

A. Moreau. "On-line, Nondestructive Mechanical Properties Measurements Using Magnetic and Ultrasonic Techniques." Annual Report produced for the "Advanced Process Control Program" of the American Iron and Steel Institute (confidential), *Industrial Materials Institute*, #IMI94RT-70300-59465-C, 1994, 7 pages.

REFERENCES

[1] Marc Dubois, André Moreau, and Jean F. Bussière. "Ultrasonic Velocity Measurements During Phase Transformations in Steels Using Laser-Ultrasonics." In preparation for publication in *Journal of Applied Physics.*

M. Dubois, M. Militzer, A. Moreau, and J. F. Bussière, "A New Technique for the Quantitative Real-Time Monitoring of Austenite Grain Growth in Steel", *Scripta Materialia* **42**, 9 (2000) p. 867-874.

M. Dubois, M. Militzer, A. Moreau, and J.F. Bussière. "Real-Time Monitoring of Austenite Grain Growth in Steel Using Laser-Ultrasonics." *Grain Growth in Polycrystalline Materials III*, Proceedings of Third International Conference on Grain Growth, Pittsburgh, PA, 14-19 June 1998. Edited by H. Weiland, B. L. Adams and A. D. Rollett. p. 593-598.

M. Dubois, A. Moreau, A. Dawson, M. Militzer and J. F. Bussière. "Laser-Ultrasonic Measurement of Microstructure Evolution During Metals Processing." NATO RTO Workshop I - Intelligent Processing of High Performance Materials, Brussels, Belgium, 13-14 May 1998. Published in *RTO MP-9* (November 1998), p. 11.1-11.9.

M. Dubois, A. Moreau, M. Militzer and J. F. Bussière. "Laser-Ultrasonic Monitoring of Phase Transformations in Steels." *Scripta Materialia* **39**, 6 (1998) p. 735-741.

M. Dubois, A. Moreau, M. Militzer and J. F. Bussière. "Monitoring of Attenuation During Phase Transformations in Steel Using Laser-Ultrasonics." *Nondestructive Characterization of Materials* **VIII**, edited by Robert E. Green, Jr. (Plenum Press, New York, 1998) p. 323-328.

[2] J.-P. Monchalin, R. Héon, P. Bouchard, C. Padioleau. "Broadband Optical Detection of Ultrasound by Optical Sideband Stripping with a Confocal Fabry-Perot." *Appl. Phys. Lett.* **55**, (1989) p. 1612-1614.

[3] A. Moreau and M. Lord. "High-Frequency Laser-Ultrasonics." *Nondestructive Characterization of Materials* **VIII**, edited by Robert E. Green, Jr. (Plenum Press, New York, 1998) p. 27-32.

[4] J.-P. Monchalin and J.-D. Aussel. "Ultrasonic Velocity and Attenuation Determination by Laser-Ultrasonics." J. of Nondestructive Evaluation **9**, 4 (1990) p. 211-221.

[5] M. Dubois, M. Viens, A. Moreau and C. K. Jen. "Ultrasonic Attenuation Measurements at 300 MHz." in *Review of Progress in Quantitative Nondestructive Evaluation* **15**, edited by D. O. Thompson and D. E. Chimenti (Plenum Press, New York, 1996) p. 1439-1446.

[6] Rohn Truell, Charles Elbaum, and Bruce B. Chick. *Ultrasonic Methods in Solid State Physics*. Academic Press, New York, 1969.

[7] Nuttall, A. H. "Some windows with very good sidelobe behavior." *IEEE Trans. on Acoust., Speech and Signal Processing* **ASSP-29**, (1981) p. 84-91.

[8] A. Moreau, D. Lévesque, M. Lord, M. Dubois, J.-P. Monchalin, C. Padioleau, and J. F. Bussière. "On-line Measurement of Texture, Thickness, and Plastic Strain Ratio Using Laser-Ultrasound Resonance Spectroscopy." Submitted to *Ultrasonics*, 1999.

[9] Rayne, J. A. and Chandrasekhar, B. S.,. "Elastic constants of iron from 4.2 to 300 K." *Phys. Rev.* **122**, (1961), p. 1714-1716.

[10] Auld, B. A. *Acoustic Fields and Waves in Solids*. Second edition. Robert E. Krieger Publishing Company, Inc., Malabar Florida, 1990. Vol. I, p. 214-219.

[11] R. L. Weaver. "Indications of materials character from the behavior of diffuse ultrasonic fields", in *Nondestructive Characterization of Materials* **II**. Edited by J. F. Bussière, J.-P. Monchalin, C. O. Ruud, and R. E. Green, Jr.. Plenum Press, New York, 1987, p. 689-695.

[12] H. Willems. "A new method for the measurement of ultrasonic absorption in polycrystalline materials", in *Review of Progress in Quantitative Nondestructive Evaluation* **6A**. Edited by D. O. Thompson and D. E. Chimenti. Plenum Press, New York, 1987, p. 473-481.

[13] A. Moreau, M. Lord, D. Lévesque, M. Dubois, and J. F. Bussière. "Laser-Ultrasonic Absorption Measurements in Low Carbon Steels." *Journal of Alloys and Compounds* **310**, 1-2 (2000), p. 427-431. *Proceedings of the Twelfth International Conference on Internal Friction and Ultrasonic Attenuation in Solids*, Buenos Aires, Argentina, 18-23 July 1999.

[14] A. Moreau et al. op. cit.

[15] H. Willems. "A New Method for the Measurement of Ultrasonic Absorption in Polycrystalline Materials." in *Review of Progress in Quantitative Nondestructive Evaluation* **6A**. Edited by D. O. Thompson and D. E. Chimenti. Plenum Press, New York, 1987. p. 473-481.

[16] R. J. Roe, "Inversion of pole figures for materials having cubic crystal symmetry", *J. Appl. Phys.* **37**, (1966) p. 2069-2072.

[17] H.-J. Bunge. *Texture Analysis in Materials Science.* Translated by Peter. R. Morris. Butterworths, London, 1982.

[18] R. Murayama, K. Fujisawa, H. Fukuoka and M. Hirao, "Development of an on-line evaluation system of formability in cold-rolled steel sheets using electromagnetic acoustic transducers (EMATs)", *NDT&E International* **29**, 141-146 (1996).

[19] D. Daniel, K. Sakata, J. J. Jonas, I. Makarow, and J. F. Bussière. "Acoustoelastic determination of the fourth order ODF coefficients and application to r-value prediction." In *Materials Research Symposium Proceedings*, **142**, *Nondestructive Monitoring of Materials Properties*, edited by John Holbrok and Jean Bussière, 77-82 (1988).

[20] M. Spies and E. Schneider, "Nondestructive analysis of the deep-drawing behavior of rolling sheets with ultrasonic techniques." *In Nondestructive Characterization of Materials* **III**", Edited by P. Höller, G. Dobmann, R. E. Green, Jr., V. Hauk, C. O. Ruud, Springer-Verlag, Berlin, 296-302 (1989).

[21] C.-S. Man. "Plastic Strain Ratio and Texture Coefficients in Orthotropic Sheets of Cubic Metals." In *Review of Progress in Quantitative Nondestructive Evaluation* **15**, edited by Donald O. Thompson and Dale E. Chimenti, Plenum, NY, 1353-1360 (1996).

[22] R. Hill. *The Mathematical Theory of Plasticity*. Clarendon Press, Oxford, 1950.

[23] William C. Leslie. *The Physical Metallurgy of Steels.* McGraw-Hill, Washington, 1981, p. 7.

[24] For example: F. B. Pickering. *Physical Metallurgy and the Design of Steels.* Applied Science Publishers Ltd, London, 1978.

[25] F. B. Pickering. *Physical Metallurgy and the Design of Steels.* Applied Science Publishers Ltd, London, 1978.

[26] R. Klinman and E. T. Stephenson. "Ultrasonic Prediction of Grain Size and mechanical Properties in Plain Carbon Steel." *Materials Evaluation* **39**, November 1981, p. 1116-1120.

[27] B. Mintz. "Importance of k_y (Hall-Petch slope) in determining strength of steels." *Metals Technology* **11**, July 1984, p. 265-271.

[28] Martin Viens. *Mesure des ratios de contraines plastiques dans des tôles d'acier.* Unpublished.

[29] F. B. Pickering. *Physical Metallurgy and the Design of Steels.* Applied Science Publishers Ltd, London, 1978.

[30] K. Kawashima, T. Hyoguchi, and T. Akagi. "On-line measurement of plastic strain ratio of steel sheet using resonance mode EMAT." *J. of Nondestructive Evaluation* **12** (1993), p. 71-77.